IDENTIFICATION OF DYNAMIC FORCE COEFFICIENTS OF A LABYRINTH AND GAS DAMPER SEALS USING IMPACT LOAD EXCITATIONS

by

David Ransom
Dr. Luis San Andrés

May 1998

TRC-SEAL-8-98

Texas A&M University
Mechanical Engineering Department

IDENTIFICATION OF DYNAMIC FORCE COEFFICIENTS OF A LABYRINTH AND GAS DAMPER SEALS USING IMPACT LOAD EXCITATIONS

David Lawrence Ransom

P.I. Dr. Luis San Andrés

TRC-Seal-2-98

April 1998

A Research Progress Report to the
Turbomachinery Research Consortium

Executive Summary

Identification of Dynamic Force Coefficients of a Labyrinth and Gas Damper Seals Using Impact Load Excitations

David Lawrence Ransom, Dr. Luis San Andrés

Experiments to identify stiffness and damping force coefficients of a two bladed teeth-on-stator labyrinth seal and a gas damper seal, both of diverging clearance, are presented. Calibrated impact guns excite a housing holding the test seal. The seal displacement and acceleration time responses in two orthogonal directions are measured. A frequency domain parameter identification procedure allows the determination of the seals' dynamic force coefficients over a frequency range. Tests are made for a centered seal condition without journal rotation and with rotation at 1,500 and 3,000 rpm. The pressure drop across the seal is controlled by increments in the inlet supply pressure to values three times the exit (ambient) pressure.

The two bladed labyrinth seal becomes less stable with increasing pressure ratio across the seal. This seal exhibits positive direct stiffness and negative direct damping. Cross-coupling effects are observed but identification of cross-coupled stiffnesses are poor. Comparison with analytical predictions is good for mass flow and direct damping coefficients. Predicted values for direct stiffness are negative, contrary to identified values. The same labyrinth seal is transformed into a four pocket damper seal and tested under identical conditions. The damper seal is shown to be more stable dynamically but can create a static instability due to excessive negative direct stiffness. In the test facility used, the seal housing does not have enough direct stiffness to support the damper seal at

pressure ratios greater than 2.0. Cross-coupled stiffness is not detected in the measurements. The direct damping coefficients are positive and large in magnitude compared to those from the labyrinth seal measurements. Analytical predictions show similar trends for mass flow, direct stiffness and direct damping coefficients. Predictions also show significant cross-coupling effects for tests with journal but these could not be identified reliably from the seal dynamic response measurements.

TABLE OF CONTENTS

Page

NOMENCLATURE vi

LIST OF FIGURES ix

LIST OF TABLES xii

INTRODUCTION 1

OBJECTIVE 3

LITERATURE REVIEW 4

Gas Seal Force Coefficients 4

Forced Excitation 6

Parameter Identification Procedures 12

TEST RIG DESCRIPTION 17

TEST PROCEDURE 23

PARAMETER IDENTIFICATION 25

Manual Curve Fitting of the Transfer Functions 27

Instrumental Variable Method 29

MEASUREMENT SENSITIVITY 32

LABYRINTH SEAL TEST RESULTS 34

Results and Predictions for Tests without Shaft Rotation 37

Results and Predictions for Tests with Shaft Rotation at 1,500 rpm 41

Results and Predictions for Tests with Shaft Rotation at 3,000 rpm 44

Test System Transfer Functions 44

Page

Coherence of Experimental Measurements 51

Conclusions 58

DAMPER SEAL TEST RESULTS 61

Results and Predictions for Tests without Shaft Rotation 64

Results and Predictions for Tests with Shaft Rotation at 1,500 rpm 64

Results and Predictions for Tests with Shaft Rotation at 3,000 rpm 67

Test System Transfer Functions 67

Coherence of Experimental Measurements 70

Conclusions 79

CONCLUSIONS 81

RECOMENDATIONS 83

REFERENCES 84

APPENDIX A 87

APPENDIX B 90

APPENDIX C 95

APPENDIX D 101

APPENDIX E 104

NOMENCLATURE

a	=	speed of sound in air [L/T]
A	=	least squares estimator matrix
C_{ij}	=	seal damping coefficients [M/T], $i,j = X,Y$
C_{hi}	=	base damping coefficient [M/T], $i= X,Y$
c	=	seal radial clearance [L]
D	=	seal journal diameter [L]
f_j	=	time domain external impact force [ML/T^2], $j = X,Y$
F_j	=	frequency domain external impact force [ML/T^2], $j = X,Y$
FFT	=	fast fourier transform
G_{ij}	=	frequency domain flexibility coefficients [T^2/M], $i,j = X,Y$
H_{ij}	=	frequency domain impedance coefficients [M/T^2], $i,j = X,Y$
I	=	identity matrix
j	=	$\sqrt{-1}$
K_{ij}	=	seal stiffness coefficients [M/T^2], $i,j = X,Y$
K_{hi}	=	base stiffness coefficient [M/T^2], $i= X,Y$
L	=	seal length [L]
Ma_{inlet}	=	V_{inlet}/a, seal inlet Mach number
M_{hi}	=	seal housing mass [M], $i= X,Y$
$\dot{m}$	=	mass flow rate through seal [M/T]
N	=	error matrix
P_{atm}	=	atmospheric (seal exit) pressure [M/LT^2]

P_{supply} = supply pressure to seal inlet [M/LT^2]

P_{ratio} = P_{supply}/P_{atm}, pressure ratio

P_1 = air line pressure before flow meters [M/LT^2]

P_2 = air line pressure after flow meters [M/LT^2]

P_3 = seal inlet pressure [M/LT^2]

P_4 = seal plenum pressure [M/LT^2]

Re_{axial} = $\dot{m} / \pi D \mu$, axial flow Reynolds number

U_f = uncertainty of measurements. Subscript indicates measurement type.

x, y = time domain seal displacements about equilibrium position [L].

$\dot{x}, \dot{y}$ = time domain seal velocities in the X, Y directions [L/T]

$\ddot{x}, \ddot{y}$ = time domain seal accelerations in the X, Y directions [L/T^2]

X, Y = frequency domain seal displacements about equilibrium position [L].

$\dot{X}, \dot{Y}$ = frequency domain seal velocities in the X, Y directions [L/T]

$\ddot{X}, \ddot{Y}$ = frequency domain seal accelerations in the X, Y directions [L/T^2]

TOR = teeth-on-rotor

TOS = teeth-on-stator

T_1 = inlet temperature of air [F]

T_2 = temperature at seal inlet [F]

T_3 = temperature at seal exit [F]

T_4 = lubricant temperature at exit of roller bearing [F]

V_{inlet} = $\mathrm{Re}_{axial}(\mu / \rho c)$, seal inlet velocity [L/T]

W = instrumental variable matrix

δ_{ij} = Dirac Delta function

Δ = $H_{XX}H_{YY} - H_{XY}H_{YX}$

μ = $1.8\ 10^{-5}$ Pa*sec, viscosity of air at $T_1 = 23$ °C [M/LT]

ρ = density of air at seal inlet [M/L^3]

ω = frequency [1/T]

ω_i = damped natural frequency [1/T], $i = X, Y$

SUBSCRIPTS

atm = refers to atmospheric pressure

d = refers to displacement measurement

h = refers to housing support parameters

i,j = corresponds to *X,Y* combinations. First subscript indicates direction of motion. Second subscript indicates direction of force.

ratio = refers to ratio of supply and atmospheric pressures

supply = refers to supply pressure at inlet of seal

SUPERSCRIPTS

T = transpose of matrix

LIST OF FIGURES

Page

Figure 1. Schematic View of Test Rig 17

Figure 2. Top View of Test Rig 18

Figure 3. Two-Bladed Labyrinth Seal 19

Figure 4. Position of Displacement and Acceleration Sensors and Coordinate System 20

Figure 5. Labyrinth Seal Mass Flow and Direct Stiffness Coefficients for No Journal Rotation and Varying Pressure Ratio 39

Figure 6. Labyrinth Seal Cross-Coupled Stiffness and Direct Damping Coefficients for No Journal Rotation and Varying Pressure Ratio 40

Figure 7. Labyrinth Seal Mass Flow and Direct Stiffness Coefficients for Journal Rotation at 1,500 rpm and Varying Pressure Ratio 42

Figure 8. Labyrinth Seal Cross-Coupled Stiffness and Direct Damping Coefficients for Journal Rotation at 1,500 rpm and Varying Pressure Ratio 43

Figure 9. Labyrinth Seal Mass Flow and Direct Stiffness Coefficients for Journal Rotation at 3,000 rpm and Varying Pressure Ratio 45

Figure 10. Labyrinth Seal Cross-Coupled Stiffness and Direct Damping Coefficients for Journal Rotation at 3,000 rpm and Varying Pressure Ratio 46

Figure 11. Labyrinth Seal Transfer Functions for No Journal Rotation and Varying Pressure Ratio 47

Page

Figure 12. Labyrinth Seal Transfer Functions for Journal Rotation at 1,500 rpm and Varying Pressure Ratio 49

Figure 13. Labyrinth Seal Transfer Functions for Journal Rotation at 3,000 rpm and Varying Pressure Ratio 50

Figure 14. Labyrinth Seal Test Coherences for No Journal Rotation and Pressure Ratio of 1.5 (X Impact) 52

Figure 15. Labyrinth Seal Test Coherences for No Journal Rotation and Pressure Ratio of 1.5 (Y Impact) 53

Figure 16. Labyrinth Seal Test Coherences for Journal Rotation at 1,500 rpm and Pressure Ratio of 1.5 (X Impact) 54

Figure 17. Labyrinth Seal Test Coherences for Journal Rotation at 1,500 rpm and Pressure Ratio of 1.5 (Y Impact) 55

Figure 18. Labyrinth Seal Test Coherences for Journal Rotation at 3,000 rpm and Pressure Ratio of 1.5 (X Impact) 56

Figure 19. Labyrinth Seal Test Coherences for Journal Rotation at 3,000 rpm and Pressure Ratio of 1.5 (Y Impact) 57

Figure 20. Labyrinth Seal Cascade Plot of Seal Displacement for Ramp-Up and Ramp-Down Test 59

Figure 21. Damper Seal Mass Flow, Direct Stiffness and Direct Damping Coefficients for No Journal Rotation and Varying Pressure Ratio 65

Page

Figure 22. Damper Seal Mass Flow, Direct Stiffness and Direct Damping Coefficients for Journal Rotation at 1,500 rpm and Varying Pressure Ratio 66

Figure 23. Damper Seal Mass Flow, Direct Stiffness and Direct Damping Coefficients for Journal Rotation at 3,000 rpm and Varying Pressure Ratio 68

Figure 24. Damper Seal Transfer Functions for No Journal Rotation and Varying Pressure Ratio 69

Figure 25. Damper Seal Transfer Functions for Journal Rotation at 1,500 rpm and Varying Pressure Ratio 71

Figure 26. Damper Seal Transfer Functions for Journal Rotation at 3,000 rpm and Varying Pressure Ratio 72

Figure 27. Damper Seal Test Coherences for No Journal Rotation and Pressure Ratio of 1.5 (X Impact) 73

Figure 28. Damper Seal Test Coherences for No Journal Rotation and Pressure Ratio of 1.5 (Y Impact) 74

Figure 29. Damper Seal Test Coherences for Journal Rotation at 1,500 rpm and Pressure Ratio of 1.5 (X Impact) 75

Figure 30. Damper Seal Test Coherences for Journal Rotation at 1,500 rpm and Pressure Ratio of 1.5 (Y Impact) 76

Figure 31. Damper Seal Test Coherences for Journal Rotation at 3,000 rpm and Pressure Ratio of 1.5 (X Impact) 77

Page

Figure 32. Damper Seal Test Coherences for Journal Rotation at 3,000 rpm and Pressure Ratio of 1.5 (Y Impact) 78

LIST OF TABLES

Table 1. Test Seal Dimensions 19

Table 2. Data Acquisition Parameters 21

Table 3. Transducer Gains 22

Table 4. Transducer Uncertainties 32

Table 5. Base Stiffness, Mass and Damping from Seal/Housing for Labyrinth Seal Tests 35

Table 6. Identified Labyrinth Seal Force Coefficients and Correlations (Centered Condition) 36

Table 7. Temperatures, Pressures and Mass Flow for Labyrinth Seal Tests (Centered Condition) 38

Table 8. Base Stiffness, Mass and Damping from Seal/Housing for Damper Seal Tests 61

Table 9. Identified Damper Seal Force Coefficients and Correlations (Centered Condition) 63

Table 10 Temperatures, Pressures and Mass Flow for Damper Seal Tests (Centered Condition) 63

Table 11. Force Coefficient Comparison of Both Seals 82

INTRODUCTION

Gas seals are used in many turbomachinery applications such as industrial compressors, aircraft engines and steam turbines to minimize leakage from a high pressure region to a low pressure region. Until the late 1970's, seal design concentrated mainly on reducing leakage. Childs (1978) reporting on the development of damper seals for the High Pressure Fuel Turbopump on the Space Shuttle Main Engine shows that seals not located at shaft vibration nodes have profound effects on the dynamics of rotors supported on bearings. Since large amplitudes of vibrations may occur at these locations, even small amounts of seal damping may decrease or even eliminate a critical speed response completely. Therefore, prediction of both seal leakage and seal forces becomes important during rotating machinery design to facilitate favorable predictions of rotor-bearing system performance.

Seal forces are general functions of the seal geometry, fluid properties, flow condition and operating conditions. For small amplitudes of rotor motion (X,Y) about an equilibrium position these forces (F_X,F_Y) are generally represented as linear stiffness $(K_{i,j})_{i,j=X,Y}$ and damping $(C_{i,j})_{i,j=X,Y}$ force coefficients (Lund, 1987, Childs, et al. 1986),

$$\begin{bmatrix} F_X \\ F_Y \end{bmatrix} = \begin{bmatrix} K_{XX} & K_{XY} \\ K_{YX} & K_{YY} \end{bmatrix} \begin{bmatrix} X \\ Y \end{bmatrix} + \begin{bmatrix} C_{XX} & C_{XY} \\ C_{YX} & C_{YY} \end{bmatrix} \begin{bmatrix} \dot{X} \\ \dot{Y} \end{bmatrix} \tag{1}$$

Fluid inertia is neglected in this description since gas densities are effectively small. These seal parameters, typically regarded as frequency independent, are necessary to predict rotor critical speeds and logarithmic decrements. The direct coefficients

---

The journal style followed is the ASME Journal of Tribology.

characterize a force that is in the same direction as the journal motion; whereas the off-diagonal (cross-coupled) coefficients represent forces that although proportional to the generalized displacement, velocity or acceleration, act in a direction perpendicular to it.

At present, there is little experimental data for the force coefficients and leakage of two bladed labyrinth seals despite their widespread use. A novel gas damper seal known as TAMSEAL™ exhibits significantly more direct damping than comparable conventional labyrinth seals as reported by Vance and Li (1995) for tests performed with and without journal rotation. For the non-rotating tests, seal direct damping is measured by the logarithmic decrement method. During coastdown tests, increased damping (due to the damper seal) is inferred by a decrease in rotor response amplitude from the baseline coastdown response. To date no systematic attempts have identified all of the rotordynamic force coefficients of the pocket damper seal. Thus, the need arises for experimental identification of all the force coefficients and seal leakage for both labyrinth seals and pocket damper seals. In the following thesis, test force coefficients and leakage rates for a two bladed labyrinth seal and a pocket damper seal are presented. The identified force coefficients demonstrate the major advantage (increased direct damping and reduced cross-coupled stiffness) of the pocket damper seal as compared to the conventional labyrinth seal.

OBJECTIVE

The objective of this research is to identify the rotordynamic force coefficients and leakage of a two bladed, teeth-on-stator (TOS) labyrinth seal and a pocket damper seal (TAMSEAL™). The experiment is performed in an existing test facility where impact guns excite the test seal and its dynamic displacements, accelerations and load are recorded as frequency response functions by a data acquisition system. The stiffness and damping force coefficients are extracted from the averaged spectral data using a frequency domain parameter identification method. The labyrinth seal test adds to the limited collection of reports concerning the measurement of force coefficients for this type of seal. The complete set of measured rotordynamic force coefficients for the pocket damper seal (direct and cross-coupled terms) is presented for the first time in this thesis. The intent is to gain better understanding of the rotordynamic force performance of both seals to be used in better designing similar seals for industrial applications.

LITERATURE REVIEW

The following review consists of three main discussions, each necessary to fully understand the task at hand. First, a brief review of the literature relevant to gas seal force coefficients is presented to insure that mistakes are not repeated and results are not duplicated unnecessarily. This is followed by a review of the literature pertaining to the experimental force coefficient identification in bearings and seals. Due to the nature of the identification task, two separate sections are necessary to discuss both the experimental procedure and the parameter identification method.

GAS SEAL FORCE COEFFICENTS

In his report on the experimental measurement of force coefficients for a two-bladed labyrinth seal (TOS), Wright (1978) presents the seal forces in terms of tangential and radial components. The direction of the tangential force determines the stability of the seal such that a positive force in the direction of whirl reduces the stability of the rotor. The author states that diverging clearance seals become increasingly unstable in backward whirl with increasing pressure ratios (seal inlet pressure/ seal exit pressure). Radial stiffness is found to be positive, increases with pressure ratio, and appears insensitive to shaft speed. In a second publication, Wright (1983) presents more experimental results from a similar test facility. A divergent labyrinth seal is found to be unstable in backward whirl although stable in forward whirl. For large pressure ratios the radial stiffness is positive and for low pressure ratios it is negative. Due to lack of an analytical model, Wright (1983) intends only to provide some data for use as a

benchmark in the development of an analysis to determine force coefficients in labyrinth seals.

In an effort to better understand and predict the rotordynamic performance of converging and diverging clearance labyrinth seals, Murphy and Vance (1980) analyze the axial flow through a typical labyrinth seal neglecting circumferential flow. The authors note that the converging clearance configuration generates a destabilizing tangential force in the direction of rotor whirl while giving a positive radial force. On the other hand, the diverging clearance configuration improves the stability of the rotor since it produces a tangential force opposing the rotor forward whirl, although producing a negative radial force.

Childs and Scharrer (1988) identify the force coefficients for teeth-on-rotor (TOR) and teeth-on-stator (TOS) labyrinth seal configurations each with 16 teeth, varying seal clearances, inlet pressures, inlet swirl conditions, and shaft speeds. Although the cross-coupled stiffness increases with seal inlet pressure for both TOR and TOS configurations, the authors find that increasing shaft speed causes cross-coupled stiffness to increase for the TOR seal and the cross-coupled stiffness to decrease for the TOS seal. Measured direct damping exhibits little sensitivity to shaft speed for both seal configurations but increases noticeably with seal inlet pressure. Independent of seal configuration and rotor speed, direct stiffness is negative, becoming less negative with increasing inlet pressure. Childs and Scharrer conclude from a stability analysis that the TOS seal is more stable than the TOR seal for positive inlet circumferential velocity ratio.

Vance, et al. (1993a) reporting on coastdown tests performed on both TOR and TOS labyrinth seals show the amplitude of the response to imbalance at the critical speed to increase with increasing pressure ratios. The largest increase occurs when the inlet pressure is twice the exit pressure corresponding to the onset of choked flow through the seal. An increase in response amplitude indicates a decrease in effective damping whether due to an increase in cross-coupled stiffness or a decrease in direct damping. Additionally, Vance, et al. show that for TOS seals the diverging clearance configuration exhibits more stability than seals with a converging clearance configuration.

Vance and Schultz (1993b) report on initial tests of a novel damper seal, TAMSEAL™. Similar in geometry to a conventional labyrinth seal, this pocket damper seal blocks circumferential flow arising from pressure variations around the seal annulus by dividing the plenum into four individual cavities. The authors perform impact load measurements in a non-rotating test apparatus, and for a range of pressure ratios extract the seal damping coefficients by the logarithmic decrement method. The authors report an increase in damping with an increase in seal inlet pressure. Vance and Schultz find that the novel damper seal has fifteen times more damping than a similar conventional labyrinth seal at a pressure ratio of 3.1.

FORCED EXCITATION

Accurate identification of seal force coefficients requires an apparatus and methodology which is unaffected by measurement noise and properly isolates the seal forces from the myriad of other forces typically found in rotating machinery. An extensive review of literature reveals that parameter identification procedures comprise

both the method to excite the test element and the method to extract the test element parameters from dynamic response measurements. Software and hardware limitations aside, the methods and procedures selected have the largest effect on the quality of the results.

In the following, three methods of forced excitation and two methods of parameter identification are examined. Each excitation method can be combined with either identification procedure, though not completely independent of each other. For instance, tests with impact load excitations excite transient rotor motions which, depending on the identification procedure selected, can be stored as time domain records or frequency domain spectra. Thus, even though the forced excitation procedures and the identification methods are discussed separately, it is important to remember that indeed they are closely related.

Three techniques of bearing excitation prevail, namely those due to vibratory loads (shakers), unbalance loads and impact loads. The number of papers available on vibratory loading indicates this to be the dominant method to date, though this method requires sophisticated test arrangements. For example, the stinger (which attaches the shaker to the test subject) must be rigid in the direction of loading, but fully flexible in all orthogonal directions. Mitchell and Elliott (1984) provide design guidelines for stinger flexural stiffness and exciter support stiffness.

Morton (1971) reports measurements made on an industrial size journal bearing using a single shaker to excite the bearing. A static load is applied using nitrogen pressurized bellows (50 tons maximum) and the dynamic load is provided by an

electrohydraulic shaker with a maximum load of two tons and top frequency of 50 Hz. Measured parameters include static force, dynamic forces, and bearing position relative to the journal. With a single shaker, movement in only one direction is not feasible without physically constraining the system. Therefore, response motions in two orthogonal directions are measured for excitation frequencies differing from the rotational speed. The amplitude of the dynamic force (two tons) provides a linear response and also a good signal to noise ratio. The resulting stiffness and damping values are found to be significantly lower than theoretical values. Morton believes theory to be deficient and states that the experimental results compare well with unbalance tests performed on a similar bearing.

Parkins (1979) introduces the selected orbit technique where the magnitude and phase of the shaker forces are controlled to render straight line motions of the test journal. The time response shows specific times when the journal displacement (relative to a static equilibrium) is null, and other times when the velocity is zero. Thus, measurements in two planes (X and Y) render eight separate equations from which eight dynamic force coefficients (stiffness and damping) are extracted. These linearized force coefficients are regarded as constants about a static equilibrium position. Parkins' measurements demonstrate that the linear assumption is not valid for motions about journal eccentricities greater than 78% of the bearing clearance, and thus, first order corrections to the test stiffness and damping coefficients become necessary. Parkins also shows static force coefficients extracted from an incremental load method on the same test apparatus. Four stiffness coefficients are determined with one added weight in each

direction and measured displacements in both directions. The dynamic values of stiffness correlate well with the incremental loading values wherever a direct comparison is made. The cross-coupled stiffness and damping coefficients (K_{XY} and C_{XY}) are shown to be nonlinear for journal eccentricity ratios greater than 0.78. All stiffness and damping coefficients are nonlinear for journal eccentricity ratios greater than 0.86 and 0.90, respectively.

Childs, et al. (1986) describe a test apparatus to extract rotordynamic coefficients from annular gas seals using a shaker in the horizontal direction. Eccentric operation is achieved by a cam displacing the shaft in the vertical direction. By exciting the system at one frequency, both stiffness and damping coefficients are identified. The extracted coefficients are assumed to be linear within a prescribed frequency range. Nelson, et al (1986) measure leakage and the rotordynamic force coefficients of a plain annular gas seal and a convergent geometry gas seal using the test rig described in Childs, et al. (1986). Tests are performed at various pressure ratios, shaking frequencies, and inlet pre-swirl conditions. The stiffness and damping coefficients are shown as a function of pressure ratio. The damping coefficients do not vary with varying inlet pre-swirl condition. Error bars on each stiffness and damping coefficient (graphical results) show that damping measurements have higher uncertainties than stiffness measurements.

A second method of dynamic force excitation is due to a rotating imbalance mass. This method requires a much less sophisticated test facility than the shaker approach and can require large amounts of testing time if numerous masses are used or if results for various rotational frequencies are desired (Goodwin, 1991). Hagg and Sankey (1956)

report on tests for a 150° hydrodynamic journal bearing and a four pad pivot bearing using this method. The rotor is mounted vertically and a static load (simulating rotor weight) is applied with a mass lever system. Vibrations are measured using the wattmeter technique, so only fundamental vibrations synchronous with journal speed are observed. The data is presented in dimensionless form for ease of comparison with other works. The results for the test journal bearing show considerable scatter, and the authors estimate uncertainties of 10 to 20%. The results for the pivot pad bearing show much less scatter and also follow theory quite well. The uncertainties are mainly due to measurement errors.

Tieu and Qiu (1994) use the unbalance mass excitation method to extract sixteen rotordynamic coefficients from two hydrodynamic journal bearings. The entire procedure requires five tests, the first with no added masses (baseline response). The second test is performed with two masses at right angles. For the third test, the same two masses in the second test merely trade positions. The fourth test corresponds to two masses directly opposing each other. Finally, in the fifth test, the same two masses from the fourth test switch places. For each test, orthogonal displacements and one pulse per revolution are recorded. This information is transformed into the frequency domain for the analysis procedure. All sixteen coefficients are successfully identified and compared to theoretical values. As also determined in other relevant works, the stiffnesses better match the theoretical values than the damping coefficients, particularly in the region of journal eccentricities below 50% of the bearing clearance. The authors state that the amplitude of the response produced by placing the masses at right angles to each other is greater

than when they are out of phase by 180°. In a situation where only a limited number of tests is available, the two tests with the masses at right angles (and the baseline test) suffice to obtain reasonable results. No values of uncertainty are presented for the coefficients in either method.

The third method of excitation is the impact or impulse method. The impact load has the distinct advantage of exciting a wide range of frequencies at one time. This range is dictated by the softness of the impact tip and the velocity of the impact. Nordmann and Schollhorn (1980) report on impact testing of a rotor supported by two fluid film bearings where the measured parameters are impact force and rotor displacements. The impact is measured by an accelerometer attached to the hammer. Displacement is measured at either end of the shaft by eddy current displacement sensors. The time data is transformed to the frequency domain and recorded on tape. Averaging several impacts eliminates noise from the response data. For comparison, a linear model is used to numerically produce the frequency response to an impulse. The values for stiffness and damping coefficients of the model are altered so that the transfer function of the linear model matches the transfer function of the rotor-bearing system. Stiffness values show good correlation with previous test results of a similar bearing; however damping values show large amounts of scatter.

Qiu and Tieu (1993) report on further measurements made using the impact method. The authors claim that their particular experiment is more applicable to industry because a rotor-bearing system with two asymmetric support bearings could be tested. By acquiring three sets of data, all sixteen rotordynamic coefficients for the rotor bearing

system can be identified. The first set of data is the initial vibration displacements (due to remnant unbalance vector). The second set is the response to an impact in the X direction, and the third is the response to an impact in the Y direction. After transforming all data to the frequency domain, the baseline vibration frequency response is subtracted from the impact frequency responses. This decreases the noise effect of the synchronous vibration response. Next, sixteen bearing parameters are extracted using the method described in the paper. The extracted parameters (force coefficients) are used to calculate time and frequency responses using a linear model, and compared to the actual acquired time and frequency responses. The authors report that the model results do compare well with the acquired data and correlate well with theory.

PARAMETER IDENTIFICATION PROCEDURES

As stated earlier, the method of forced excitation is only one part of the parameter identification process. The actual identification of the rotordynamic force coefficients requires a procedure to analyze the test data in either the time domain or the frequency domain. Hagg and Sankey (1956) record time responses of journal motion for a bearing subjected to both static and imbalance loads. By defining a Cartesian coordinate system with the (X,Y) axes along the major and minor axes of the journal orbit, the authors are able to determine the exact instants in time when the journal displacements are zero on each axis. The damping and stiffness coefficients are determined from the solution of two uncoupled steady state equations of journal motion. The authors state that the inaccuracies in the parameter values are mostly due to phase measurement errors.

Parkins (1979,1981,1995) uses the selected orbit technique which allows for exact measurement of times when journal velocities and displacements are null. However, Parkins uses two coupled equations to describe the journal motion, thus resulting in direct and cross-coupled terms. As mentioned previously, Parkins measures non-linear coefficients, so all values are presented in terms of a *zero value* and a gradient. The test *zero values* show very little spread, while the gradient terms show large scatter and do not seem useful. Parkins concludes that the measurements could have been improved with an on-line subtraction of journal center coordinates (runout removal).

In an effort to overcome the synchronous noise problem described in Parkins (1979,1981,1995), Burrows and Sahinkaya (1982) perform an analysis of a frequency-domain estimation method. The system is modeled by two coupled equations of motion excited by a Schroeder-phased harmonic signal which contains 100 harmonics. The identification procedure requires four inputs: two displacement time records and two force time records (one for each orthogonal direction). The input signals are then transformed to the frequency domain and used to fill two matrices, one containing displacements and applied forces, and another containing displacements only. These two matrices can be applied to a least squares estimator equation which renders the eight rotordynamic force coefficients. In an effort to estimate the effect of bias on parameter estimation, another form of the least squares estimator is used which includes a noise term. In one set of response data, a noise level of 5% completely destroys the method's ability to estimate parameters accurately. However, by taking an average frequency response, the authors found that the effect of 5% noise is almost eliminated. In another

test, the authors use actual experimental data to determine the coefficients of a squeeze-film damper bearing. The results of this frequency technique are compared with the results of a time domain method used on the same data. The frequency domain method shows much less scatter than the time domain method. In addition, three of the four damping coefficients obtained with the frequency domain method are found to be in close agreement with the π-film theory for squeeze-film damper bearings.

Tieu and Qiu (1994) measure a rotor-bearing system forced response to imbalance and transform it to the frequency domain where bearing impedances are identified. To prove the ability of the *FFT* (Fast Fourier Transform) procedure, the authors plot the inverse *FFT* of each measured signal against the original time data and show there is virtually no difference. The test results appear to be repeatable, although no particular information is given regarding the uncertainty of the estimated force coefficients. Also, the frequency domain least squares estimation requires much less effort than does a non-linear curve fit of time domain data.

Rouvas (1993) uses the power spectral density method to identify the rotordynamic force coefficients of hydrostatic bearings. Rouvas states that although the method is intended for random vibrations, it can be used successfully for deterministic vibrations as well. There are two distinct advantages to the power spectral density method. First, if two signals are statistically independent, the cross spectral density of those two signals is zero. This characteristic allows the effect of noise to be eliminated from the frequency response function. Time domain analysis methods require that for multiple excitations, each excitation must start at a similar point in the cycle and the excitations must have the

same magnitude. The power spectral density method does not require either of the two previous conditions.

Fritzen (1985) and Massmann and Nordmann (1985) present the instrumental variable (IV) method for use in identifying the force coefficients of a mechanical system. The IV method is an extension of a least-squares estimation procedure, and minimizes the error between identified coefficients and the actual coefficients which make up the test frequency response function. The IV method has the advantage of eliminating bias typically seen in an estimator due to measurement noise. Fritzen compares analytical transfer functions generated by coefficients extracted by a least-squares estimator and those functions generated by coefficients extracted by the IV method, and demonstrates clearly that the latter procedure is much more capable of recreating the experimentally acquired transfer function.

Ewins (1986) discusses coherence as an important measure of causality between an output response and an input force in the frequency domain. Coherence has a value between zero and one such that the stronger the relationship between the input and the output, the closer the coherence is to one. There are several possible reasons to have poor coherence (much less than unity), many of which are related to failure of the instrumentation, but the most relevant relate to measurements contaminated with extraneous *noise* during the testing. Therefore, signal coherence is a useful tool for verifying the quality of the measurement although it does not provide information regarding the cause of poor measurements.

This literature review provides relevant information on gas seal force coefficients and experimental procedures to identify the same. A clear understanding of gas seal literature enables the author to make informed decisions about test procedures and provides some idea of expected results. The extensive review of parameter identification literature eliminates much of the uncertainty in establishing an excitation procedure and an analysis method so that confidence in the identified coefficients continues to improve.

TEST RIG DESCRIPTION

A cross-section of the test rig is shown in Figure 1. Robison, et al. (1995) describes the original facility and experimental results for a squeeze film damper. The driver is a 7.5 kWatt (10 hp) DC motor utilizing a belt-pulley system to turn the test shaft to a maximum speed of 14,400 rpm. The base block is made of steel and weighs 104 kg (230 lb). The test shaft is held in the base by three precision angular contact ball bearings which are lubricated by a dedicated oil pump with a 144 liter (38 gallon) reservoir. A journal is mounted on the end of the shaft with a key and has a measured mechanical runout of 25.4 μm (0.001 inches). The natural frequency of the test shaft with the journal in place is 417 Hz.

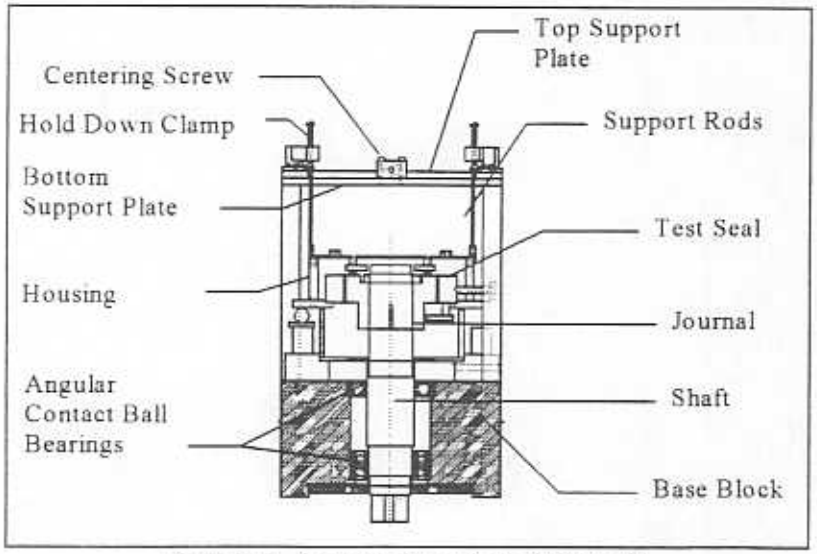

Figure 1 - Schematic view of test rig

The aluminum housing containing the test seal is suspended by four threaded mild steel rods, each 8 mm (5/16 inches) in diameter and 152.4 mm (6.0 inches) long. These

rods are bolted to the top support plate which rests flat on the bottom support plate. Figure 2 shows a view of the top and bottom support plates. The four positioning screws shown in the figure provide the ability to center the seal relative to the journal by moving the top support plate. To insure minimal friction when sliding, the mating surfaces for both plates (each 0.0127 m [0.5 inches] thick) are flat within 25.4 μm (1 mil). Four clamps hold the top plate in its desired place and prevent it from raising when the housing is pressurized.

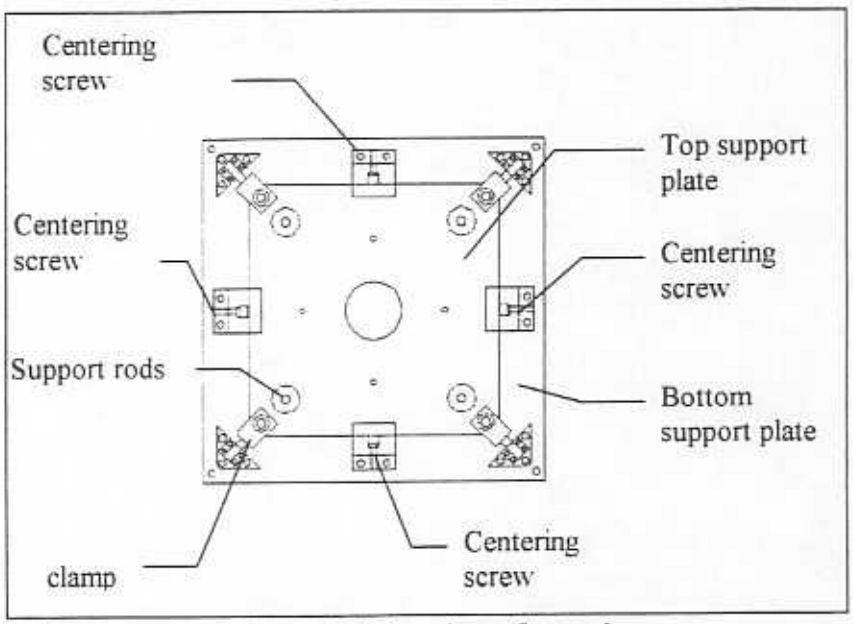

Figure 2 - Top view of test rig

The test seal is a two bladed labyrinth seal (TOS) with diverging clearance (Figure 3). The nominal dimensions are listed in Table 1. After the seal is tested in its original form, it is altered and tested as a pocket damper seal. The modification involves insertion

of four partition walls into the labyrinth deep groove dividing it into four cavities of equal size. The aluminum housing holding the seal also contains four eddy current displacement sensors fastened to the housing cap, and two (23 gr) piezoelectric accelerometers mounted to the side of the housing with magnetic bases. Figure 4 shows the position of the displacement sensors and accelerometers.

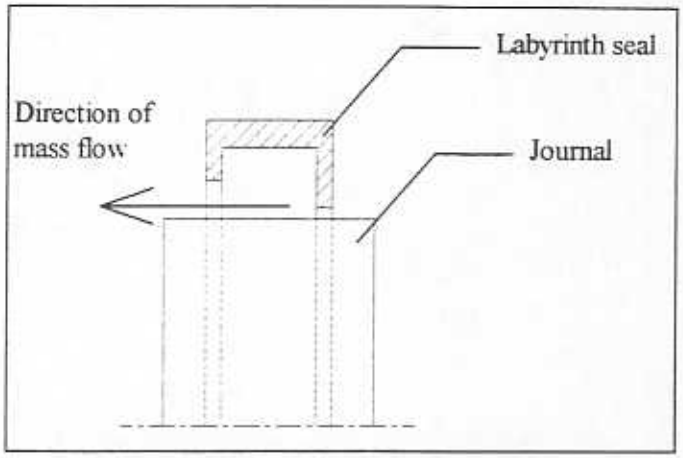

Figure 3 - Two bladed labyrinth seal

Table 1 - Test seal dimensions

Outer Diameter	17.780 cm (7.000 in)
Inlet Blade Diameter	12.725 cm (5.010 in)
Exit Blade Diameter	12.751 cm (5.020 in)
Journal Diameter (D)	12.700 cm (5.000 in)
Inlet Radial clearance (c)	127 μm (5 mils)
Exit Radial clearance (c)	254 μm (10 mils)
Length (L)	4.064 cm (1.6 in)
Material	Aluminum
Weight	1.0 kg (2.1 lb)

uncertainty ±12.7 μm (0.5 mils)

Pressurized air is delivered to the seal through a flexible hose containing a K-type thermocouple, and a visual flow meter and a turbine type flow meter. Pressure regulation is performed well upstream of the test seal. The inlet air pressure to the seal is measured with a strain gauge pressure transducer mounted on the housing cap. The air flow through the seal exhausts to atmospheric conditions. The discharge lubricant temperature from the rolling element bearings in the test rig base is measured with a K-type thermocouple.

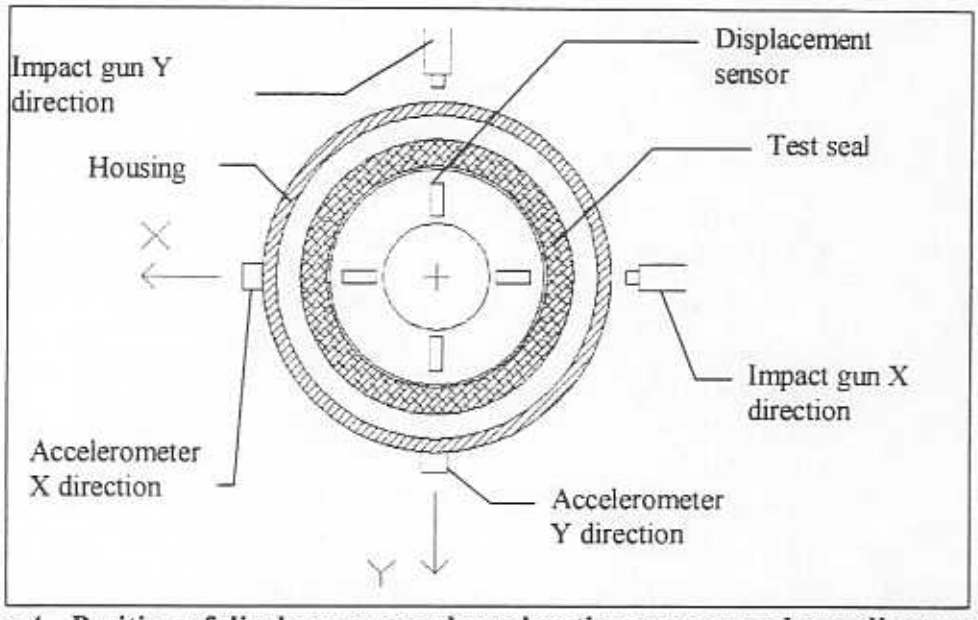

Figure 4 - Position of displacement and acceleration sensors and coordinate system

The data acquisition is performed by an eight channel simultaneous sampling *FFT* analyzer with a maximum rate of 20,000 samples/sec. Table 2 lists the acquisition parameters used in the testing. The sampling rate is a compromise between resolution for the measurement (in time) of the impact loads and resolution of the seal displacement and

acceleration frequency spectra. Impacts imparted with soft tips in the guns last ~3 milliseconds, while the seal dynamic motion lasts well over 0.5 sec. A sampling rate of 6,600 samples/sec leads to a resolution in the frequency domain of 0.813 Hz, and where the impact is described by twenty discrete data points.

Table 2 - Data acquisition parameters

Acquisition Parameter	Value
Sampling frequency	6,600 samples/sec
Number of samples	8,192 per test
Total sampling time	1.24 sec
Full scale voltage (FSV)	4.7 volts all channels
Windowing	none
Pre-trigger	5 samples

The full scale voltage (FSV) in the data acquisition process is an important parameter and must be considered carefully. In terms of measurement accuracy it is best for each motion transducer to use as much of the FSV as possible. Different transducers operate in different ranges and the data acquisition system allows each channel to have a different range. However, the post process requires that all D/A channels must have the same FSV. The piezoelectric accelerometers produce significantly smaller voltage signals than the eddy current sensors and the impact gun load cells. Therefore, the accelerometer outputs are pre-amplified by a factor of 10 with a signal conditioner. The sensitivity for each transducer is listed below in Table 3.

Each transducer is calibrated before use in the test facility. Displacement sensors are calibrated on a translating table with electronic position reading accurate to 12.7 μm

(0.0005 inches). Accelerometers are calibrated with an electric shaker designed to shake at a frequency of 100 Hz and an acceleration equal to 1 g.. Load cells are calibrated by impacting a mass suspended from the ceiling and measuring its acceleration with a previously calibrated accelerometer.

Table 3 - Transducer gains

Transducer	Gain
Displacement X	124 μm/volt
Displacement Y	126 μm/volt
Acceleration X	9.225 g/volt × 10
Acceleration Y	9.461 g/volt × 10
Force X	44.11 N/volt
Force Y	43.67 N/volt

The data acquisition is initiated by an increase of 7% of FSV on the impact load cell channel. However, since the impacts last very briefly, the data points before the trigger 7% value are also required. A built-in pre-trigger function allows recovery of the data to the instant when the impact just initiates. Experiments show that 7% of FSV for the impact loads amounts to the first 5 data points. Therefore, the pre-trigger is set to exactly 5 data points.

Despite the time and effort invested in the rig, there exist a few pitfalls which are encountered during testing. Due to the flexibility of the support structure, the seal alignment is altered with a change in seal inlet pressure. This requires the seal to be re-centered for each pressure ratio. In addition, the bias of the displacement transducers must be null for each pressure ratio (DC offset) which requires adjustments to the signal conditioner any time the inlet pressure changes.

TEST PROCEDURE

The experiments are performed without journal rotation (0 rpm) and at journal speeds of 1,500 and 3,000 rpm. The seal is centered statically with respect to the journal and no effort is made to induce fluid pre-swirl. For each shaft speed, four pressure ratios are tested and each test is repeated once. A *pressure ratio* is defined as the ratio of the absolute supply pressure (P_{supply}) to the absolute discharge pressure (P_{atm}) corresponding to ambient conditions (101.3 kPa). All experiments are conducted at a mean air temperature equal to 73 °F (23 °C).

The gun triggering and the data acquisition procedure are fully controlled from a PC computer. For each impact in either the X or Y directions, the signals from the gun load cell, two accelerometers, and two displacement sensors are acquired and stored temporarily. The seal dynamic responses are evaluated graphically before permanent storage. The impact test is repeated if the response is not acceptable. Impact responses can be discarded for various reasons such as occurrences of a double impact, impact too large, impact too small, or a failed transducer during acquisition. For each test condition, the impact guns are adjusted so that the seal and housing move approximately 55-65% of the seal clearance in the first oscillation. The entire frequency domain response data is saved upon acceptance. Every test consists of 16 impacts in each direction (X and Y) for a given test condition (journal speed and pressure ratio).

Once all impacts are complete, the responses are frequency averaged and stored. Finally, the coefficients are identified using a frequency domain method described in the

following section. The identified force coefficients are valid for the entire range of frequencies excited by the impact force.

An effort is made to correlate the experimental measurements with predictions from a code presented by Li et al. (1997). The one control-volume bulk-flow model determines the seal force coefficients for the pocket damper seal and for conventional see through labyrinth seals with either converging or diverging clearances. Perturbation equations for seal cavity flow, flow across the partition walls, and axial mass flow rate are derived for a centered seal condition. Flow turbulence is accounted for by using turbulent shear stress parameters and Moody's friction factors in the circumferential bulk-flow momentum equation. The flow equations are numerically solved and a computer program is developed correspondingly. Sample input data for the analysis code is provided in APPENDIX A.

PARAMETER IDENTIFICATION

The identification of the seal dynamic force coefficients is performed by analysis of the seal forced response and impact load in the frequency domain. The housing and seal, considered as a rigid mass supported by the four elastic rods, move in a horizontal plane under the forced excitation of the impact guns. The equations of motion for small amplitudes about an equilibrium position are described in linear form by,

$$\begin{aligned} M_h\ddot{x} + \left(C_{XX} + C_{hX}\right)\dot{x} + C_{XY}\dot{y} + \left(K_{XX} + K_{hX}\right)x + K_{XY}y &= f_X \\ M_h\ddot{y} + \left(C_{YY} + C_{hY}\right)\dot{y} + C_{YX}\dot{x} + \left(K_{YY} + K_{hY}\right)y + K_{YX}x &= f_Y \end{aligned} \tag{2}$$

where $\{f_i\}_{i=X,Y}$ are external forces, M_h is the combined housing and seal mass, $\{K_{hi}, C_{hi}\}_{i=X,Y}$ are the support rod stiffness and damping coefficients, and $\{K_{ij}, C_{ij}\}_{i,j=X,Y}$ are the gas seal dynamic stiffness and damping force coefficients, respectively.

The model for equations (2) assumes the journal motion in the lateral directions (X,Y) to be negligible (i.e. no runout) and does not include the effects of random noise due to fluctuations in the air pressure and local flow turbulence. The journal lateral motion is indeed small since the shaft support is nearly rigid at the test conditions. However, some amplitude of shaft runout (25.4 μm [1.0 mil]) at synchronous frequency is present in the tests at 1,500 and 3,000 rpm. The effects of random noise are minimized by averaging 16 impact responses and seal forced frequency responses. Equations (2) in matrix form become

$$\mathrm{M}_h\begin{bmatrix}\ddot{x}\\ \ddot{y}\end{bmatrix} + \begin{bmatrix} C_{XX}+C_{hX} & C_{XY} \\ C_{YX} & C_{YY}+C_{hY}\end{bmatrix}\begin{bmatrix}\dot{x}\\ \dot{y}\end{bmatrix} + \begin{bmatrix} K_{XX}+K_{hX} & K_{XY} \\ K_{YX} & K_{YY}+K_{hY}\end{bmatrix}\begin{bmatrix}x\\ y\end{bmatrix} = \begin{bmatrix}f_X\\ f_Y\end{bmatrix} \tag{3}$$

Let

$$X(\omega) = FFT\big(x(t)\big), \quad Y(\omega) = FFT\big(y(t)\big), \quad F_i(\omega) = FFT\big(f_i(t)\big) \tag{4}$$

be the *Fourier transforms* of the dynamic seal responses and of the applied impact loads, respectively. By definition,

$$\begin{aligned} \dot{X} &= \mathbf{j}\omega X & \dot{Y} &= \mathbf{j}\omega Y \\ \ddot{X} &= -\omega^2 X & \ddot{Y} &= -\omega^2 Y \end{aligned} \tag{5}$$

where $\mathbf{j} = \sqrt{-1}$ and (ω) is the frequency[1]. Application of the *Fourier transform* to the linear ordinary differential equations (3) gives the following set of algebraic equations in the frequency domain,

$$-\omega^2 \mathrm{M}_h \begin{bmatrix} X \\ Y \end{bmatrix} + \mathbf{j}\omega \begin{bmatrix} C_{XX}+C_{hX} & C_{XY} \\ C_{YX} & C_{YY}+C_{hY} \end{bmatrix} \begin{bmatrix} X \\ Y \end{bmatrix} + \begin{bmatrix} K_{XX}+K_{hX} & K_{XY} \\ K_{YX} & K_{YY}+K_{hY} \end{bmatrix} \begin{bmatrix} X \\ Y \end{bmatrix} = \begin{bmatrix} F_X \\ F_Y \end{bmatrix} \tag{6}$$

Complex *impedances* $\{H_{ij}\}_{i,j=X,Y}$ are defined as

$$H_{ij} = \Big[\big(K_{ij} + K_{hi}\delta_{ij}\big) - \omega^2 M_{hi}\delta_{ij}\Big] + \mathbf{j}\omega\big(C_{ij} + C_{hi}\delta_{ij}\big) \tag{7}$$

where $\delta_{ij} = 1$ for $i = j = X,Y$; zero otherwise. The impedances are composed of real and imaginary parts, both functions of frequency (ω). The real part denotes the dynamic stiffness, while the imaginary part is proportional to the damping coefficient. Substitution of the impedance definitions into the frequency domain equations (6) leads to:

---

[1] Measurements of housing acceleration show this to be the case, i.e. the *FFT* of the acceleration is identical to $-\omega^2 \ddot{X}$. This is of course since the journal does not vibrate with large amplitude motions.

$$\begin{bmatrix} H_{XX} & H_{XY} \\ H_{YX} & H_{YY} \end{bmatrix} \begin{bmatrix} X \\ Y \end{bmatrix} = \begin{bmatrix} F_X \\ F_Y \end{bmatrix} \tag{8}$$

These represent two algebraic equations and four unknown impedances $(H_{ij})_{i,j=X,Y}$. For two independent impact excitations $(f_X,0)^T$ and $(0,f_Y)^T$, the equations of motion are:

$$\begin{bmatrix} X_X & Y_X \\ X_Y & Y_Y \end{bmatrix} \begin{bmatrix} H_{XX} \\ H_{XY} \end{bmatrix} = \begin{bmatrix} F_X \\ 0 \end{bmatrix}$$

$$\begin{bmatrix} X_X & Y_X \\ X_Y & Y_Y \end{bmatrix} \begin{bmatrix} H_{YX} \\ H_{YY} \end{bmatrix} = \begin{bmatrix} 0 \\ F_Y \end{bmatrix} \tag{9}$$

where X_Y is the *Fourier transform* of the seal displacement in the X direction due to an impact load in the Y direction, etc. Equations (9) represent four independent equations with four unknowns, $(H_{ij})_{i,j=X,Y}$, easily found using Cramers' rule.

MANUAL CURVE FITTING OF THE TRANSFER FUNCTIONS

At this point, one of two methods is used to actually identify the force coefficients contained in the impedances described previously. As noted above, the impedances are general functions of frequency and follow typical formulations for linear systems. The parameters of the system, $\{M,K,C\}_{i,j=X,Y}$ are determined by curve fitting of the discrete impedances $\{H_{ij}\}$ over a certain range of frequencies. The real part of an impedance is modeled as a quadratic polynomial, $\mathrm{Re}(H) \sim K - M\omega^2$, and from which the system stiffness and inertia coefficients are obtained. The imaginary part of an impedance is represented as a first order polynomial or straight line, $\mathrm{Im}(H) \sim \omega C$, and whose slope renders the damping coefficient. The quality (goodness) and certainty of the identified system parameters depends on how well the analytical curve fits the test data over the selected

frequency range. Of course, the linearity of the system response and the invariance of the force coefficients with frequency must also be accounted for in the procedure.

The system impedances, $(H_{ij})_{i,j=X,Y}$, are (in principle) valid for the entire frequency spectrum and only limited in practice by instrumentation and methodology. In the current tests, the accelerometers are only calibrated to a low value of 10 Hz. However, the measured accelerations are not used in the current procedure since it is verified in the frequency domain that $\ddot{X} = -\omega^2 X$. Furthermore, it is found in the procedure that subtracting the housing inertia force, $\left(-M_h \times \ddot{X}\right)$ degrades the quality of the curve fit for the real portion of the impedances. Therefore, the identification method is valid for the lowest measurable frequency (0.813 Hz). The measurements at exactly 0 Hz are not useful due to a small dc offset (bias) from the transducers. The upper limit of the frequency range is determined by the frequency range excited by the impact gun. The seal displacement frequency response extends up to about 90 Hz for gun excitations with a soft tip. Therefore, the frequency domain curve fitting is performed in the frequency range of 1-90 Hz. However, the experimental impedances (especially the imaginary portion) show considerable scatter for such a wide frequency range. Thus, identification of the slope (damping coefficient) of the imaginary portion becomes too inaccurate. Therefore, in the present procedure, the method described is valuable to identify preliminary seal parameters. These seal coefficients are adjusted when reproducing the system (output/input) transfer functions.

System transfer functions (output/input) are used to obtain more precise measurements of the annular seal force coefficients. In terms of impedance $(H_{ij})_{i,j=X,Y}$, the analytical system transfer functions are generated by the following equations

$$G_{XX} = TF(X_X) = \frac{H_{YY}}{\Delta} \qquad G_{XY} = TF(X_Y) = \frac{-H_{XY}}{\Delta}$$
$$G_{YX} = TF(Y_X) = \frac{-H_{YX}}{\Delta} \qquad G_{YY} = TF(Y_Y) = \frac{H_{XX}}{\Delta} \tag{10}$$

where $\Delta = H_{XX}H_{YY} - H_{XY}H_{YX}$. The transfer functions calculated from the experimental data are evaluated, and the magnitude of analytical transfer functions using the preliminary estimates for the seal force coefficients are also determined from equations (10). At first, the test and calculated transfer functions are not likely to match very well over the selected frequency range. However, at this point small adjustments to the seal stiffness and damping values in the analytical model quickly lead to a better match between the model and the experimental results. Unfortunately this method looses effectiveness when trying to curve fit all four transfer functions simultaneously. It is far too difficult to determine which ones of the twelve coefficients need be altered to improve all four curve fits. A method which does not require user input and can simultaneously curve fit all four transfer functions is desired.

INSTRUMENTAL VARIABLE METHOD

The instrumental variable (IV) method described by Fritzen (1985) and Massmann and Nordmann (1985) has the ability to simultaneously curve fit all four transfer functions. The IV method is an extension of a least-squares estimation method.

Massmann and Nordmann (1985) apply the least-squares and IV methods to identify annular gas seal coefficients. The flexibility matrix (G) is defined as the matrix of transfer functions in equations (10). Since flexibility (or compliance) is the inverse of impedance ($G=H^{-1}$), then theoretically the product of both matrices is the identity matrix, I. In reality there is some noise associated with the experimental measurements and so an error matrix, N, is introduced into the following relationship.

$$G \cdot H = G\left[K - \omega^2 M + \mathbf{j}\omega C\right] = I + N \tag{11}$$

where K, M and C are the stiffness, mass and damping coefficient matrices. Equation (11) is rearranged as follows

$$A\begin{bmatrix} K \\ M \\ C \end{bmatrix} = I + N \tag{12}$$

where A consists of the measured transfer functions and the unknown force coefficients are contained in the stiffness, mass and damping matrices on the left hand side of the equation. Solution of equation (12) by least-squares requires minimization of the loss function defined by the Euclidean norm of N. This minimization leads to the normal equations,

$$A^T A\begin{bmatrix} K \\ M \\ C \end{bmatrix} = A^T I \tag{13}$$

where A^T is a weighting function which places more weight on the resonance frequencies. The first set of coefficients of the stiffness, mass and damping matrices are determined

from these equations. At this point, the instrumental variable extension is used to identify the force coefficients and eliminate the effect of measurement noise.

Analytical transfer functions are generated from the stiffness, mass and damping matrices found by the least-squares minimization. The weighting function, A^T, is replaced by a new matrix, W^T, which is created from these analytical transfer functions. This new weighting function is free of measurement noise and contains a peak only at the resonant frequency which is determined from the first estimates for stiffness, mass and damping. The new normal equation is

$$W^T A \begin{bmatrix} K \\ M \\ C \end{bmatrix} = W^T I \tag{14}$$

so that an improved set of force coefficients are determined. The new coefficients are used to recalculate analytical transfer functions and next the weighting function, W^T. The new set of identified coefficients are compared with the previous set and the procedure is complete if correlation is within a desired tolerance. If the tolerance is not met, then the procedure just repeats until such time. The software used to perform the identification is produced by Mr. Sergio Diaz, a graduate student in the Rotordynamics Laboratory. APPENDIX B presents the program developed in Mathcad. Notice the surprising simplicity of the programmed algorithm.

MEASUREMENT SENSITIVITY

The measurement uncertainties for displacement, acceleration, force, seal inlet pressure and mass flow rate are given in Table 4. These uncertainties combine the precision uncertainty of the sensors and the uncertainties resulting from the analog to digital conversion. The seal inlet pressure defines the *pressure ratio* (P_{supply}/P_{amb}), and since the seal discharges to atmospheric conditions (14.7 psia), the uncertainty of the test *pressure ratio* is only 0.3%. The uncertainty for mass flow rate corresponds to that of the turbine flow meter.

Table 4 - Transducer uncertainties

Transducer	Uncertainty
Displacement	± 2.0 μm (0.08 mils)
Acceleration	± 0.001 g
Force	± 0.04 N (0.009 lb)
Seal inlet pressure	± 0.34 MPa (0.05 psi)
Mass flow rate	± 0.0006 kg/sec (0.001 lb/sec)

The uncertainties for displacement and force measurements are only valid for single sample experiments in the time domain. However, the stiffness and damping coefficients are identified in the frequency domain. Thus, magnitudes of uncertainty for the estimated force coefficients must be obtained from a method which transforms the time domain measurement uncertainties to the frequency domain.

Two sets of time domain signals are necessary in the sensitivity procedure devised. First, an impulse force and associated displacement time response for known values of force coefficients are generated using analytical formulae for a simple mass,

spring and damper linear system. A second set of derived responses is generated using an impulse force whose original value is lowered by one magnitude of force uncertainty, and a displacement response taken as the superposition of the original response and one magnitude of displacement uncertainty. The original and derived time responses are brought into the frequency domain, and the parameter identification method (described earlier) determines the system impedances; and from these, stiffness and damping coefficients are identified over a certain frequency range . The difference between the original magnitudes of stiffness and damping coefficients and the values identified from the second set of responses reveals the measurement uncertainty for both force coefficients. As expected, the uncertainties vary with the magnitude of the original parameters. The largest uncertainty magnitudes for the stiffness and damping coefficients are equal to 6 kN/m and 3 N sec/m, respectively. Of course, this method does not address the uncertainty introduced by measurement noise. However, it is expected that the averaging procedure and the IV method combined minimize this effect. APPENDIX C details the sensitivity analysis performed to estimate the uncertainty of the identified parameters.

LABYRINTH SEAL TEST RESULTS

As described in the formulation of the parameter identification method, the base stiffness, mass and damping coefficients of the test housing must be subtracted from all identified coefficients in order to obtain the coefficients attributed solely to the gas seal. To measure the base coefficients, the impact testing is performed with no journal rotation and no air mass flow across the seal. The base stiffness, mass and damping coefficients are identified as described above in the parameter identification section.

Initially, base direct damping is too small so that the seal becomes dynamically unstable at pressure ratios greater than 2.0. To increase base damping, four sections of rubber hose are wedged between the support rods which suspend the housing and the support columns which support the plate assembly. Vertical placement of the rubber inserts determines the amount of added damping. Measurements show that the optimum position for each rubber insert is half way between the top of the housing and the bottom of the support plates. The test structure is not completely symmetric as indicated by the base coefficients listed in Table 5. The structure exhibited a measurable amount of cross-coupled behavior as seen by the cross-coupled terms also presented.

Table 5 - Base stiffness, mass and damping from seal/housing for labyrinth seal tests

Parameter	Value	Uncertainty
K_{hXX}	327 kN/m (1870 lb/in)	6.0 kN/m (34 lb/in)
K_{hXY}	14 kN/m (80 lb/in)	0.4 kN/m (2 lb/in)
K_{hYX}	-4 kN/m (-23 lb/in)	0.4 kN/m (2 lb/in)
K_{hYY}	293 kN/m (1676 lb/in)	5.5 kN/m (31 lb/in)
C_{hXX}	89 N sec/m (0.51 lb sec/in)	1.5 N sec/m (0.01 lb sec/in)
C_{hXY}	3 N sec/m (0.02 lb sec/in)	0.5 N sec/m (0.00 lb sec/in)
C_{hYX}	-1 N sec/m (-0.01 lb sec/in)	0.5 N sec/m (0.00 lb sec/in)
C_{hYY}	69 N sec/m (0.40 lb sec/in)	1.3 N sec/m (0.01 lb sec/in)
M_{hXX}	7.0 kg (15.4 lb)	0.2 kg (0.4 lb)
M_{hXY}	0.0 kg (0.0 lb)	0.2 kg (0.4 lb)
M_{hYX}	0.0 kg (0.0 lb)	0.2 kg (0.4 lb)
M_{hYY}	6.3 kg (13.9 lb)	0.2 kg (0.4 lb)
ω_X	34.4 Hz	0.8 Hz
ω_Y	34.3 Hz	0.8 Hz

Identified seal coefficients for a centered seal at all test conditions are listed in Table 6. The base coefficients described previously are subtracted so that the values listed in the table are contributions of the active labyrinth seal only. The correlation between the experimental transfer function and the curve fit is also listed in Table 6. There are four correlation values corresponding to the four transfer functions, two direct transfer functions (*XX* and *YY*) and two indirect transfer functions (*XY* and *YX*). The correlation has a value between zero and one so that a value of one indicates perfect correlation (in the selected frequency range) between the experimental transfer function and the analytical transfer function generated from the identified values of stiffness, mass and damping. Almost every transfer function has a high correlation (well into the 0.9 region) with the exception of a few at a journal speed of 3,000 rpm. For reference, APPENDIX D shows typical time traces of load, displacement and acceleration

Table 6 - Identified labyrinth seal force coefficients and correlations (centered condition)

Speed (RPM)	Pressure Ratio	K_{XX} (kN/m)	K_{XY} (kN/m)	K_{YX} (kN/m)	K_{YY} (kN/m)	C_{XX} (N sec/m)	C_{XY} (N sec/m)	C_{YX} (N sec/m)	C_{YY} (N sec/m)	$Corr_{XX}$	$Corr_{XY}$	$Corr_{YX}$	$Corr_{YY}$
0	1.50	25	-3	3	26	-15	1	1	-10	0.99	0.98	0.97	0.99
	1.50	23	-4	4	21	-12	1	-1	-12	0.99	0.98	0.98	0.99
	2.00	49	2	2	51	-23	3	-2	-10	0.99	0.97	0.97	0.99
	2.00	40	-1	5	42	-19	3	-3	-14	0.99	0.97	0.98	0.99
	2.50	67	-3	-4	70	-28	2	0	-9	0.99	0.96	0.96	0.99
	2.50	65	-3	2	66	-25	1	-1	-11	0.99	0.96	0.97	0.99
	3.00	88	-12	-11	83	-30	1	1	-6	0.99	0.94	0.93	0.98
	3.00	78	-9	-13	79	-35	2	0	-7	0.99	0.96	0.94	0.98
1,500	1.50	26	-18	15	27	-21	-5	-2	-9	0.99	0.98	0.99	0.99
	1.50	20	-2	-7	30	-11	0	-7	-5	0.99	0.98	0.99	0.99
	1.75	26	-8	0	26	-15	3	-5	-3	0.99	0.98	0.98	0.99
	2.00	22	-19	-1	78	-20	0	-6	-8	0.99	0.96	0.97	0.99
	2.00	39	-6	-2	38	-25	2	-6	-5	0.99	0.96	0.97	0.99
	2.50	54	-4	-9	49	-33	3	-7	0	0.99	0.95	0.97	0.99
	2.50	50	-9	6	47	-29	3	-11	-4	0.98	0.95	0.97	0.99
	3.00	73	-5	-5	68	-32	5	-1	-1	0.99	0.95	0.96	0.98
	3.00	61	-20	-7	62	-38	-1	-10	-2	0.99	0.88	0.96	0.98
3,000	1.50	28	-25	10	35	-20	-5	-1	-7	0.99	0.97	0.99	1.00
	1.50	-7	-15	28	9	-20	1	-6	-3	0.99	0.97	0.99	0.99
	1.75	43	4	4	39	-16	-2	2	0	0.99	0.97	0.98	0.99
	2.00	42	-10	-12	4	-14	7	2	0	0.98	0.91	0.96	0.98
	2.00	64	4	-34	80	-18	-3	0	2	0.99	0.91	0.97	0.99
	2.50	51	-29	55	61	-39	1	-2	-1	0.99	0.61	0.98	0.99
	2.50	75	-35	-19	30	-33	3	-8	7	0.99	0.67	0.95	0.97
	3.00	84	-14	46	83	-31	3	0	9	0.99	0.73	0.96	0.97
	3.00	76	-6	-28	84	-38	1	-15	5	0.99	0.83	0.96	0.98

* Maximum uncertainties for stiffness and damping coefficients are 6 kN/m and 3 N sec/m respectively

transducers for labyrinth seal tests. Also included are samples of curve fit transfer functions as they compare to test data.

Table 7 lists values for inlet air temperature, seal top temperature, seal bottom temperature, roller bearing lubricant discharge temperature, air pressure before flow meters, air pressure after flow meters, seal inlet air pressure, plenum pressure, mass flow as measured with the turbine type flow meter, axial flow Reynolds number and seal inlet Mach number. All of the temperatures are listed in degrees Celsius and the pressures listed are gauge, not absolute.

RESULTS AND PREDICTIONS FOR TESTS WITHOUT SHAFT ROTATION

Predicted and measured mass flow and identified seal direct stiffness coefficients are shown in Figure 5 as a function of pressure ratio. Predictions are based on Li et al.'s (1997) analysis for no fluid pre-swirl and excitation frequency of 37 Hz. As expected, mass flow steadily increases with pressure ratio, ranging from 0.011 kg/sec to 0.026 kg/sec. The predicted mass flow rate is marginally higher than the measured values. The direct stiffness coefficients (K_{XX}, K_{YY}) are positive and also increase linearly with increasing seal inlet pressure. This is contrary to the predicted values which show the coefficients to be negative.

Identified cross-coupled stiffness and direct damping are shown in Figure 6. The cross-coupled stiffness values are small and are generally positive except for the highest pressure ratio where all identified values are negative. Predictions show cross-coupled stiffness to be zero for all pressure ratios. The direct damping coefficients (C_{XX}, C_{YY}) are negative, although it is peculiar that the C_{YY} damping coefficient does not change with

Table 7 - Temperatures, pressures, mass flow, axial Reynolds number and seal inlet Mach number for labyrinth seal tests (centered condition)

Speed (RPM)	Pressure Ratio	T_1 (C)	T_2 (C)	T_3 (C)	T_4 (C)	P_1 (KPa)	P_2 (KPa)	P_3 (KPa)	P_4 (KPa)	$\dot{m}$ (kg/sec)	Re_{axial}	Ma_{inlet}
0	1.50	23	23	23	23	655	621	51	14	0.0109	1,518	0.341
	1.50	23	23	23	23	655	621	51	14	0.0111	1,540	0.346
	2.00	22	23	23	23	655	607	101	21	0.0169	2,353	0.397
	2.00	23	23	23	23	655	607	101	22	0.0167	2,323	0.391
	2.50	22	23	23	23	655	607	152	31	0.0217	3,027	0.407
	2.50	23	23	23	23	655	607	152	31	0.0220	3,061	0.412
	3.00	22	23	23	23	655	607	203	42	0.0261	3,636	0.408
	3.00	23	23	23	23	655	593	203	42	0.0262	3,643	0.409
1,500	1.50	21	23	23	32	655	621	51	14	0.0111	1,545	0.347
	1.50	21	23	24	34	655	621	51	14	0.0112	1,561	0.350
	1.75	21	22	23	31	655	607	76	17	0.0140	1,947	0.373
	2.00	20	22	23	28	655	607	101	21	0.0170	2,365	0.399
	2.00	20	22	23	32	655	607	101	22	0.0168	2,344	0.395
	2.50	20	22	22	29	655	607	152	31	0.0219	3,045	0.409
	2.50	21	22	22	30	655	593	152	31	0.0219	3,050	0.410
	3.00	20	21	21	29	655	607	203	42	0.0263	3,659	0.410
	3.00	20	22	21	26	655	593	203	43	0.0262	3,653	0.410
3,000	1.50	21	23	24	38	655	621	51	14	0.0111	1,540	0.345
	1.50	21	23	24	41	655	621	51	14	0.0111	1,550	0.348
	1.75	21	23	24	38	655	607	76	18	0.0141	1,969	0.377
	2.00	21	22	23	36	655	607	101	21	0.0169	2,355	0.397
	2.00	21	23	23	38	655	607	101	21	0.0168	2,338	0.394
	2.50	20	22	23	37	655	607	152	31	0.0219	3,056	0.411
	2.50	20	22	23	36	655	593	152	31	0.0217	3,028	0.407
	3.00	20	22	22	34	655	593	203	42	0.0262	3,648	0.409
	3.00	21	22	22	32	655	593	203	42	0.0265	3,686	0.413

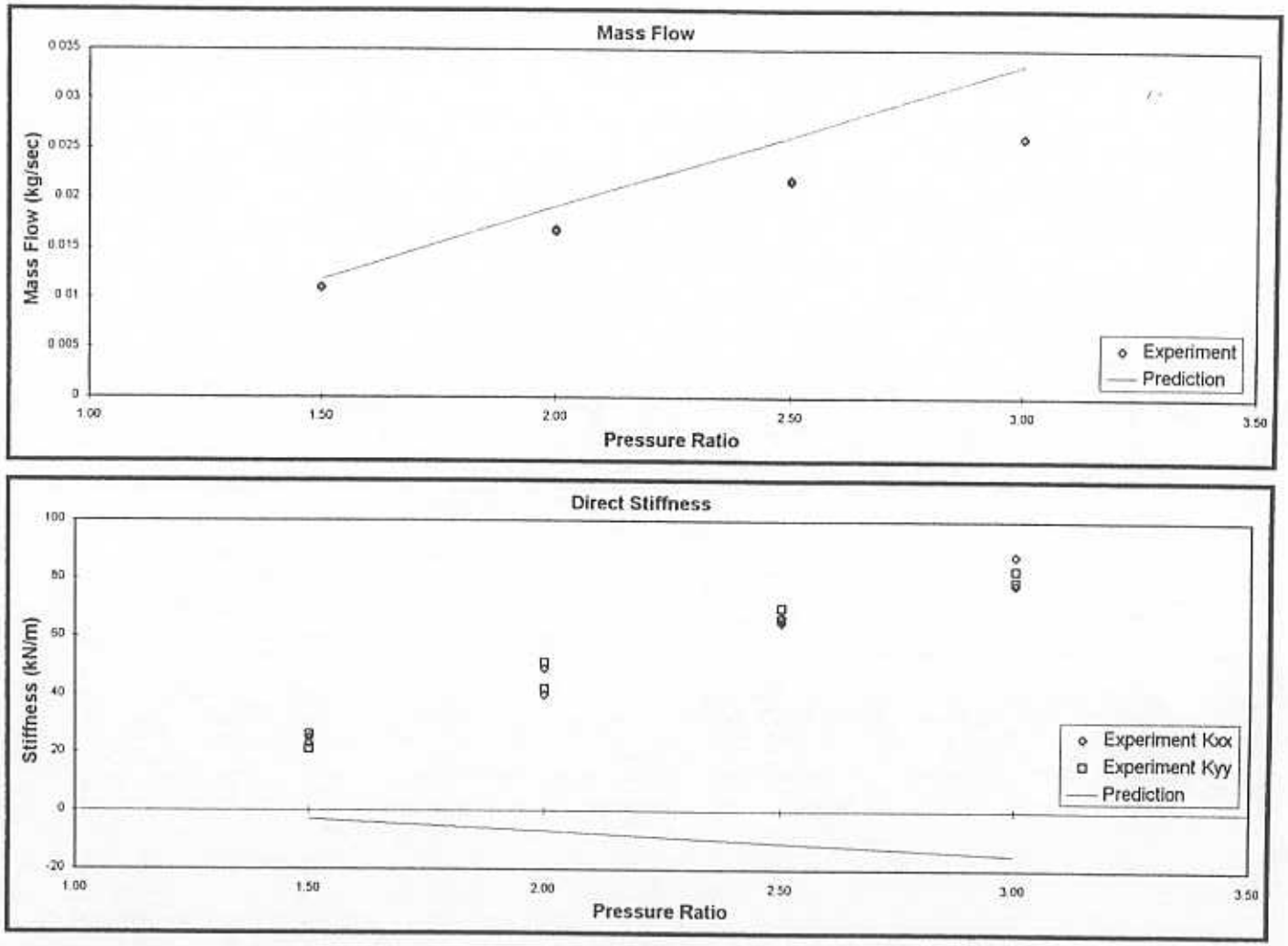

Figure 5 - Labyrinth seal mass flow and direct stiffness coefficients for no journal rotation and varying pressure ratio

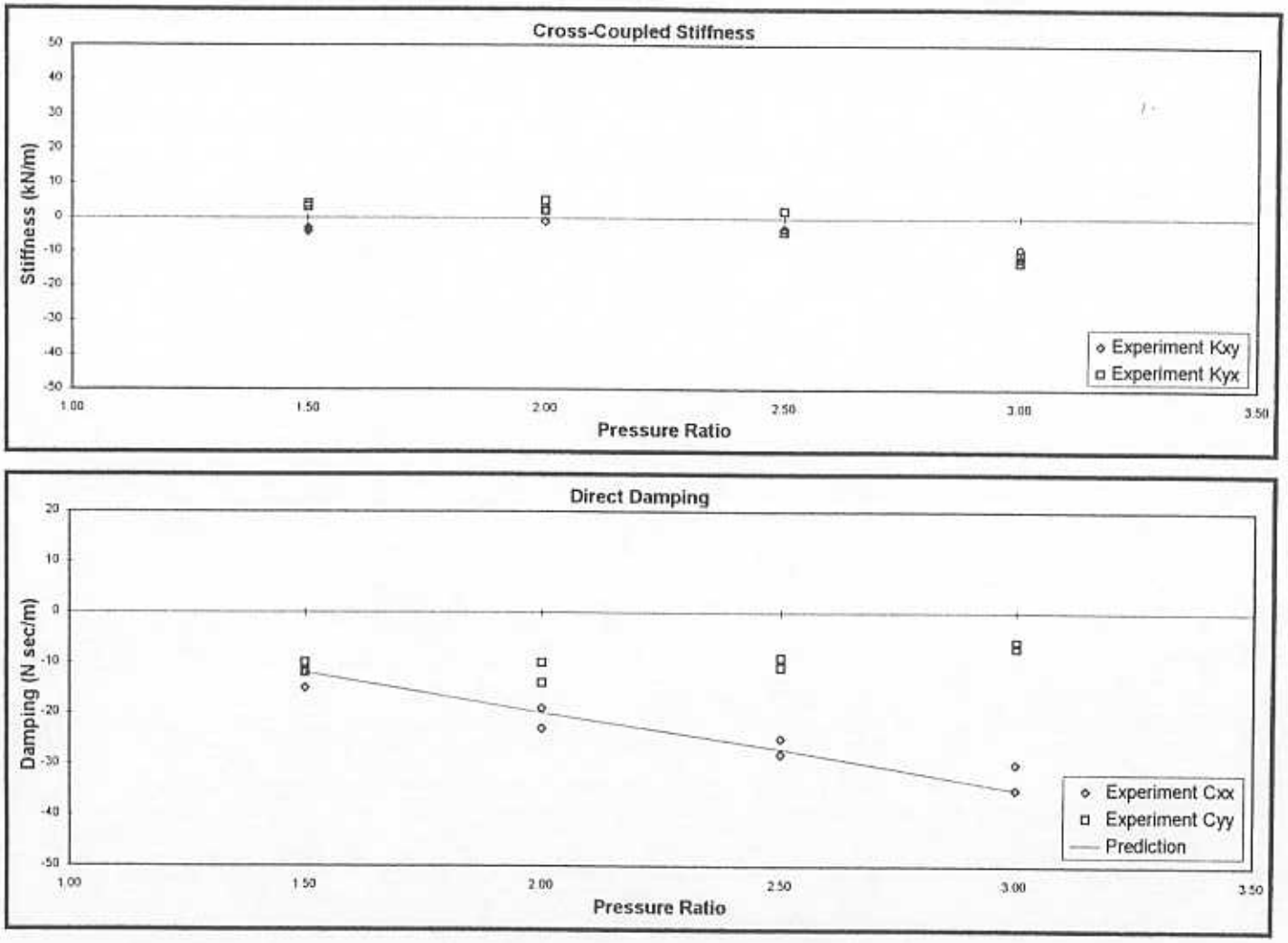

Figure 6 - Labyrinth seal cross-coupled stiffness and direct damping coefficients for no journal rotation and varying pressure ratio

pressure ratio. The direct damping coefficient (C_{XX}) continually becomes more negative with increasing inlet pressure which is demonstrated by predictions as well.

RESULTS AND PREDICTIONS FOR TESTS WITH SHAFT ROTATION TO 1,500 RPM

Test results for journal speed of 1,500 rpm are shown in Figure 7 for mass flow and direct stiffness as functions of pressure ratio. The mass flow measurements are nearly identical to the non-rotating mass flow measurements, and again the predicted values are higher than measured values. Identified direct stiffness coefficients (K_{XX}, K_{YY}) show a trend similar to the non-rotating tests with the exception of a couple scattered points. The direct stiffness becomes more positive with increasing inlet pressure, contrary to the predictions. The values of direct stiffness are approximately 10 kN/m less than the non-rotating tests for all pressure ratios.

Figure 8 shows the cross-coupled stiffness and direct damping coefficients for a journal speed of 1,500 rpm. The cross-coupled stiffness values are widely scattered (within uncertainty) making it difficult to identify a clear trend. The prediction shows K_{XY} to be negative and becoming more negative with increasing pressure ratio. The direct damping coefficients (C_{YY}) are similar to the non-rotating tests except that the damping slightly increases with pressure ratio, having a null value at the highest inlet pressure. The direct damping (C_{XX}) is negative and becomes more so with increasing pressure ratio, agreeing well with predictions.

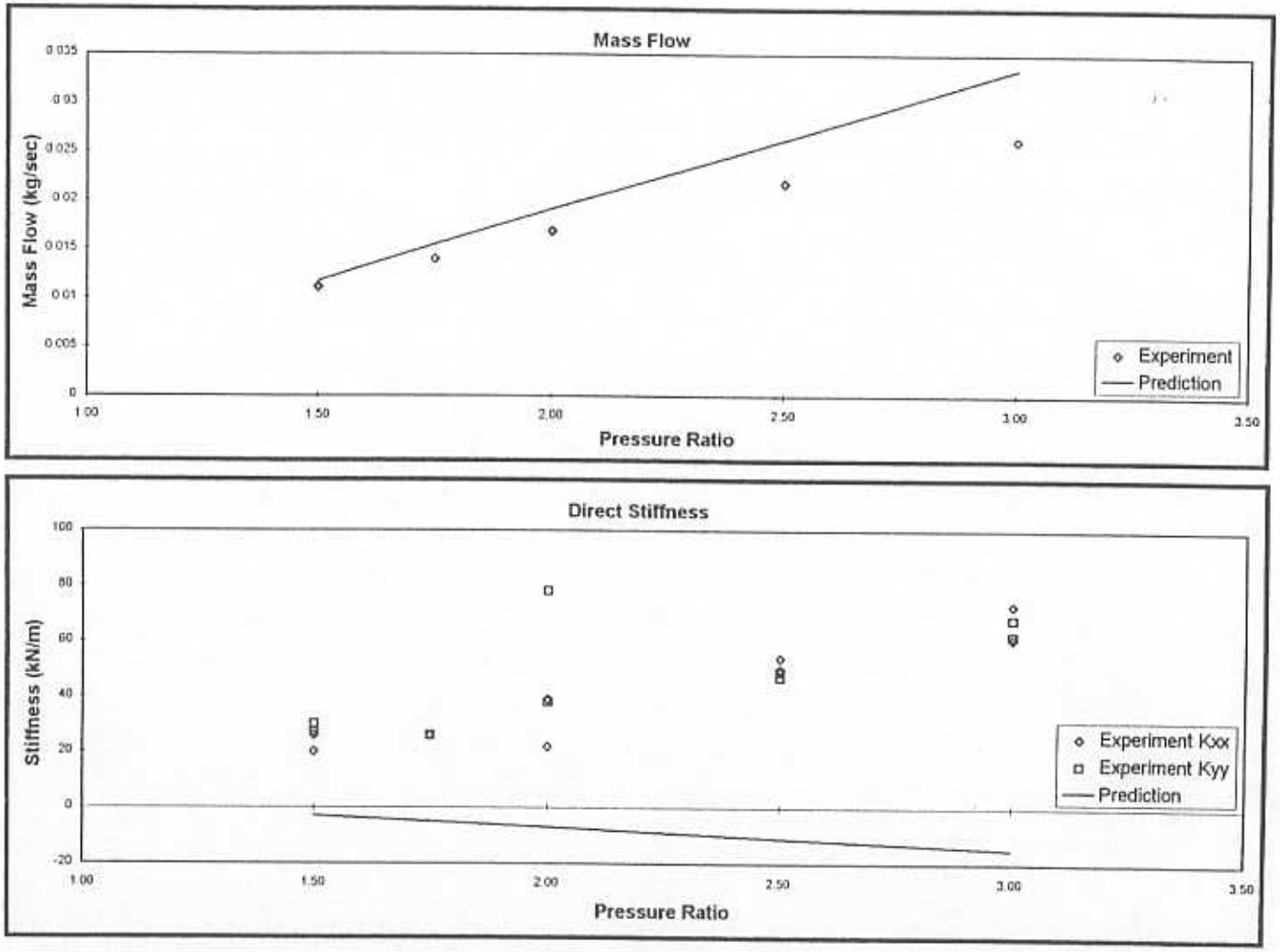

Figure 7 - Labyrinth seal mass flow and direct stiffness coefficients for journal rotation at 1,500 rpm and varying pressure ratio

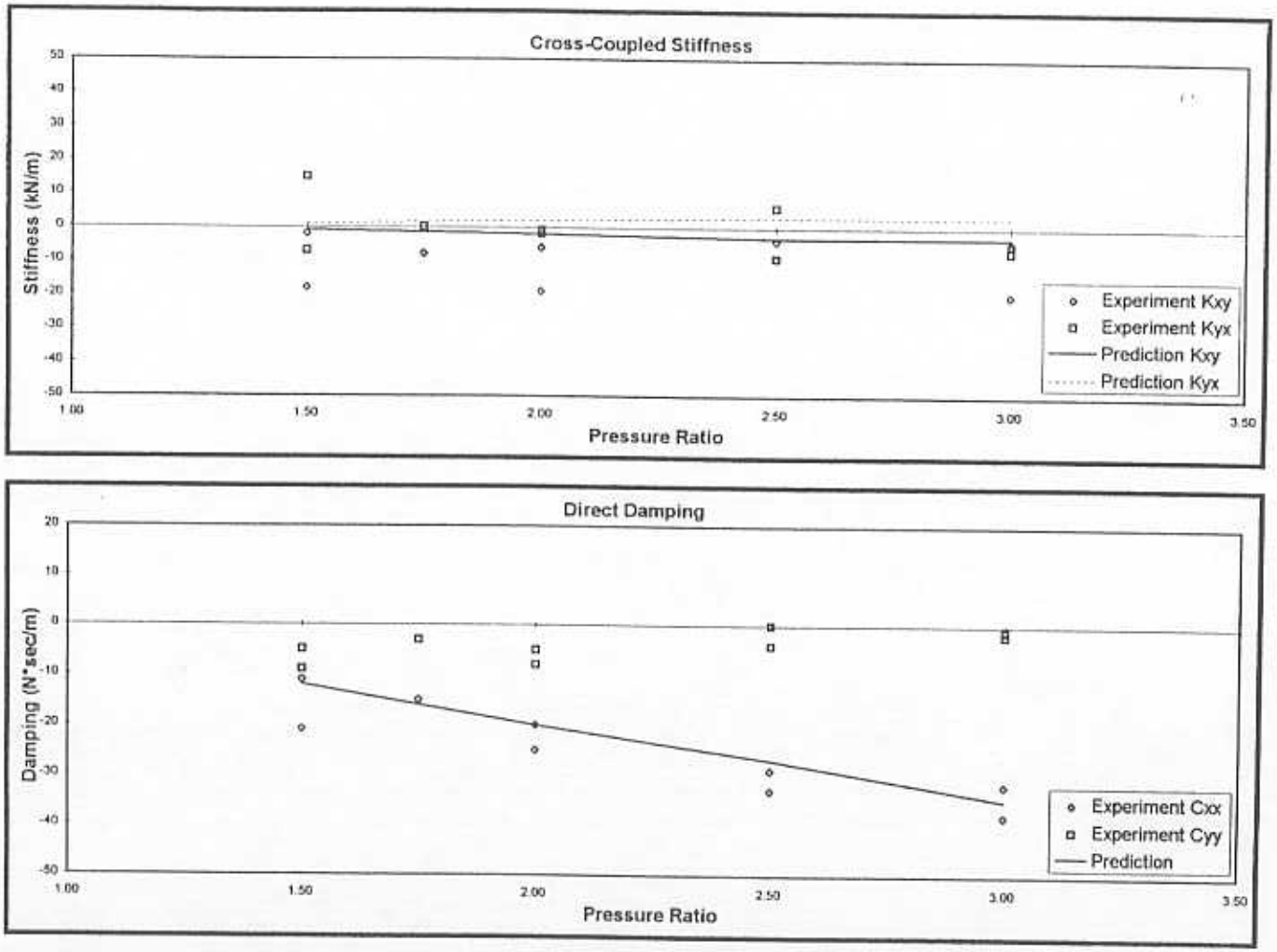

Figure 8 - Labyrinth seal cross-coupled stiffness and direct damping coefficients for journal rotation at 1,500 rpm and varying pressure ratio

RESULTS AND PREDICTIONS FOR TESTS WITH SHAFT ROTATION TO 3,000 RPM

Figure 9 provides the mass flow and direct stiffness measurements for the 3,000 rpm tests. Again, mass flow increases with pressure ratio and is nearly identical to the earlier measurements at 0 and 1,500 rpm. Mass flow rate predictions are higher than measured values. Direct stiffness (K_{XX}, K_{YY}) shows considerably more scatter due to an unusually large synchronous motion but maintains the trend found in the previous tests. Due to the excessive scatter it is difficult to comment on the magnitude of the coefficients in comparison to the previous test conditions.

The cross-coupled stiffness and direct damping values are shown in Figure 10. The cross-coupled stiffness coefficients (K_{XY}, K_{YX}) are even more scattered than the 1,500 rpm results. The direct damping (C_{YY}) continues to behave as in previous tests with the exception that the damping is actually positive at the higher two pressure ratios. The direct damping (C_{XX}) also maintains the same characteristics as in previous tests and becomes increasingly negative with increasing pressure ratio and continues to correlate well with predictions.

TEST SYSTEM TRANSFER FUNCTIONS

Figure 11 shows the direct transfer functions (G_{XX} and G_{YY}) for the non-rotating tests. Each transfer function represents a different pressure ratio. Although the changes are not large, it is easy to see that both the damped natural frequency and the amplitude of vibration are increasing with increasing pressure ratio for the X direction (Figure 11, top). This trend supports the identified coefficients as direct stiffness increases with

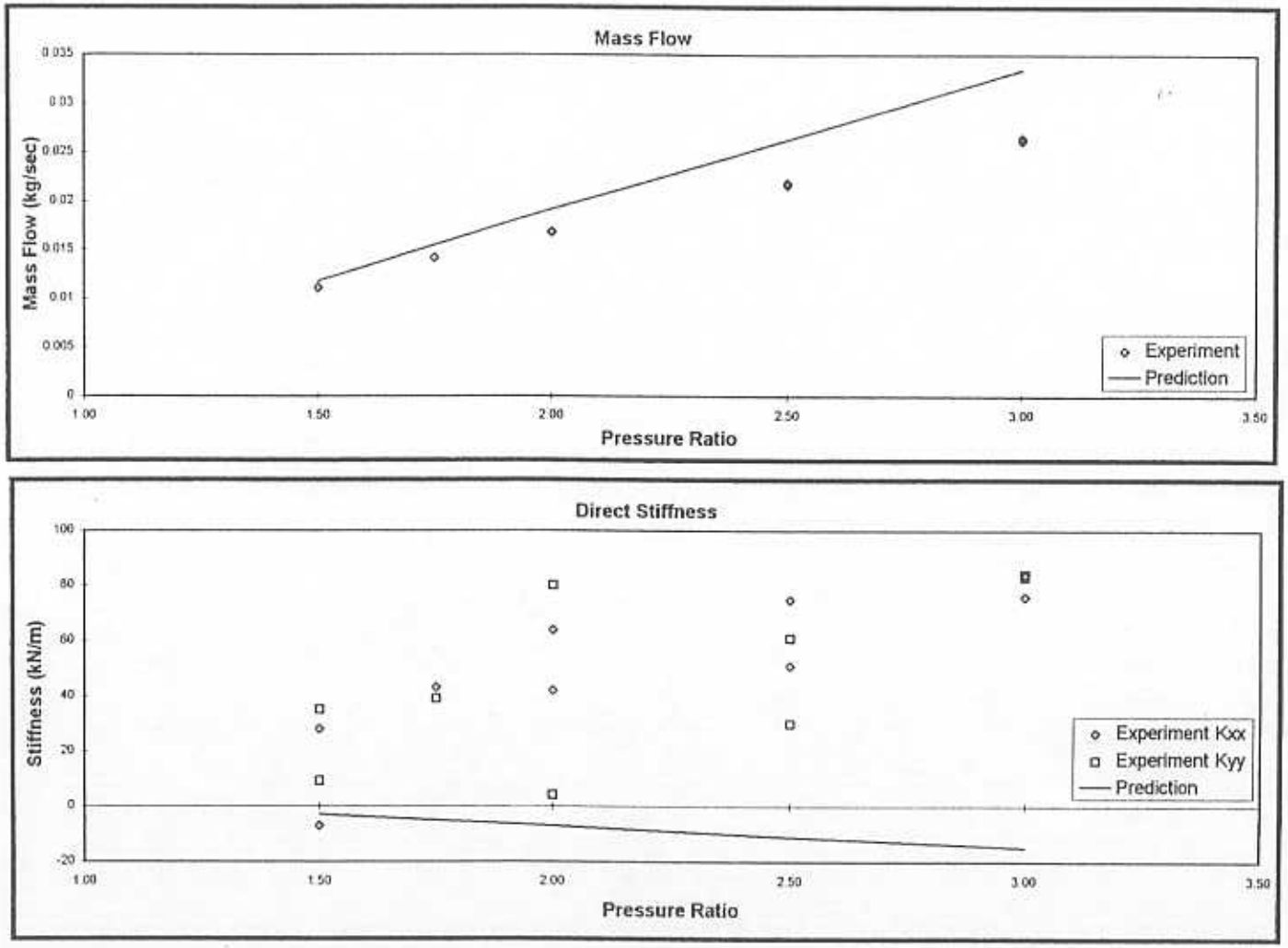

Figure 9 - Labyrinth seal mass flow and direct stiffness coefficients for journal rotation at 3,000 rpm and varying pressure ratio

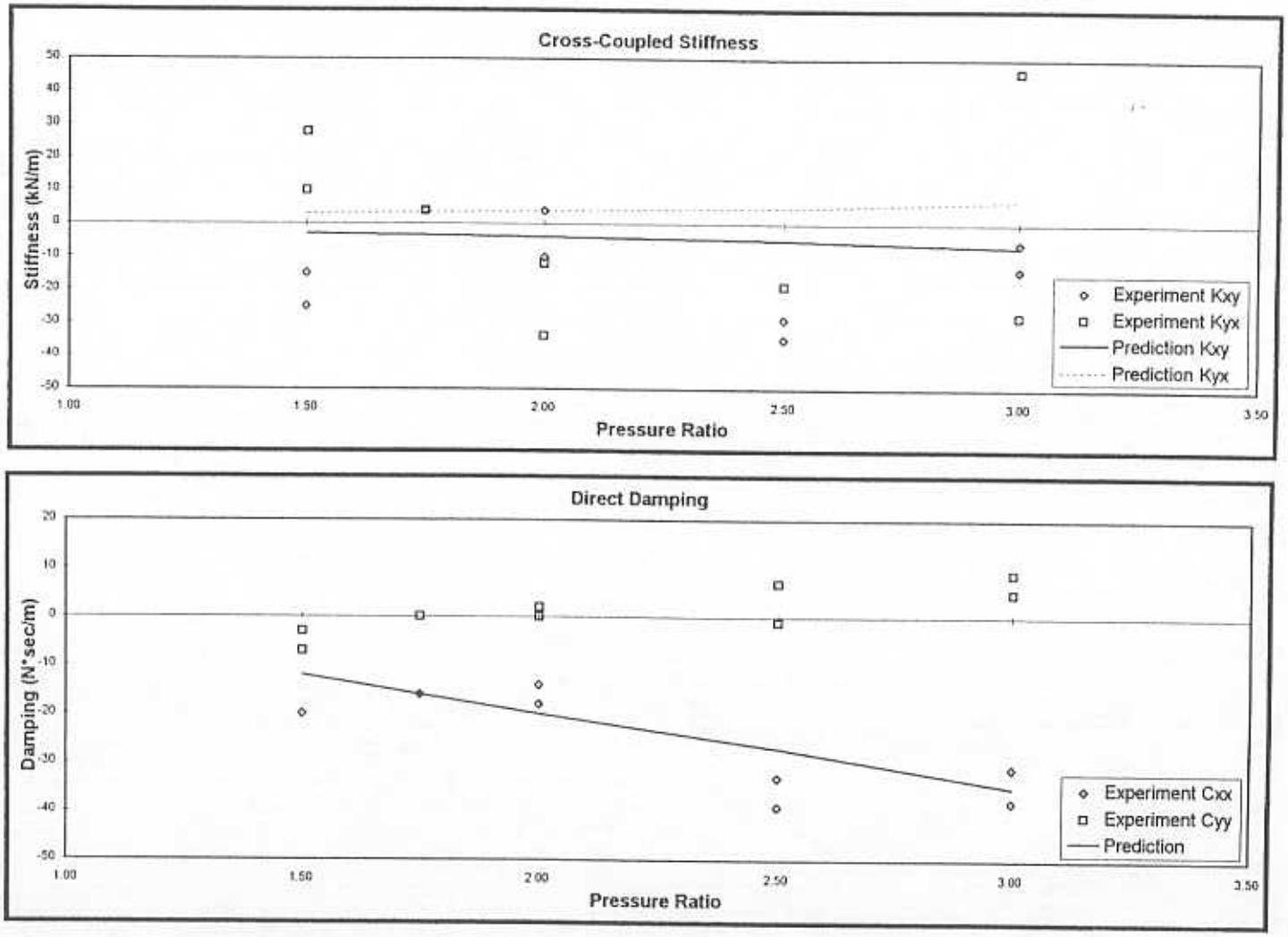

Figure 10 - Labyrinth seal cross-coupled stiffness and direct damping coefficients for journal rotation at 3,000 rpm and varying pressure ratio

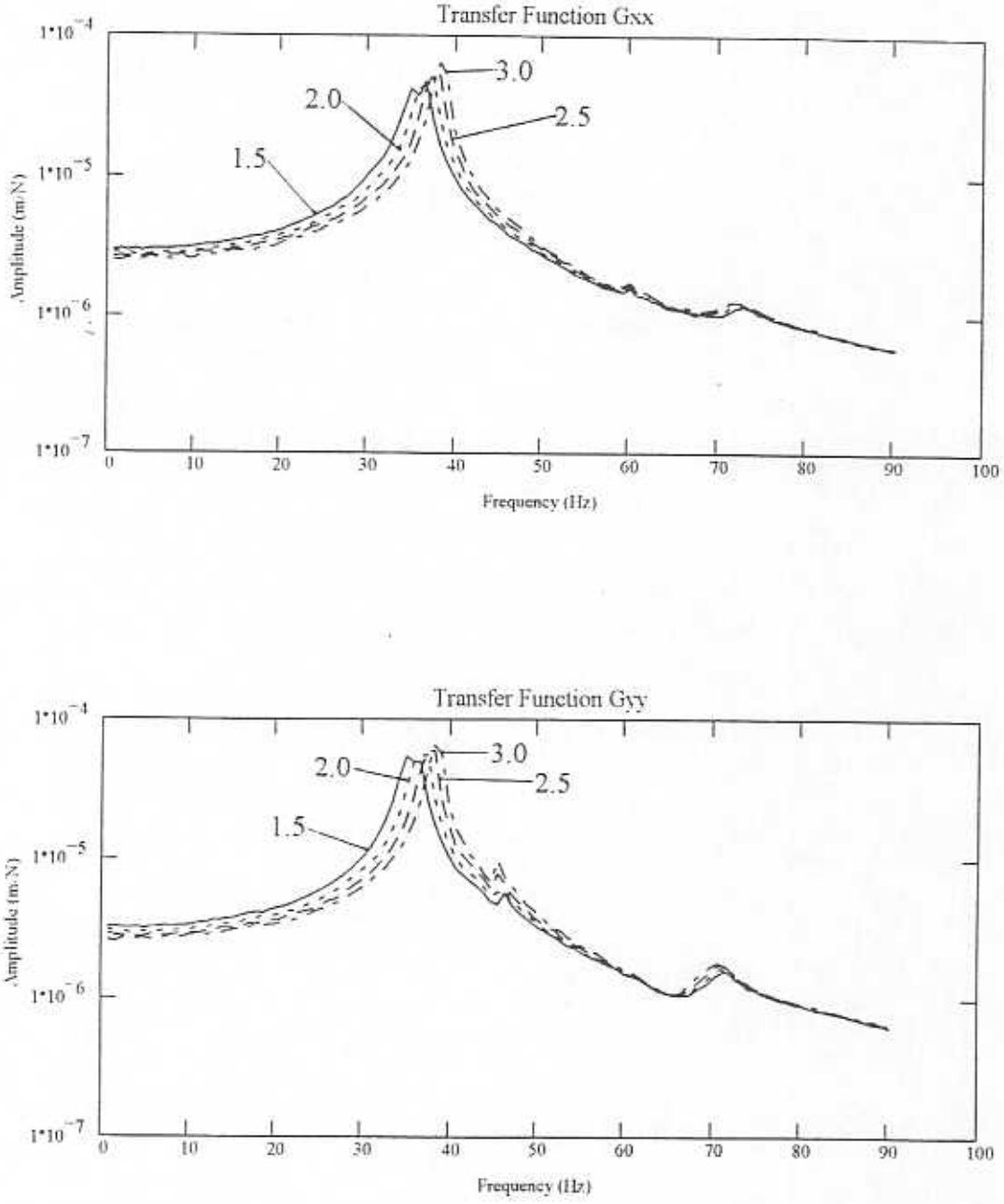

Figure 11 - Labyrinth seal transfer functions for no journal rotation and varying pressure ratios

pressure ratio and direct damping decreases with increasing pressure ratio. In the *Y* direction (Figure 11, bottom) the damped natural frequency also increases with pressure ratio but the increase in amplitude of vibration is not as pronounced as in the *X* direction. This also supports the identified coefficients in that the direct stiffness increases with pressure ratio but direct damping shows very little change with respect to pressure ratio.

The direct transfer functions for the 1,500 rpm tests are shown in Figure 12. The synchronous response due to mechanical runout is seen at 25 Hz. There are also two and three times running speed components. There is also one sub-synchronous response at about 10 Hz. None of the above mentioned responses are related to the impact load as they exist even when the seal is not excited by the impact guns. Despite the steady state excitations, the transfer functions add strength to the identified coefficients as the damped natural frequency and the amplitude both increase with increasing pressure ratio for the *X* direction. The damped natural frequency in the *Y* direction also increases but the amplitude of the response shows very little change with increasing pressure ratio.

The 3,000 rpm transfer functions are shown in Figure 13. The synchronous response due to the mechanical runout is seen at 50 Hz. The next multiple of the running speed is 100 Hz and therefore is not shown. There is a sub-synchronous response which has increased from 10 Hz for the 1,500 rpm tests to 20 Hz for the 3,000 rpm tests. Once again, the *X* direction transfer functions supports the identified coefficients. However, the *Y* direction does not indicate the same increase in damping as is seen in the identified direct damping coefficients. In both cases, the direct stiffness increase is supported by increasing damped natural frequency.

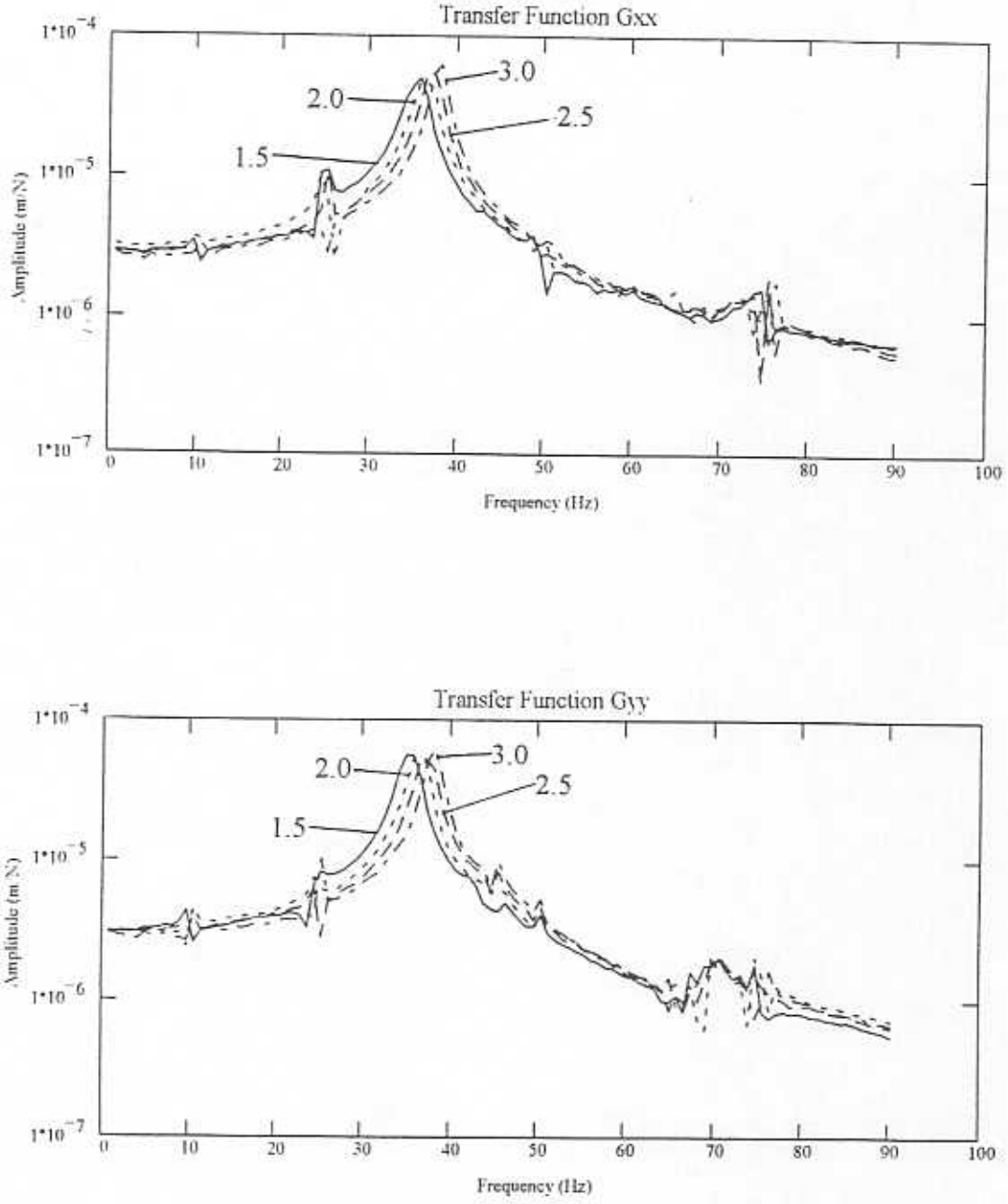

Figure 12 - Labyrinth seal transfer functions for journal rotation at 1,500 rpm and varying pressure ratios

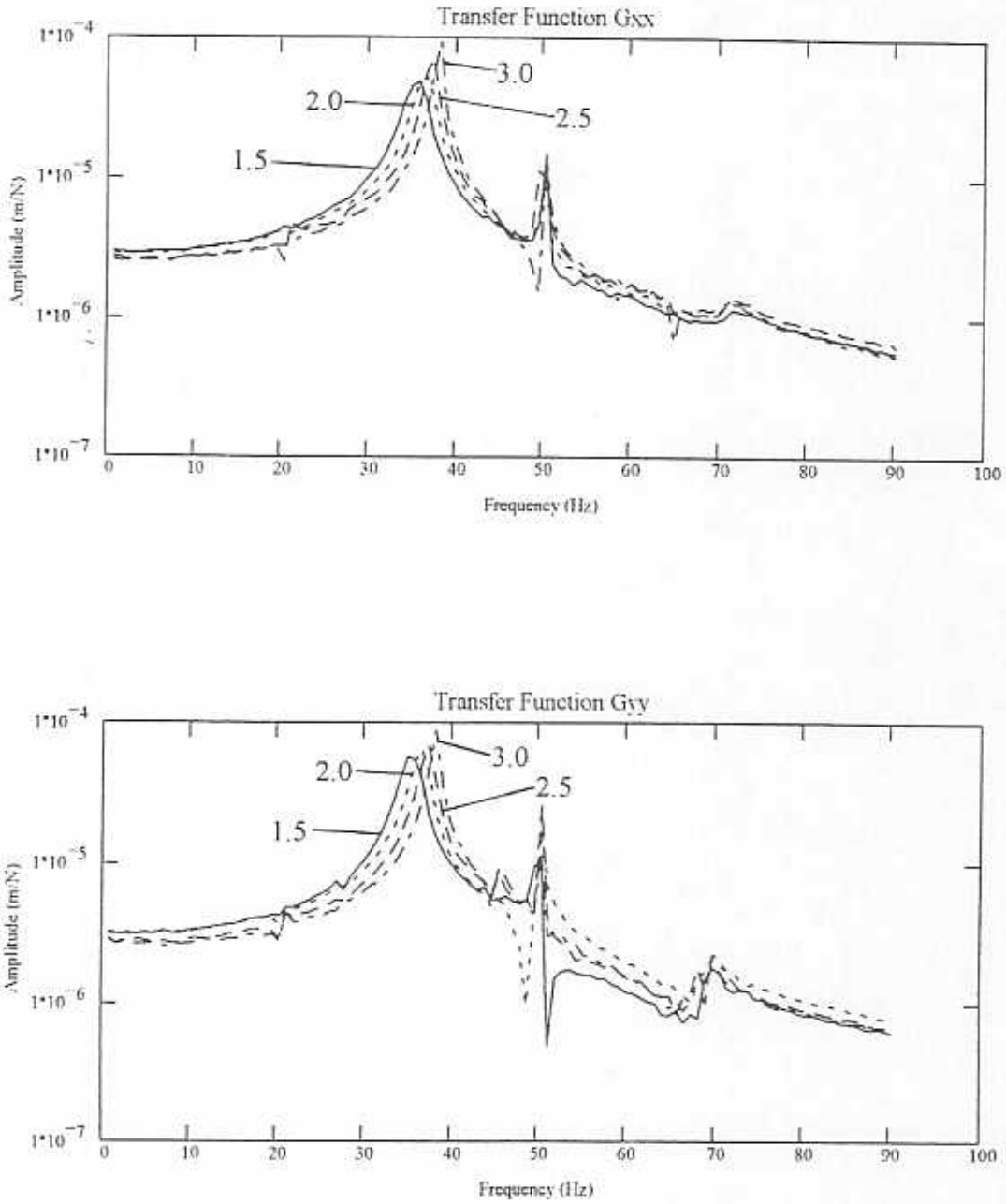

Figure 13 - Labyrinth seal transfer functions for journal rotation at 3,000 rpm and varying pressure ratios

COHERENCE OF EXPERIMENTAL MEASUREMENTS

A sample of measured coherence is provided for each test speed at a pressure ratio of 1.5 in Figures 14 through 19. The coherence does not change noticeably with increasing pressure ratio for any journal speed, so it is not necessary to view all of the results. Figures 14 and 15 show the coherence for all transducers for the non-rotating tests and noted as:

a) X displacement measurement to X impact load

b) Y displacement measurement to X impact load

c) X acceleration measurement to X impact load

d) Y acceleration measurement to X impact load.

The coherence for the X direction displacement and acceleration is excellent for the entire frequency range. The poor coherence at the low frequencies of the accelerometer measurements is due to the instrument limitations. For the Y direction measurements the coherence suggests a weak relationship between the Y motion and the X impact. Figure 15 shows the coherence of all displacement and acceleration transducers with respect to the Y impact. Again, the coherence for the direct motion is excellent for all frequencies. However, the coherence for the indirect motion is very poor for almost all frequencies. This shows of course that cross-coupled terms may be highly inaccurate.

Figures 16 and 17 show the coherence for the 1,500 rpm tests. In all cases the coherence is poor at 10 Hz, 25 Hz, 50 Hz, 75 Hz and 100 Hz. These frequencies correspond to the steady state vibrations induced by shaft rotation. In other words, these motions are not related to the impact load, F_X. The coherence measurements for the

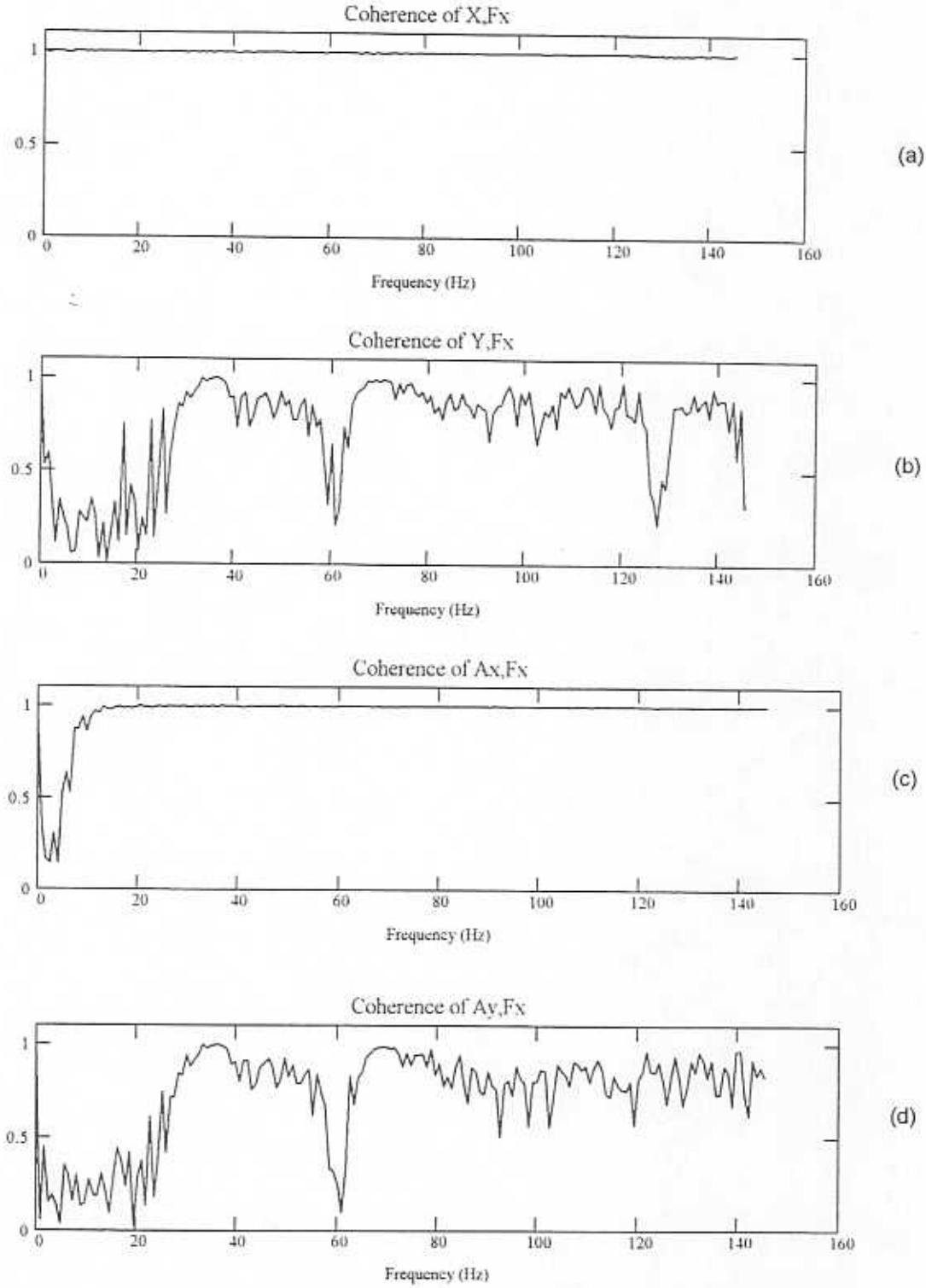

Figure 14 - Labyrinth seal test coherences for no journal rotation and pressure ratio of 1.5 (X Impact)

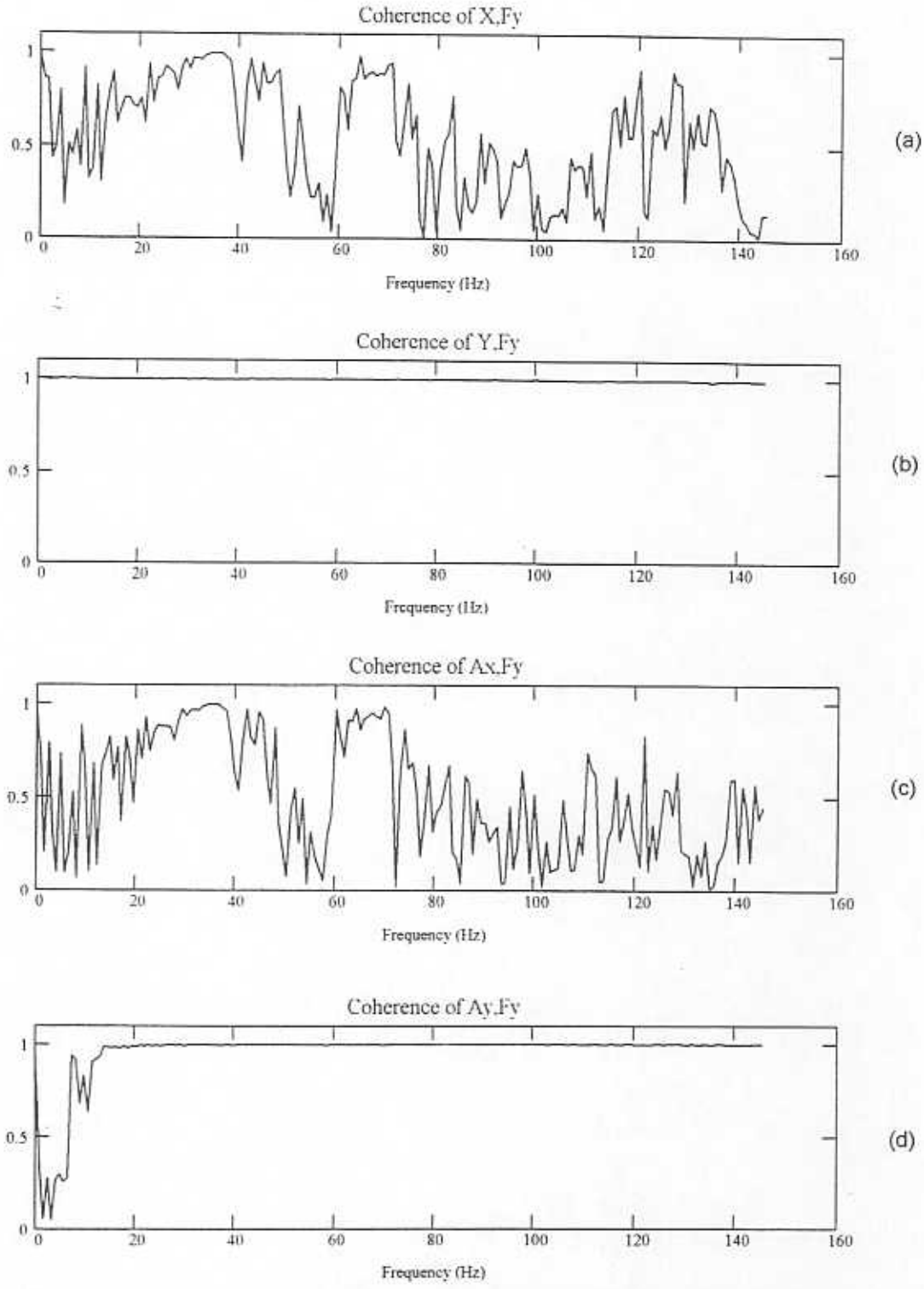

Figure 15 - Labyrinth seal test coherences for no journal rotation and pressure ratio of 1.5 (Y Impact)

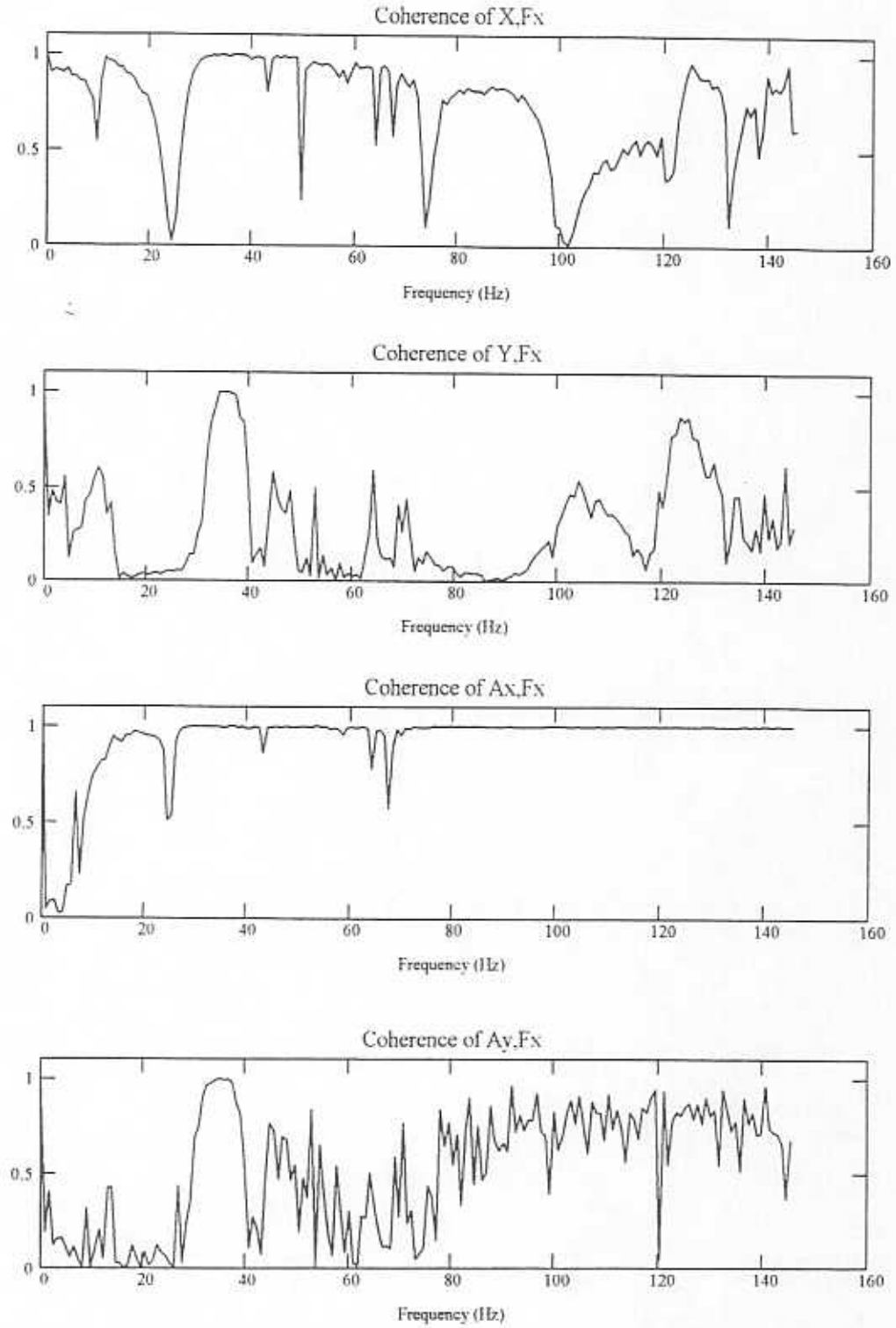

Figure 16 - Labyrinth seal test coherences for journal rotation at 1,500 rpm and pressure ratio of 1.5 (X Impact)

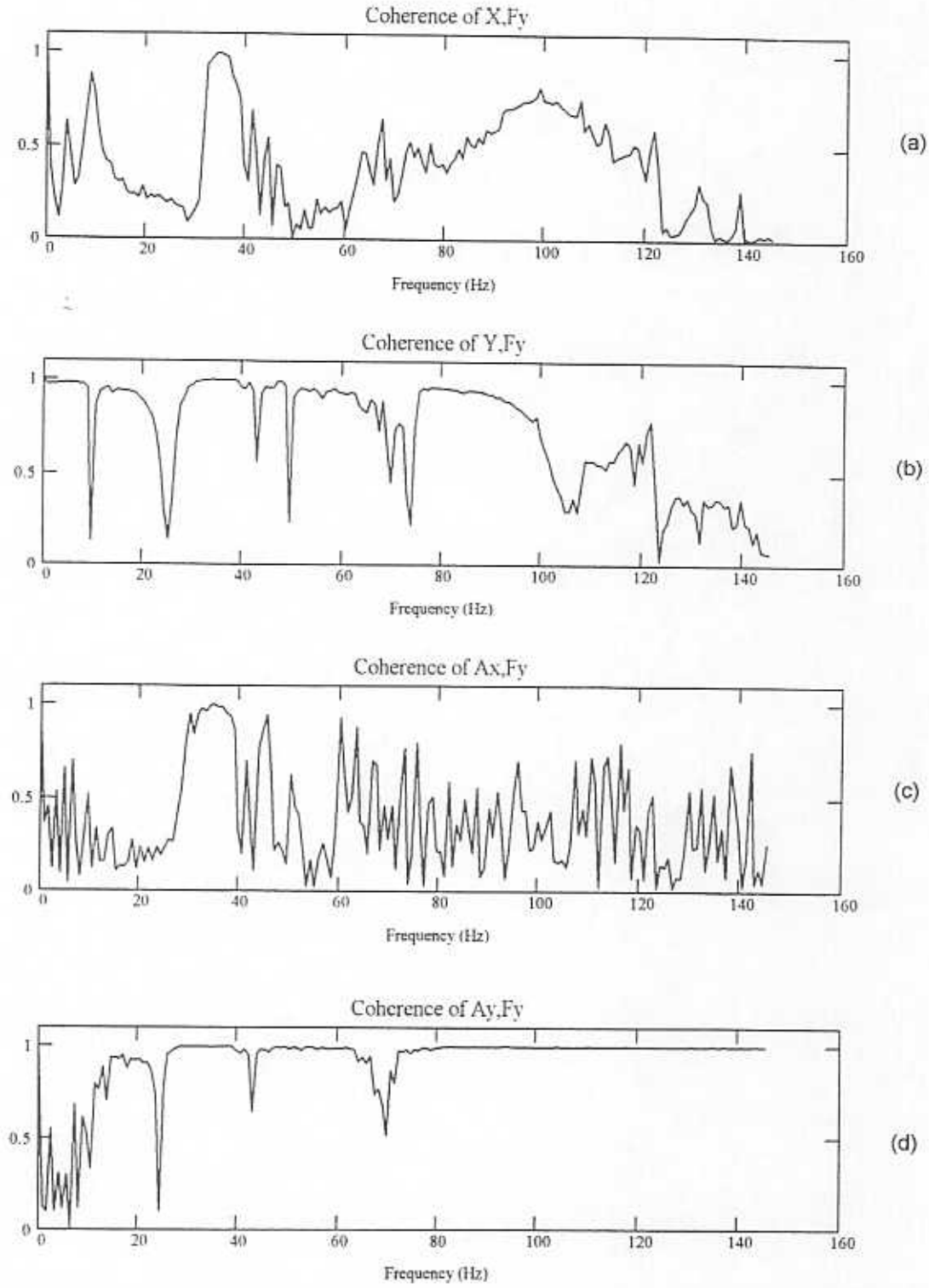

Figure 17 - Labyrinth seal test coherences for journal rotation at 1,500 rpm and pressure ratio of 1.5 (Y Impact)

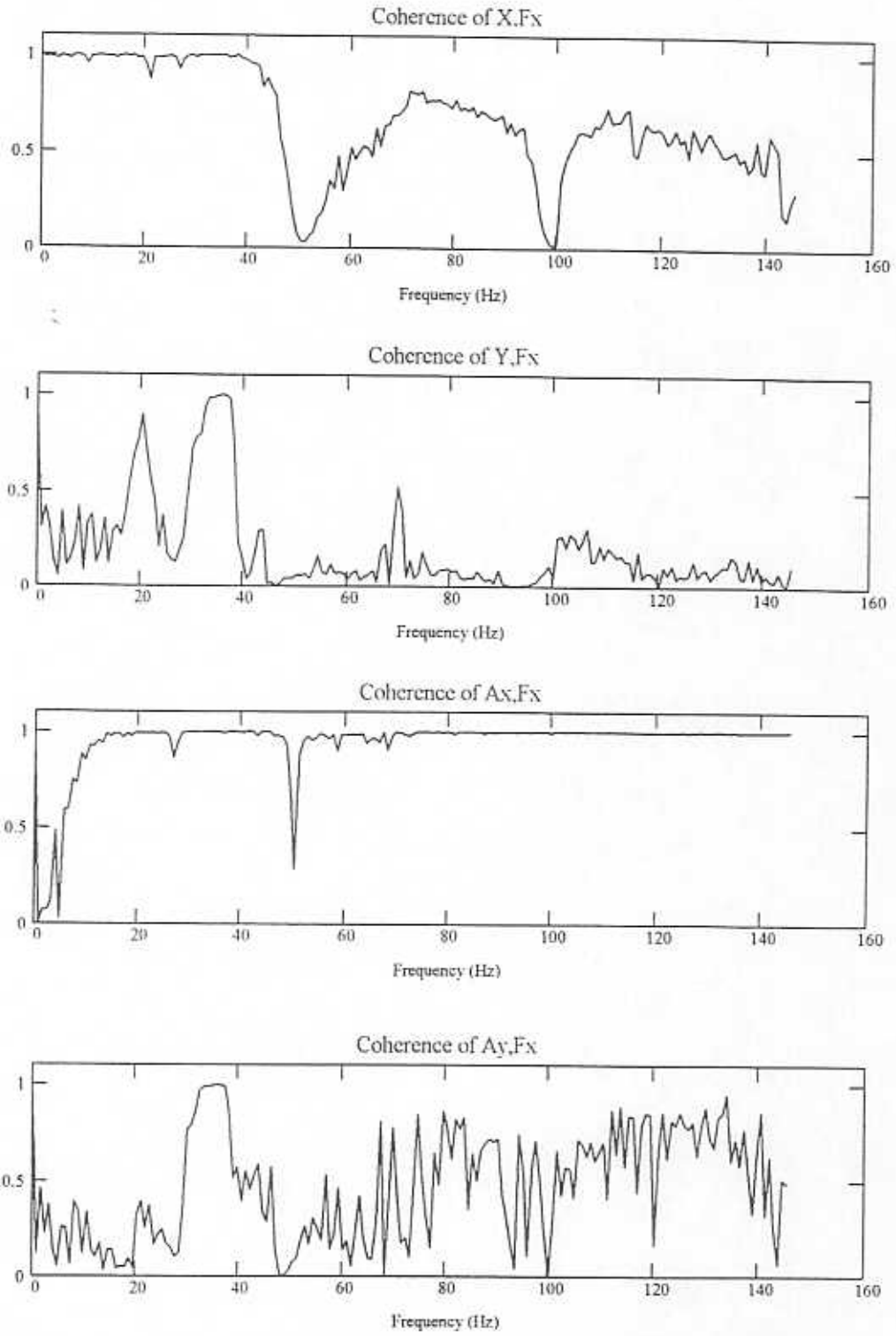

Figure 18 - Labyrinth seal test coherences for journal rotation at 3,000 rpm and pressure ratio of 1.5 (X Impact)

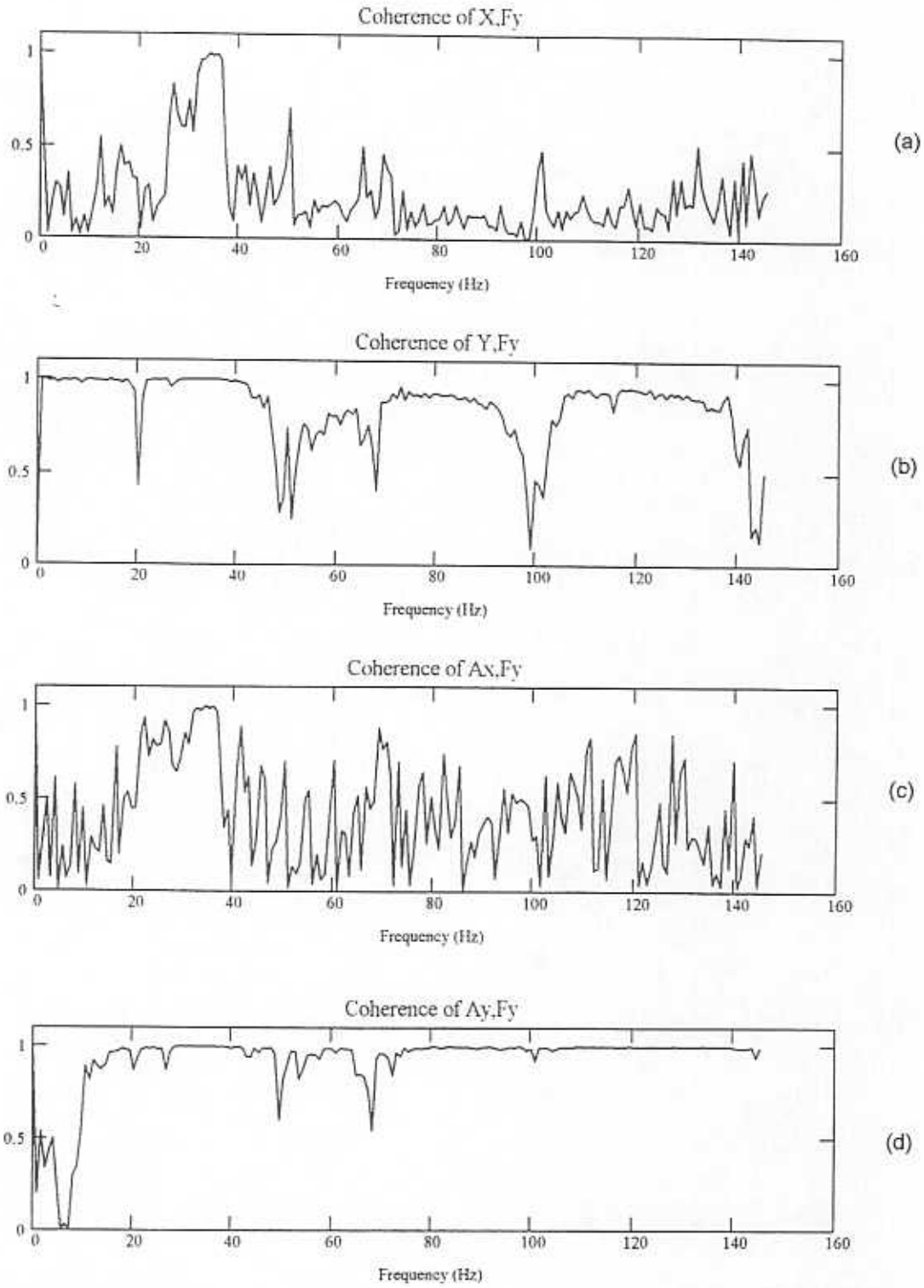

Figure 19 - Labyrinth seal test coherences for journal rotation at 3,000 rpm and pressure ratio of 1.5 (Y Impact)

3,000 rpm tests are given in Figures 18 and 19. The coherence is poor at 50 and 100 Hz, both due to the motion of the journal. For both rotating test speeds, the coherence of the indirect terms is very poor and suggests a weak relationship between impacts and orthogonal motions.

CONCLUSIONS

The following conclusions are made for the two-bladed labyrinth seal (TOS) with diverging clearance tested at 0, 1,500 and 3,000 rpm journal speeds and seal pressure ratios ranging from 1.5 to 3.0. The measured mass flow and all rotordynamic force coefficients are insensitive to shaft rotation except for the increase in scatter of the data. The trends observed in all measured values at 0 rpm are also obvious at 1,500 and 3,000 rpm.

The labyrinth seal has a positive direct stiffness and increases with increasing seal inlet pressure, contrary to predictions. The cross-coupled stiffness is small and difficult to measure with certainty using this facility. No distinct trend is identified due to the scatter in the results. Direct damping C_{XX} is certainly negative and becomes more negative with increasing pressure ratio and agrees well with predictions. For reasons unknown, the C_{YY} coefficient does not present the same behavior. The author suspects asymmetry in the test facility to be the most likely cause of this observation.

A cascade plot of seal displacement response from a speed ramp-up and ramp-down test is presented in Figure 20. As seen in the cascade plot, the seal exhibits a sub-synchronous whirl instability which starts at about 3,700 rpm. With all certainty, it is seen that the two-bladed labyrinth seal with diverging geometry does not exhibit

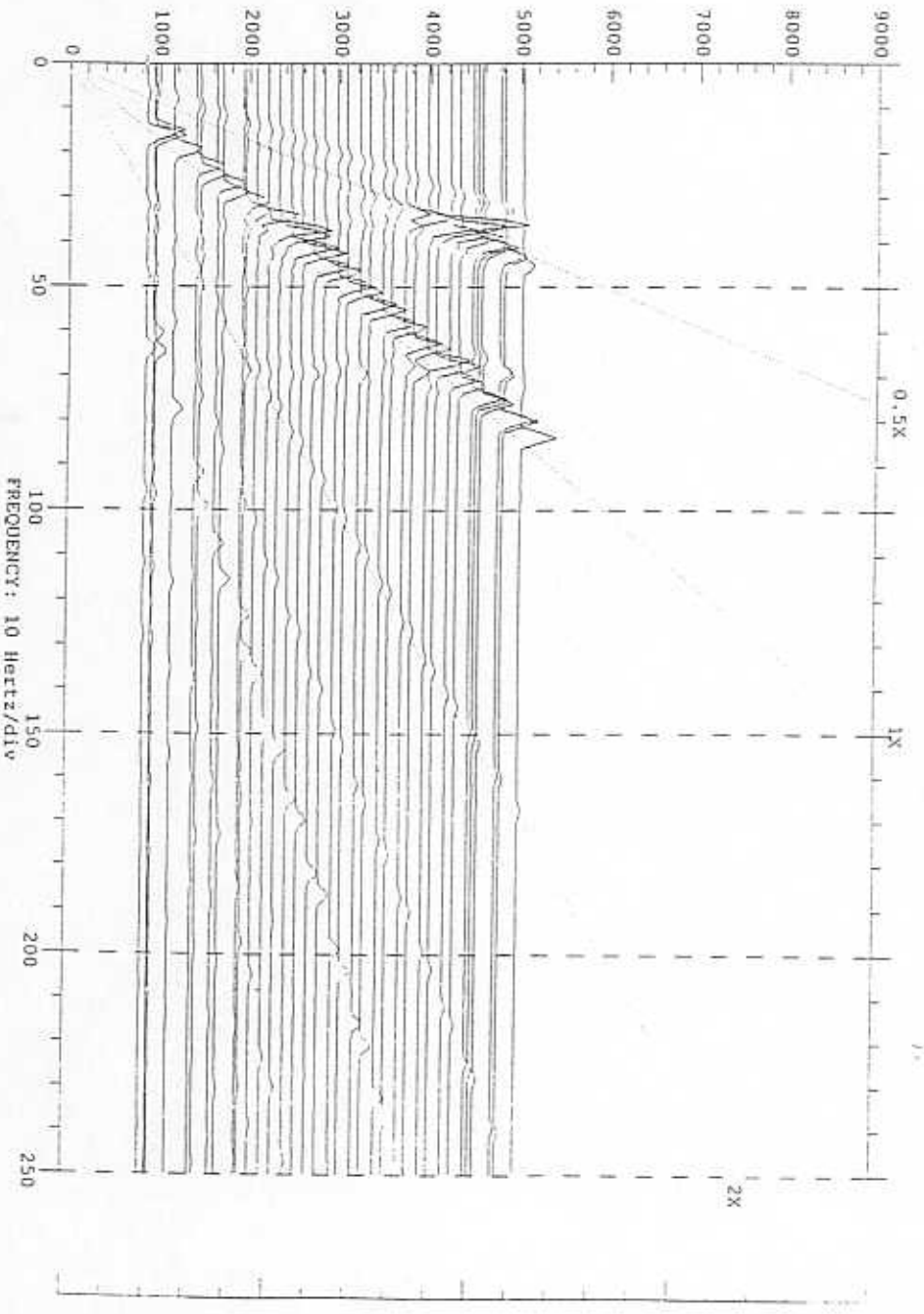

Figure 20 - Labyrinth seal cascade plot of seal displacement for ramp-up and ramp-down test

significant positive damping and becomes less stable with increasing pressure ratio across the seal.

DAMPER SEAL TEST RESULTS

Next the labyrinth seal is altered and tested as a pocket damper seal. The modification involves insertion of four partition walls into the labyrinth deep groove dividing it into four cavities of equal size. As with the labyrinth seal, the base stiffness, mass and damping coefficients are identified before any tests are conducted with an active seal (Table 8). In an effort to increase the direct stiffness of the structure, the added rubber inserts are moved further down the support rods so that they contribute more to the structural properties. This allows seal testing at a pressure ratio of 2.0, whereas without the added stiffness tests above a pressure ratio of 1.5 are not possible.

Table 8 - Base stiffness, mass and damping from seal/housing structure for damper seal tests

Parameter	Value	Uncertainty
K_{hXX}	608 kN/m (3478 lb/in)	6.0 kN/m (34 lb/in)
K_{hXY}	-22 kN/m (-126 lb/in)	0.5 kN/m (3 lb/in)
K_{hYX}	-23 kN/m (-132 lb/in)	0.5 kN/m (3 lb/in)
K_{hYY}	607 kN/m (3472 lb/in)	6.0 kN/m (34 lb/in)
C_{hXX}	463 N sec/m (2.65 lb sec/in)	3.0 N sec/m (0.02 lb sec/in)
C_{hXY}	38 N sec/m (0.22 lb sec/in)	0.5 N sec/m (0.00 lb sec/in)
C_{hYX}	36 N sec/m (0.21 lb sec/in)	0.5 N sec/m (0.00 lb sec/in)
C_{hYY}	373 N sec/m (2.14 lb sec/in)	3.0 N sec/m (0.02 lb sec/in)
M_{hXX}	6.5 kg (14.3 lb)	0.2 kg (0.4 lb)
M_{hXY}	0.0 kg (0.0 lb)	0.2 kg (0.4 lb)
M_{hYX}	0.0 kg (0.0 lb)	0.2 kg (0.4 lb)
M_{hYY}	6.3 kg (13.9 lb)	0.2 kg (0.4 lb)
ω_X	48.7 Hz	0.8 Hz
ω_Y	49.4 Hz	0.8 Hz

The damper seal is tested at journal speeds of 0, 1,500 and 3,000 rpm and pressure ratios of 1.5 and 2.0. For a pressure ratio higher than 2.0, the negative direct stiffness of the

damper seal overcomes the base direct stiffness (Table 8) causing the seal to suck against the journal. It is not possible to perform the impact testing due to this static instability.

Identified damper seal coefficients for centered condition and all test conditions are listed in Table 9. The base coefficients described previously are subtracted so that the values listed in the table are contributions of the active damper seal only. The correlation between the experimental transfer function and the curve fit is also listed in Table 9. All the direct transfer functions have high correlation (well into the 0.9 region). The correlation for all the indirect transfer functions is very poor indicating that the measured parameters do not represent the real system accurately. Therefore, either the parameter identification method is not working properly or the damper seal does not produce any significant cross-coupled forces. The later is most likely since the seal does not exhibit any cross-coupled behavior during testing. For this reason, test cross-coupled stiffness and cross-coupled damping terms are not discussed any further for the damper seal. For reference, APPENDIX E shows typical time traces of load, displacement and acceleration transducers for damper seal tests. Also included are samples of curve fit transfer functions as they compare to test data.

Table 10 lists values for inlet air temperature, seal top temperature, seal bottom temperature, roller bearing lubricant discharge temperature, air pressure before flow meters, air pressure after flow meters, seal inlet air pressure, plenum pocket pressure, mass flow as measured with the turbine type flow meter, axial flow Reynolds number and seal inlet Mach number. All of the temperatures are listed in degrees Celsius and the pressures listed are gauge, not absolute.

Table 9 - Identified damper seal force coefficients and correlations (centered condition)

Speed (RPM)	Pressure Ratio	K_{XX} (kN/m)	K_{XY} (kN/m)	K_{YX} (kN/m)	K_{YY} (kN/m)	C_{XX} (N sec/m)	C_{XY} (N sec/m)	C_{YX} (N sec/m)	C_{YY} (N sec/m)	$Corr_{XX}$	$Corr_{XY}$	$Corr_{YX}$	$Corr_{YY}$
0	1.50	-88	-1	-1	-117	44	4	13	102	0.95	0.85	0.79	0.96
	1.50	-70	-2	0	-92	64	3	13	117	0.93	0.83	0.80	0.95
	2.00	-206	8	8	-132	186	-13	-4	261	0.94	0.52	0.49	0.96
	2.00	-190	8	4	-216	196	-6	1	261	0.94	0.61	0.59	0.97
1,500	1.50	-106	-41	-35	-111	74	-11	4	107	0.92	0.67	0.43	0.94
	1.50	-71	-10	11	-108	43	-7	15	124	0.94	0.67	0.69	0.95
	2.00	-231	4	9	-259	277	5	11	367	0.94	0.28	0.25	0.95
	2.00	-199	2	0	-258	200	-6	34	357	0.94	0.54	0.52	0.96
3,000	1.50	-81	3	7	-143	25	-16	-4	127	0.95	0.62	0.67	0.95
	1.50	-105	4	6	-139	63	-5	30	121	0.95	0.74	0.83	0.96
	2.00	-230	9	3	-243	266	-8	38	234	0.95	0.37	0.44	0.97
	2.00	-208	11	5	-258	208	13	12	279	0.94	0.51	0.56	0.97

* Maximum uncertainties for stiffness and damping coefficients are 6 kN/m and 3 N sec/m respectively

Table 10 - Temperatures, pressures, mass flow, axial Reynolds number and seal inlet Mach number for damper seal tests (centered condition)

Speed (RPM)	Pressure Ratio	T_1 (C)	T_2 (C)	T_3 (C)	T_4 (C)	P_1 (KPa)	P_2 (KPa)	P_3 (KPa)	P_4 (KPa)	$\dot{m}$ (kg/sec)	Re_{axial}	Ma_{inlet}
0	1.50	23	23	23	23	655	621	51	12	0.0113	1,567	0.352
	1.50	23	23	23	23	655	621	51	13	0.0117	1,632	0.366
	2.00	23	23	23	23	655	607	101	19	0.0173	2,404	0.405
	2.00	23	23	23	23	655	607	101	19	0.0173	2,409	0.406
1,500	1.50	21	23	24	33	655	621	51	12	0.0117	1,627	0.365
	1.50	21	22	23	27	655	621	51	12	0.0115	1,605	0.360
	2.00	21	22	23	26	655	607	101	19	0.0173	2,404	0.405
	2.00	21	23	23	30	655	607	101	19	0.0172	2,393	0.403
3,000	1.50	21	23	24	34	655	621	51	12	0.0117	1,627	0.365
	1.50	21	23	24	37	655	621	51	12	0.0116	1,610	0.361
	2.00	21	23	24	34	655	607	101	18	0.0171	2,387	0.402
	2.00	21	23	24	35	655	607	101	19	0.0172	2,393	0.403

RESULTS AND PREDICTIONS FOR TESTS WITHOUT SHAFT ROTATION

Predicted and measured mass flow, direct stiffness and direct damping coefficients for non-rotating damper seal tests are shown in Figure 21. Predictions are based on Li et al.'s (1997) analysis for no fluid pre-swirl and excitation frequency of 37 Hz. It is noted that the damper seal predictions are only preliminary as the analysis code is still in the development phase. Mass flow measurements for the damper seal are about three percent higher than the labyrinth seal measurements and the predicted mass flow is still too high for a pressure ratio of 2.0. Experimentally identified direct stiffness' (K_{XX}, K_{YY}) agree well with predicted values having a negative value at a pressure ratio of 1.5 and becoming more negative with an increase in pressure ratio. Both experimental and predicted direct damping coefficients are positive and increase with inlet pressure. Although not shown, the theory predicts a cross-coupled stiffness (K_{XY}) of about 1 kN/m at a pressure ratio of 1.5 for the non-rotating tests. As mentioned previously, experimental results indicate that cross-coupling is not present in the damper seal.

RESULTS AND PREDICTIONS FOR TESTS WITH SHAFT ROTATION TO 1,500 RPM

Figure 22 shows the test results for the 1,500 rpm measurements. The mass flow continues to be about three percent larger than labyrinth seal measurements and is over-predicted by theory. Direct stiffness is negative and becomes more negative with the increase in inlet pressure. Prediction shows the same trend except with a higher magnitude of stiffness. Direct damping is positive and raises with an increase in inlet pressure. There is some scatter in the damping coefficients but the trend is clear. Unlike

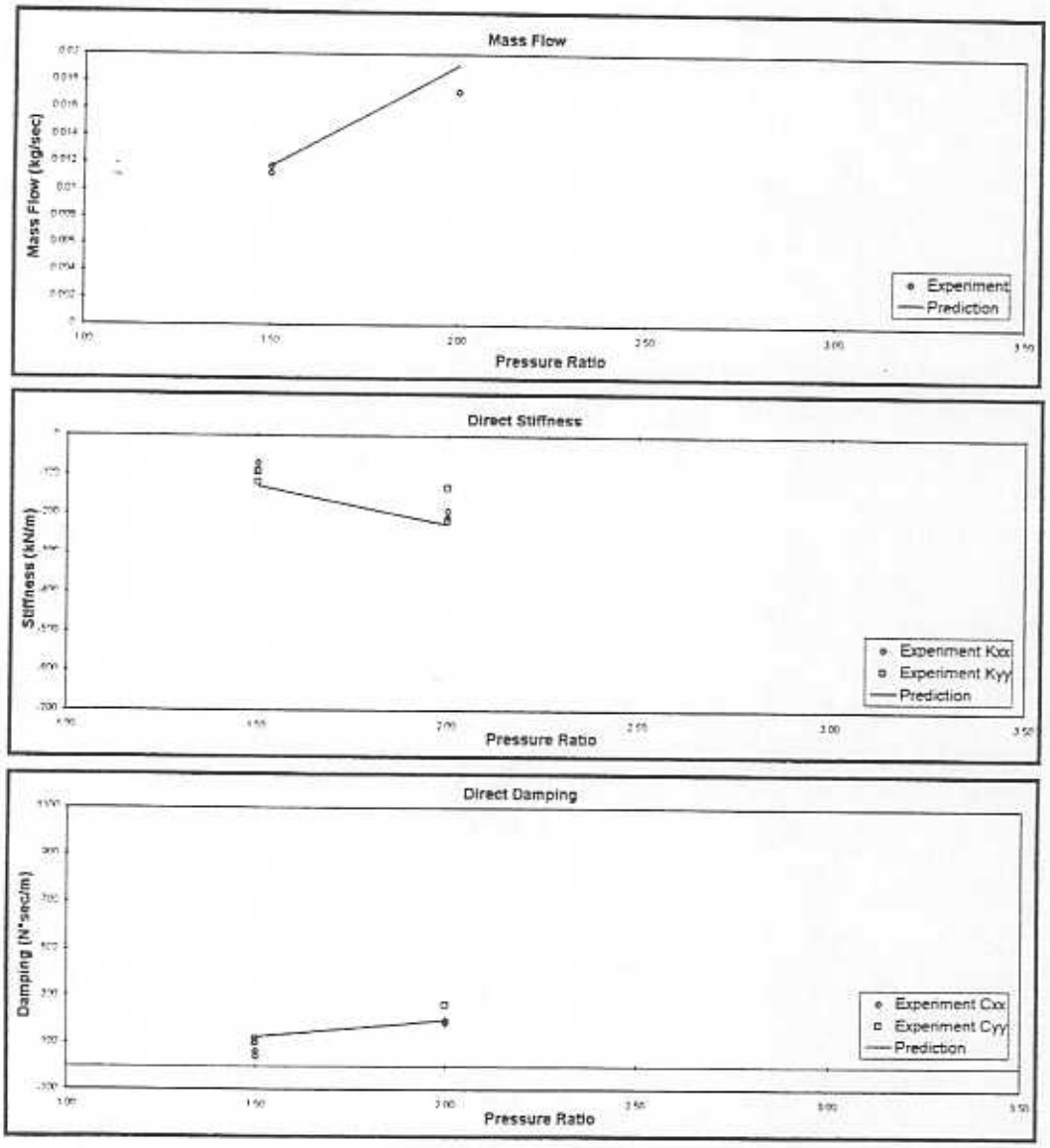

Figure 21 - Damper seal mass flow, direct stiffness and direct damping coefficients for no journal rotation and varying pressure ratio

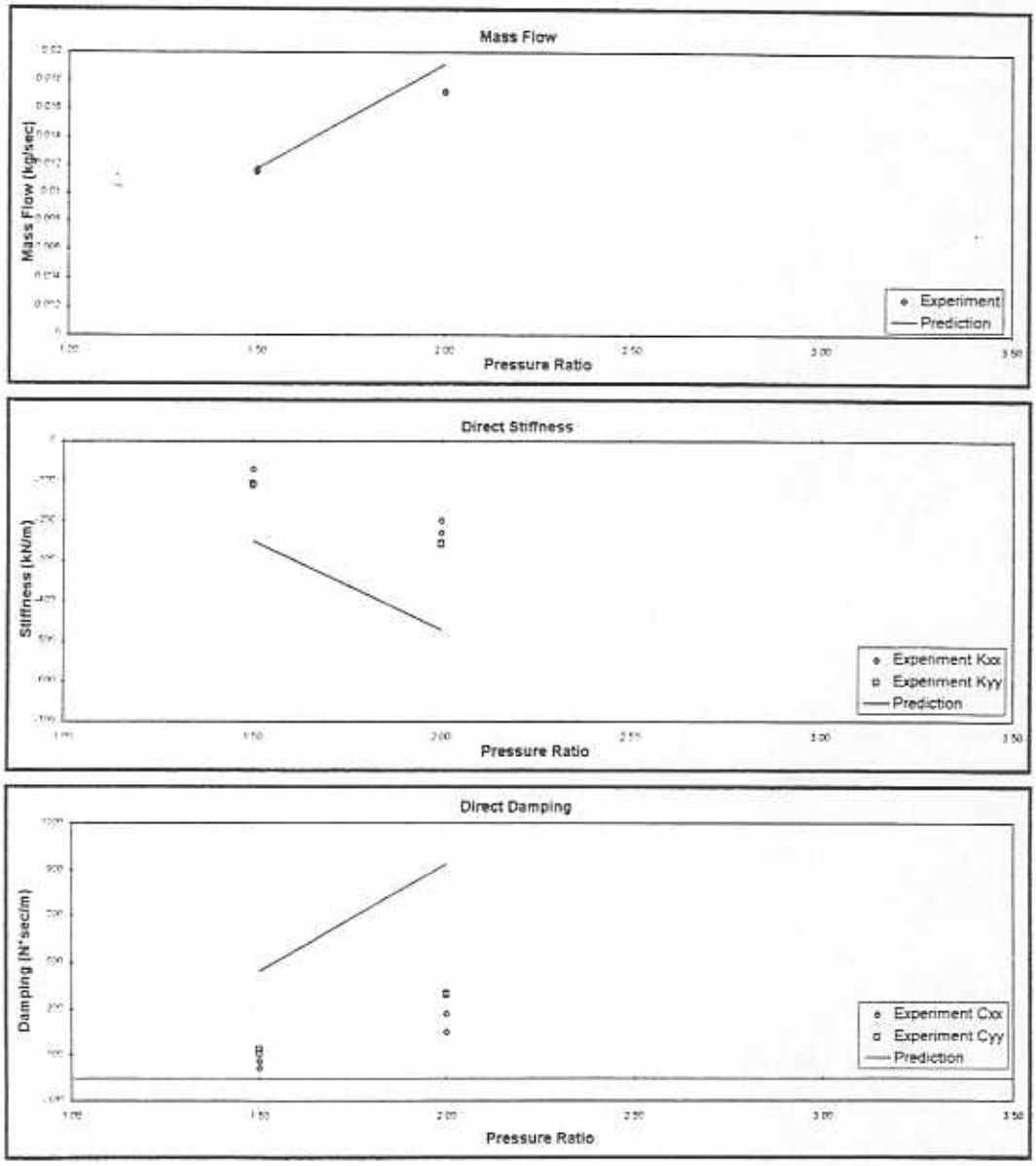

Figure 22 - Damper seal mass flow, direct stiffness and direct damping coefficients for journal rotation at 1,500 rpm and varying pressure ratio

the non-rotating test predictions, the direct damping is severely over-predicted. Predictions show the seal to have a cross-coupled stiffness (K_{XY}) of about 10 kN/m at a pressure ratio of 1.5 and 14 kN/m at a pressure ratio of 2.0 for a journal speed of 1,500 rpm. This is not observed in the experimental results.

RESULTS AND PREDICTIONS FOR TESTS WITH SHAFT ROTATION TO 3,000 RPM

The 3,000 rpm test results are presented in Figure 23. The mass flow measurements are consistent with the previous two sets of damper seal results. Experimental values of direct stiffness coefficients are much smaller in magnitude than indicated predictions for this journal speed. Direct damping coefficients demonstrate the same trend as in previous tests but are severely over-predicted by theory. Predictions for cross-coupled stiffness (K_{XY}) at 3,000 rpm are much larger than for the previous journal speeds (19 kN/m at pressure ratio of 1.5 and 26 kN/m at pressure ratio of 2.0) despite the lack of any observed cross-coupled behavior on the test seal.

TEST SYSTEM TRANSFER FUNCTIONS

The direct transfer functions (G_{XX} and G_{YY}) for the non-rotating damper seal tests are presented in Figure 24. The damped natural frequency of the seal and housing is shown to be around 40 Hz. There is an additional response at about 75 Hz which is much smaller in magnitude and is found to be the natural frequency of the support structure from which the seal is suspended. This frequency does not appear in the labyrinth seal tests because the connection between the seal housing and the support structure is much more flexible. However, in order to counter the negative direct

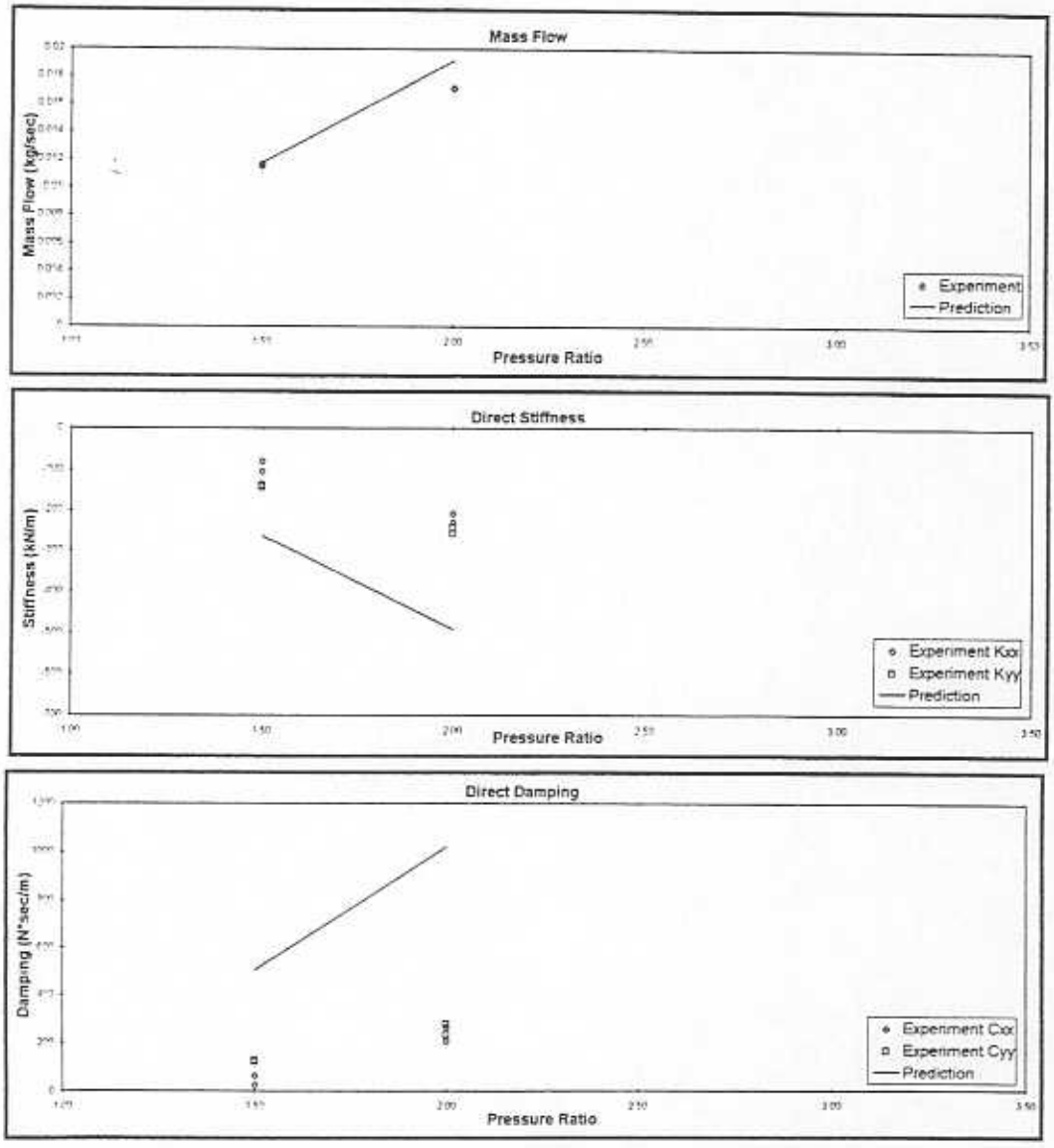

Figure 23 - Damper seal mass flow, direct stiffness and direct damping coefficients for journal rotation at 3,000 rpm and varying pressure ratio

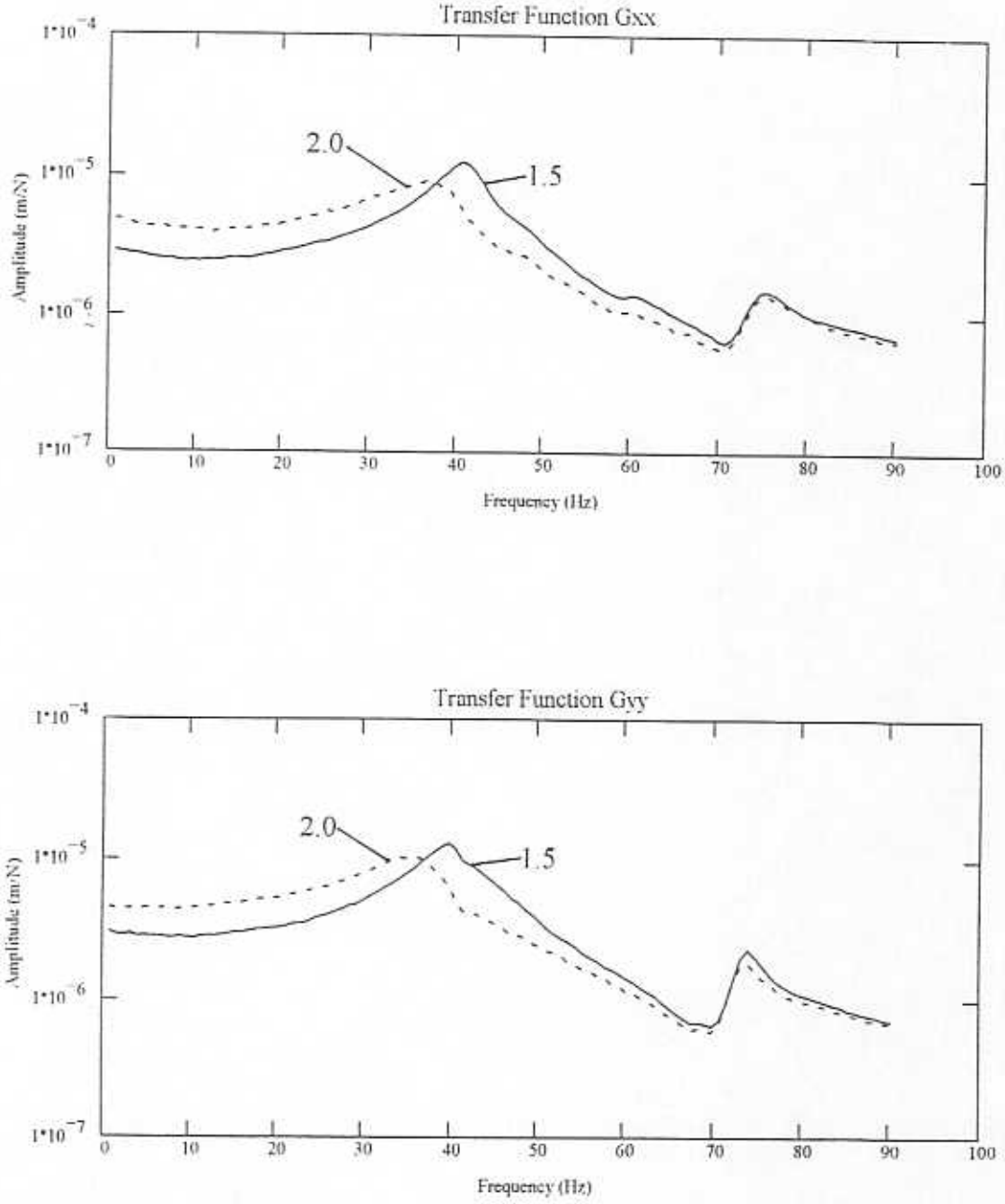

Figure 24 - Damper seal transfer functions for no journal rotation and varying pressure ratios

stiffness of the damper seal, the stiffness of the seal housing is increased which makes the link between the support structure and the housing more rigid.

At any rate, the transfer functions clearly demonstrate the decrease in direct stiffness and the increase in direct damping for both the X and Y directions. The transfer functions for a journal speed of 1,500 rpm are shown in Figure 25. Aside from the steady state responses at 10 and 25 Hz (also seen in the labyrinth seal tests), the figures are very similar to the non-rotating transfer functions shown previously. Figure 26 shows the transfer functions for the 3,000 rpm tests. It is more difficult to see the running speed response because it is close to the damped natural frequency of the seal and housing. The 20 Hz response discussed earlier is present for the damper seal tests as well. Once again, the decrease in direct stiffness and the increase in direct damping is obvious.

COHERENCE OF EXPERIMENTAL MEASUREMENTS

Samples of measured coherences are provided for each test speed at a pressure ratio of 1.5 in Figures 27 through 32. The coherence does not change significantly with increasing pressure ratio for any journal speed, so it is not necessary to view all of the results for the damper seal either. Figures 27 and 28 show the coherence for all transducers for the non-rotating tests. The coherence for the X direction displacement and acceleration with respect to F_X is excellent for the entire frequency range. The same observation holds for the Y displacement and acceleration with respect to F_Y. The poor coherence at the low frequencies of the accelerometer measurements is due to the instrument limitations. Indirect coherence (for example Y displacement with respect to

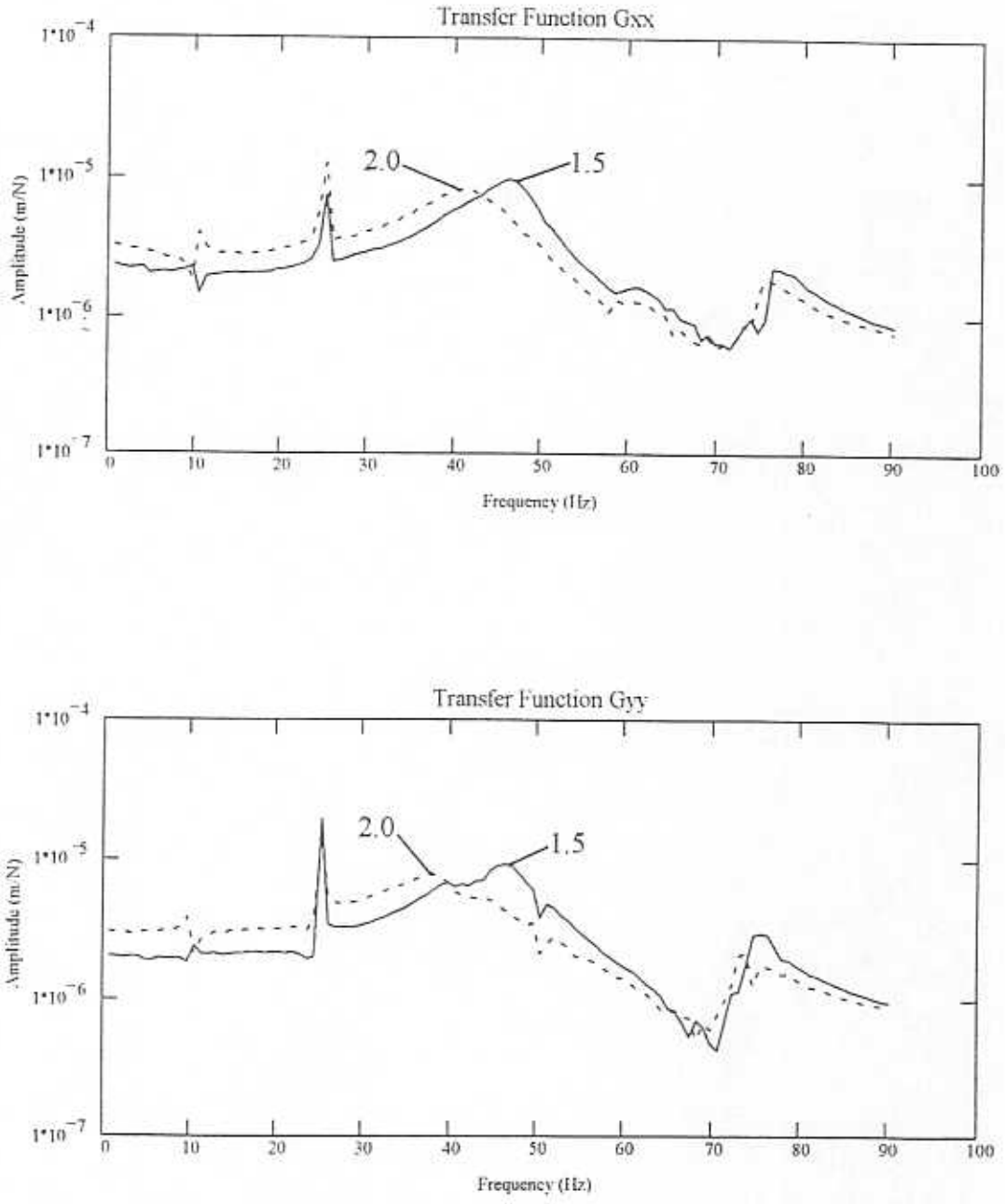

Figure 25 - Damper seal transfer functions for journal rotation at 1,500 rpm and varying pressure ratios

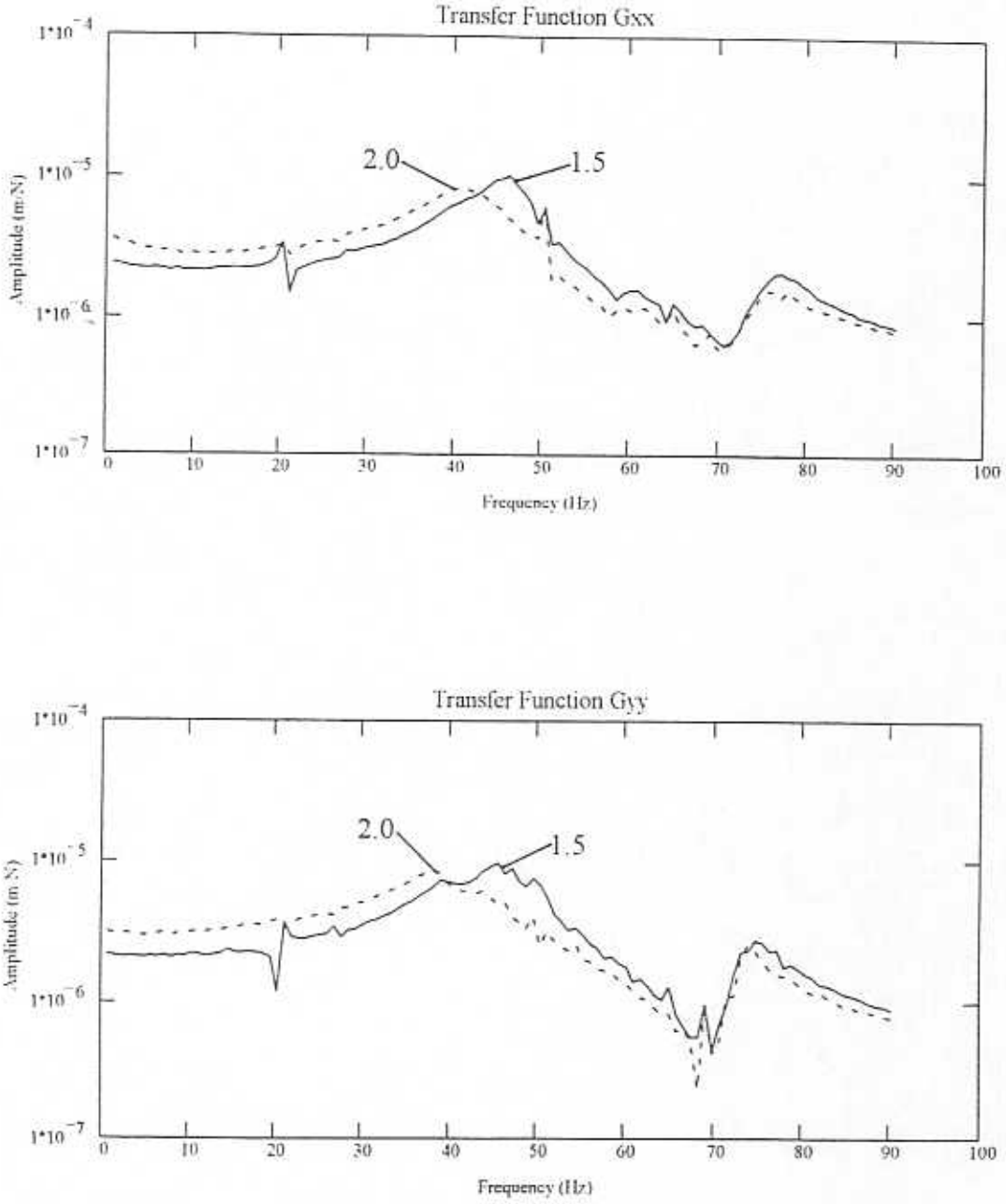

Figure 26 - Damper seal transfer functions for journal rotation at 3,000 rpm and varying pressure ratios

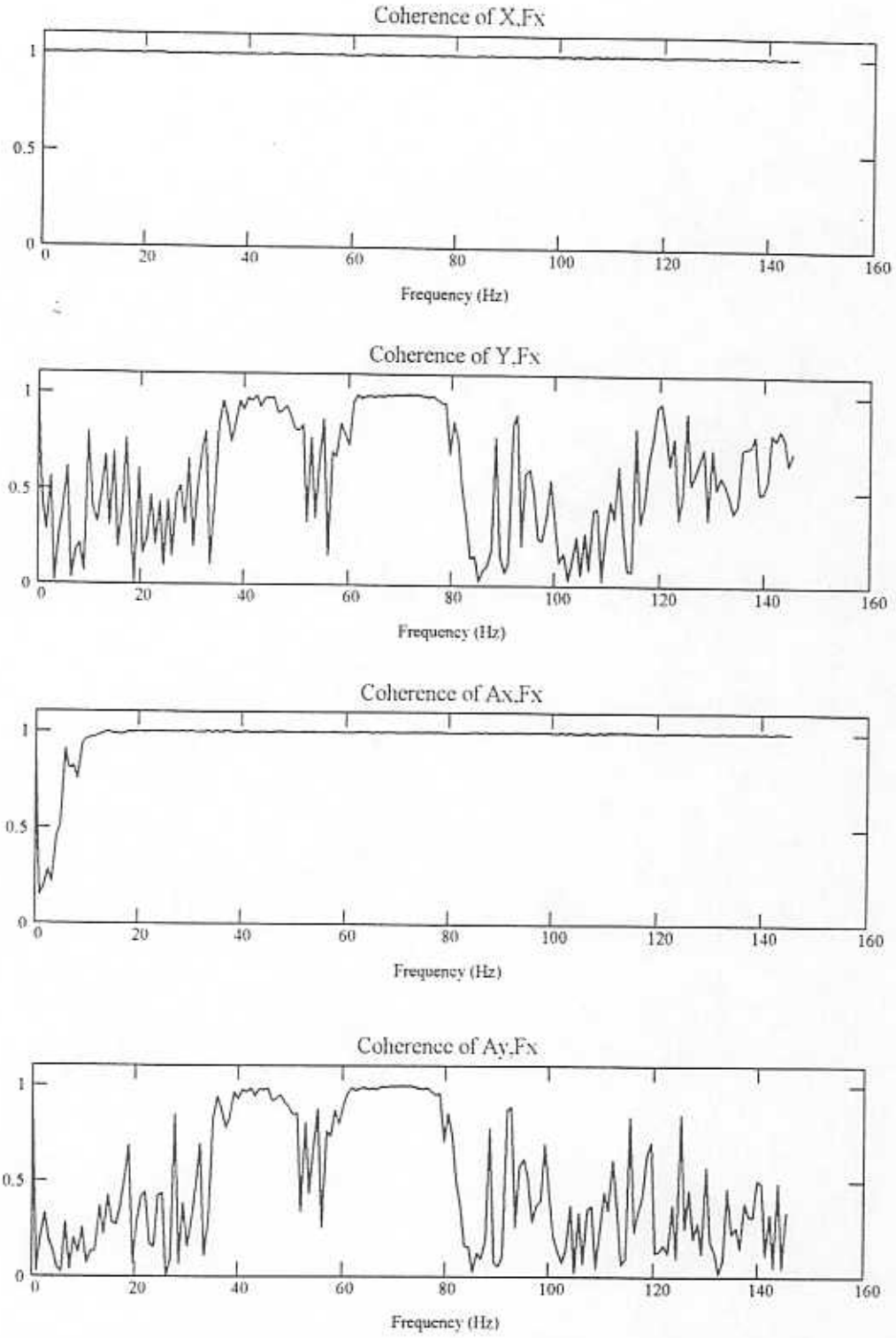

Figure 27 - Damper seal test coherences for no journal rotation and pressure ratio of 1.5 (X Impact)

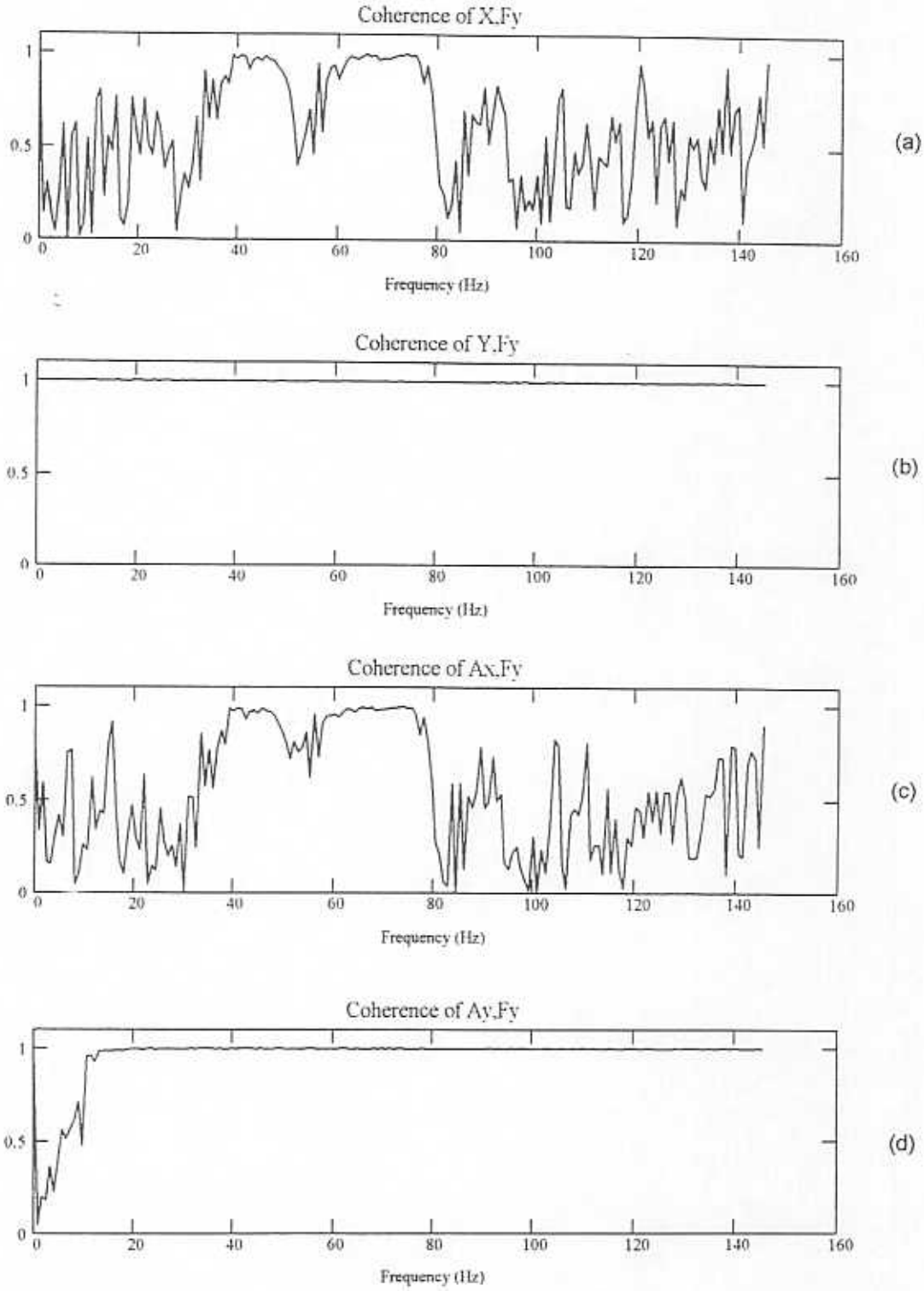

Figure 28 - Damper seal test coherences for no journal rotation and pressure ratio of 1.5 (Y Impact)

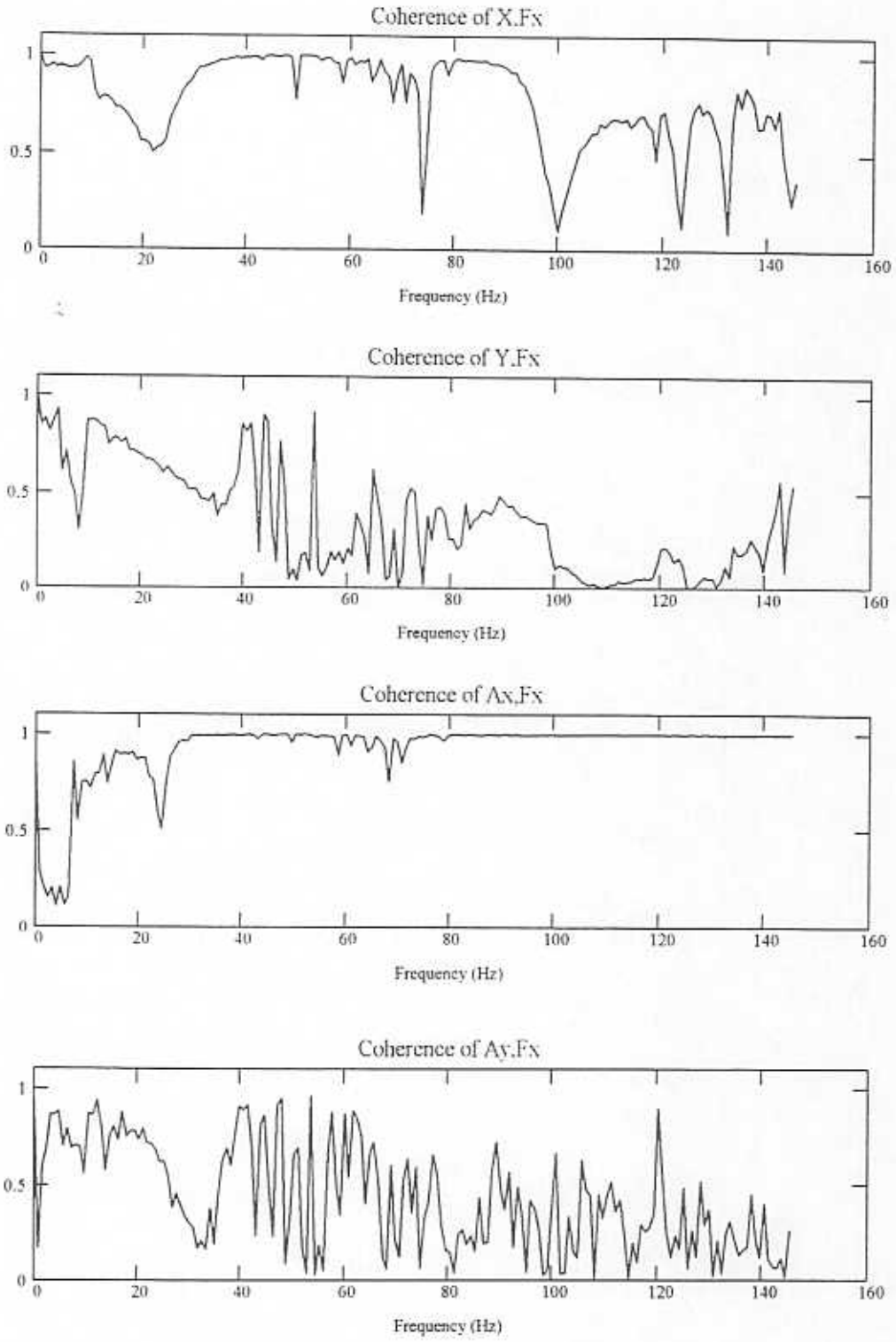

Figure 29 - Damper seal test coherences for journal rotation at 1,500 rpm and pressure ratio of 1.5 (X Impact)

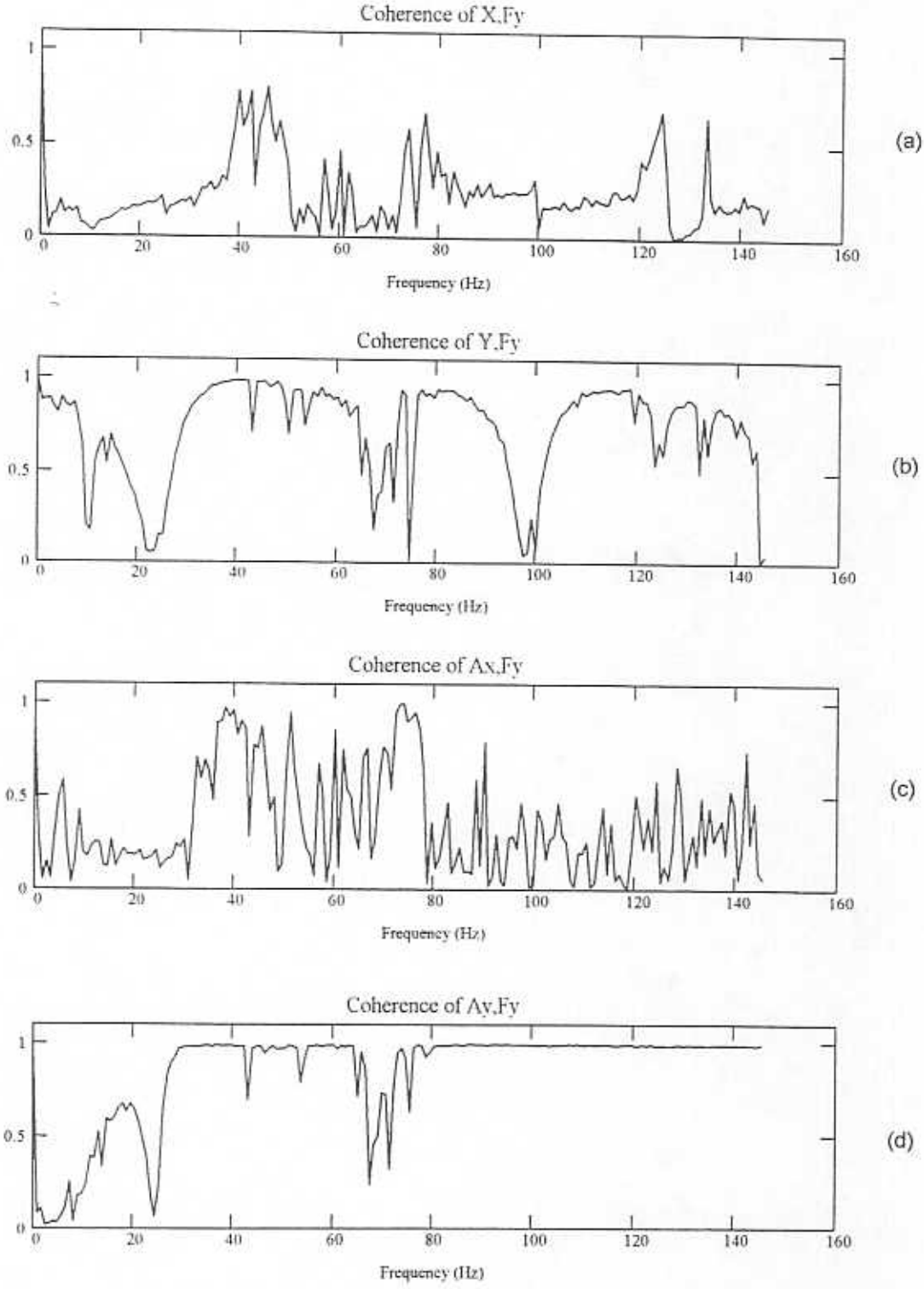

Figure 30 - Damper seal test coherences for journal rotation at 1,500 rpm and pressure ratio of 1.5 (Y Impact)

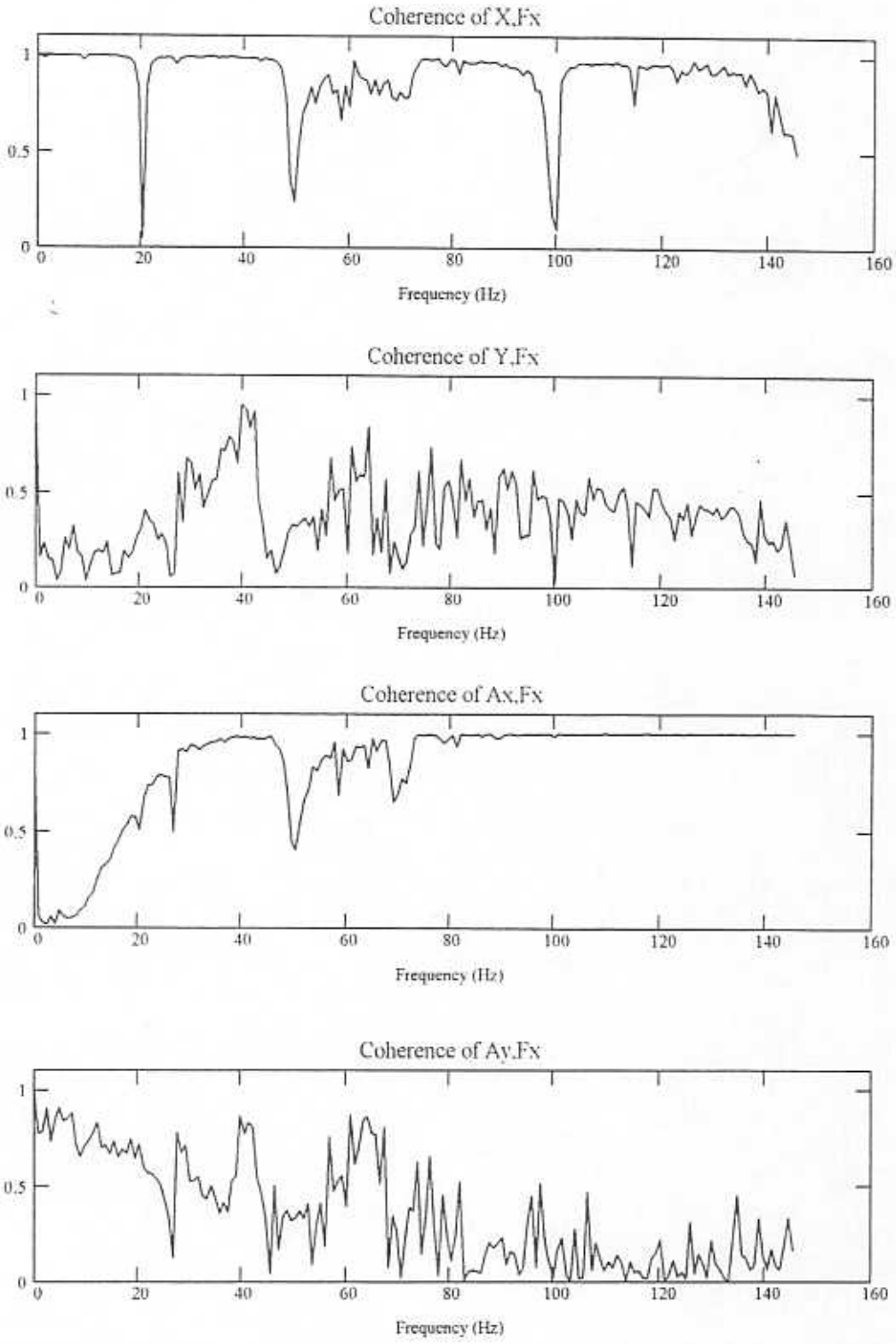

Figure 31 - Damper seal test coherences for journal rotation at 3,000 rpm and pressure ratio of 1.5 (X Impact)

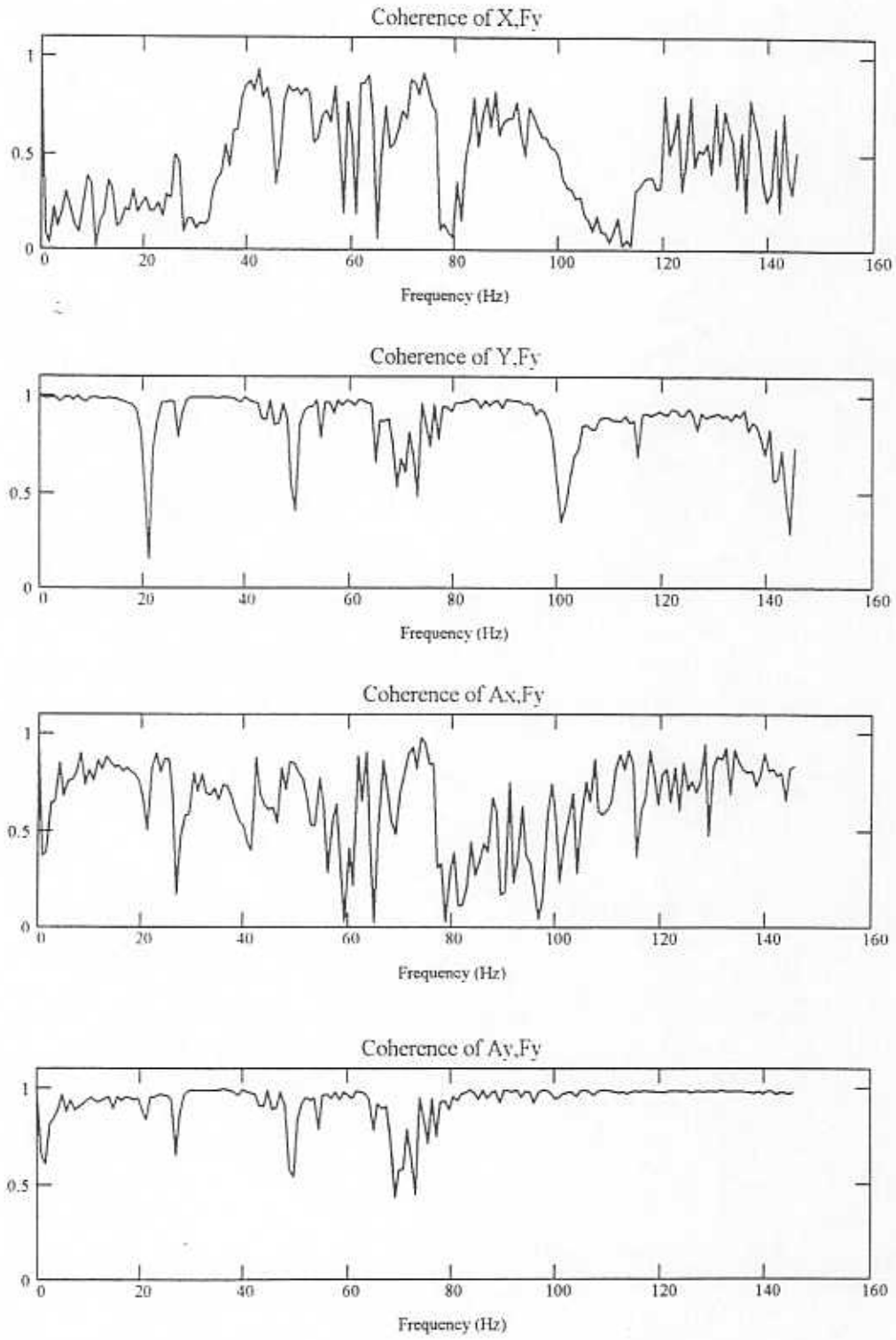

Figure 32 - Damper seal test coherences for journal rotation at 3,000 rpm and pressure ratio of 1.5 (Y Impact)

F_X) is poor for both directions indicating a weak relationship between an impact and the corresponding orthogonal motion.

Figures 29 and 30 show the coherence for the 1,500 rpm tests. In general the coherence is poor at 10, 25, 50, 75 and 100 Hz much like the labyrinth seal tests already discussed. The coherence measurements for the 3,000 rpm tests are given in Figures 31 and 32. The coherence is poor at 20, 50 and 100 Hz. For both rotating test speeds, the coherence of the indirect terms is very poor and suggests a weak relationship between impacts and orthogonal motions.

CONCLUSIONS

The following conclusions are made for the centered, two-bladed damper seal (TOS) with diverging clearance tested at 0, 1,500 and 3,000 rpm journal speeds and seal pressure ratio of 1.5 and 2.0. Measured mass flow is insensitive to journal rotation speed. Comparison of force coefficients from one journal speed to another is not particularly revealing due to the small number of data points and the amount of scatter in the identified coefficients. Certainly, the same trends which are observed in the non-rotating tests are also observed in the rotating journal tests.

The pocket damper seal exhibits large amounts of negative direct stiffness and becomes more negative with an increase in pressure ratio, as is also indicated by the predictions. Although predictions also show sizable cross-coupled stiffness, tests show cross-coupled stiffness' to be extremely small and do not appear in the response data for damper seal impact tests. Direct damping is positive and raises with an increase in pressure ratio, agreeing with predictions. Overall, the damper seal becomes more

dynamically stable but becomes unstable statically due to the overwhelming amount of the negative direct stiffness. This characteristic prevents tests at pressure ratios higher than 2.0 in the current facility.

CONCLUSIONS

Measurements of the leakage and identification of the rotordynamic force coefficients of two gas seals are successfully made. The test labyrinth seal (TOS) is shown to become less stable with increasing pressure ratios for a range of 1.5 to 3.0. Particularly, the seal exhibits positive direct stiffness and negative direct damping. Cross-coupled effects are also observed but measurement of cross-coupled stiffness is poor (high uncertainty). The same labyrinth seal is modified into a four pocket damper seal and tested under identical conditions. The damper seal is shown to be more stable dynamically but can create a static instability in this test facility due to excessive negative direct stiffness. For the test facility described, the seal housing does not have enough direct stiffness to support the damper seal at pressure ratios greater than 2.0. Cross-coupled stiffness is not detected from the measurements. The direct damping coefficients are positive and large in magnitude compared to the labyrinth seal test measurements. Table 11 emphasizes the difference in rotordynamic performance between the two seal configurations for identical test conditions. Mass flow measurements for the labyrinth seal are approximately three percent smaller than corresponding damper seal measurements.

Table 11 - Force coefficient comparison of both seals

Speed (RPM)	Pressure Ratio	Parameter	Labyrinth Seal	Damper Seal
0	1.5	K_{XX} (kN/m)	25	-88
	1.5	C_{XX} (N sec/m)	-15	44
	2.0	K_{XX} (kN/m)	49	-206
	2.0	C_{XX} (N sec/m)	-23	186
1,500	1.5	K_{XX} (kN/m)	26	-106
	1.5	C_{XX} (N sec/m)	-21	74
	2.0	K_{XX} (kN/m)	22	-231
	2.0	C_{XX} (N sec/m)	-20	277
3,000	1.5	K_{XX} (kN/m)	28	-81
	1.5	C_{XX} (N sec/m)	-20	25
	2.0	K_{XX} (kN/m)	42	-230
	2.0	C_{XX} (N sec/m)	-14	266

RECOMMENDATIONS

Further testing of pocket damper seals is desired since they show increased damping in comparison to conventional labyrinth seals. The following recommendations will enhance the capabilities of the test rig. The seal support direct stiffness must be increased to withstand higher pressure ratios. This can be accomplished with thicker support rods. Consequently, the support structure stiffness must be increased so that housing motions due not translate into large structure motions. This can be accomplished by inserting thicker columns in place of the current set.

The conflict between the identified cross-coupled stiffness values from the labyrinth seal tests and the associated coherences suggests that the orthogonal motion is due to another excitation besides the impact. It is hypothesized that the motion is due to the impact striking the housing away from the actual mass center. Doing so causes the seal to be excited in the direction orthogonal to the impact as well as the impact direction. It is recommended that some effort be made to ensure that the guns fire directly along the mass center of the seal and housing to eliminate this possibility.

Finally, in an effort to accurately remove all synchronous responses from the acquired impact spectra, the once-per-revolution tachometer signal can be used to trigger the impact guns and the data acquisition. In this way, the motions induced by shaft rotation are removed from the measured displacements long before the parameter identification process. These problems aside, the test facility has proven to be capable of extracting reliable rotordynamic force coefficients for a labyrinth seal and a pocket damper seal.

REFERENCES

Burrows, C.R., and M.N. Sahinkaya, 1982, "Frequency-Domain Estimation of Linearized Oil-Film Coefficients," ASME Journal of Lubrication Technology, Vol. 104, pp. 210-215.

Childs, D.W., 1978, "The Space Shuttle Main Engine High-Pressure Fuel Turbopump Rotordynamic Instability Problem," ASME Journal of Engineering for Power, Vol. 100, pp. 48-57.

Childs, D.W., C.E. Nelson, C. Nicks, J. Scharrer, D. Elrod, and K. Hale, 1986, "Theory Versus Experiment for the Rotordynamic Coefficients of Annular Gas Seals: Part 1 - Test Facility and Apparatus," ASME Journal of Tribology, Vol. 108, pp. 426-432.

Childs, D.W., and J.K. Scharrer, 1988, "Theory Versus Experiment for the Rotordynamic Coefficient of Labyrinth Gas Seals: Part II - A Comparison to Experiment," ASME Journal of Vibration, Acoustics, Stress, and Reliability in Design, Vol. 100, pp. 281-287.

Ewins, D.J., 1986, *Modal Testing: Theory and Practice*, Research Studies Press LTD, Letchworth, England.

Fritzen, C.-P., 1985, "Identification of Mass, Damping, and Stiffness Matrices of Mechanical Systems," submitted to 10th ASME Conference on Mechanical Vibration and Noise, Cincinnati.

Goodwin, M.J., 1991, "Experimental Techniques for Bearing Impedance Measurement," ASME Journal of Engineering for Industry, Vol. 113, pp. 335-342.

Hagg, A.C., and G.O. Sankey, 1956, "Some Dynamic Properties of Oil-Film Journal Bearings with Reference to the Unbalance Vibration of Rotors," ASME Journal of Applied Mechanics, Vol. 23, No. 1, pp. 302-306.

Li, J., L. San Andrés and J. Vance, 1997, "A Bulk-Flow Analysis of a Novel Gas Damper Seal," Report to the Turbomachinery Research Consortium, Texas A&M University, May.

Lund, J.W., 1987, "Review of the Concept of Dynamic Coefficients for Fluid Film Journal Bearings," ASME Journal of Tribology, Vol. 109, pp. 37-41.

Massmann, H., and R. Nordmann, 1985, "Some New Results Concerning the Dynamic Behavior of Annular Turbulent Seals," Rotordynamic Instability Problems of High Performance Turbomachinery, Proceedings of a workshop held at Texas A&M University, Dec, pp. 179-194.

Mitchell, L.D., and K.B Elliott, 1984, "How to Design Stingers for Vibration Testing of Structures," Sound and Vibration Magazine, April, pp. 14-18.

Morton, P.G., 1971, "Measurement of the Dynamic Characteristics of a Large Sleeve Bearing," ASME Journal of Lubrication Technology, January, pp. 143-150.

Murphy, B.T., and J.M. Vance, 1980, "Labyrinth Seal Effects on Rotor Whirl Instability," IMechE, C306/80, pp. 369-373.

Nelson, C.C., D.W. Childs, C. Nicks, and D. Elrod, 1986, "Theory Versus Experiment for the Rotordynamic Coefficients of Annular Gas Seals: Part 2 - Constant-Clearance and Convergent-Tapered Geometry," ASME Journal of Tribology, Vol. 108, pp. 433-438.

Nordmann, R., and K. Schollhorn, 1980, "Identification of Stiffness and Damping Coefficients of Journal Bearings by Means of the Impact Method," Proceedings. 2nd International Conference On Vibrations in Rot. Mach., IMechE, pp.231-238.

Parkins, D.W., 1979, "Theoretical and Experimental Determination of the Dynamic Characteristics of a Hydrodynamic Journal Bearing," ASME Journal of Lubrication Technology, Vol. 101, pp. 129-137.

Parkins, D.W., 1981, "Measured Characteristics of a Journal Bearing Oil Film," ASME Journal of Lubrication Technology, Vol. 103, pp. 120-125.

Parkins, D.W., 1995, "Measurement of Oil Film Journal Bearing Damping Coefficients - An Extension of the Selected Orbit Technique," Journal of Tribology, Vol. 117, October, pp. 696-701.

Qiu, Z.L., and A.K. Tieu, 1993, "Full Determination of Dynamic Coefficients of Fluid Film Bearings from Impulse Responses," Proceedings of 4th ASIA-PACIFIC Vibration Conference, Kitakyushu, Japan, Nov. 14-18, Vol. 2, pp. 527-532.

Robison, M, G. Arauz, and L. San Andrés, 1995, "A Test Rig for the Identification of Rotordynamic Force Coefficients of Fluid Film Bearing Elements," ASME Paper, 95-GT-431.

Rouvas, Constantinos, 1993, "Parameter Identification of the Rotordynamic Coefficients of High-Reynolds-Number Hydrostatic Bearings," Ph.D. Dissertation, Texas A&M University.

San Andrés, L., 1991, "Analysis of Variable Fluid Properties, Turbulent Annular Seals," ASME Journal of Tribology, Vol. 113, pp. 694-702.

Swanson, E.E., and R.G. Kirk, 1996, "Survey of Experimental Data for Fixed Geometry Hydrodynamic Journal Bearings," ASME Paper 96-Trib-65.

Tieu, A.K., and Z.L. Qiu, 1994, "Identification of Sixteen Dynamic Coefficients of Two Journal Bearings from Experimental Unbalance Responses," Wear, Vol. 177, pp. 63-69.

Vance, J.M, and R.R. Schultz, 1993, "A New Damper Seal for Turbomachinery," Vibration of Rotating Systems, ASME DE-Vol. 60.

Vance, J.M, J.J., Zierer Jr., and E.M. Conway, 1993, "Effect of Straight-Through Labyrinth Seals on Rotordynamics," 14th Biannual ASME Vibration Conference, September.

Vance, J.M., and J. Li, 1995, "Test Results of a New Damper Seal for Vibration Reduction in Turbomachinery," ASME Paper 95-GT-36.

Wright, D.V., 1978, "Air Model Tests of Labyrinth Seal Forces on a Whirling Rotor," ASME Journal of Engineering for Power, Vol. 100, pp. 533-543.

Wright, D.V., 1983, "Labyrinth Seal Forces on a Whirling Rotor," Rotordynamic Instability, Proceedings of the ASME Applied Mechanics, Bioengineering and Fluids Engineering Conference, Houston, TX, pp. 19-31.

APPENDIX A

SAMPLE INPUT FILES FOR BOTH LABYRINTH SEAL AND DAMPER SEAL PREDICTIONS

The following two pages show the input parameters necessary for the analysis code of Li et al. (1997). The conditions are listed for shaft speed of 3,000 rpm and a pressure ratio of 3.0. The first section describes the geometry of the seal. The second section describes the operating conditions such as pressure ratio, temperature, pre-swirl, rotating speed and analysis frequency. In these predictions, 37 Hz is used as a close estimate of the housing/seal natural frequency. The remaining sections are used by the analyst to calibrate the code to a particular set of experimental data.

Two-Bladed Labyrinth Seal
3000 rpm, P_{Ratio} = 3.0

********** Input Data Sheet **********

------- Seal Configuration ----------
Number of cavities NC, NW: 1 1
Rotor radius and Seal bottom radius Rr, Rs: 0.635000E-01 0.703580E-01(m)
Seal inside pitch length L: 0.348996E-01(m)
Upstream and Downstream strip height Bs, Bb: 0.673100E-02 0.660400E-02(m)
Upstream and Downstream clearances Hs, Hb: 0.127000E-03 0.254000E-03(m)
Types of Upstream and Downstream clearances: 1 1
Types of seal cavity: 1
Rotor and stator surface roughness : 0.000000E+00 0.000000E+00(m)

---------- Operating Conditions ----------
Supply pressure and Back pressure Ps, Pb: 0.303900E+01 0.101300E+01(Bar)
Gas constant Rg and Temperature T (K)): 0.287000E+03 0.295000E+03
Specific heat ratio Gamma and Gas viscosity EMU(N-s/m**2): 0.140000E+01
0.182000E-04
Pre-swirl velocity ratio UIRATIO: 0.000000E+00
Rotor Rotational Frequency (SPEED): 0.300000E+04(RPM)
Rotor Whirling Frequency (OMEGA): 0.370000E+02(Hz)

----- Empirical Parameters for the partition wall ------
Velocity modification factor BETAw: 0.100000E+01

------ Parameters of Moody Shear Stress Model -------
AMOD= 1.3749999999999999E-03 BMOD= 1000000.000000000 EXPO=
0.3333300000000000

----- Parameter relative to Numerical Computation -----
No. of grids in one circumferential cavity NCV: 40
Underrelaxation factors ALFU, ALFP: 0.500000E+00 0.500000E+00
Underrelaxation factors ALFU1, ALFP1: 0.700000E+00 0.700000E+00
Underrelax factor at the partitin wall ALFuw: 0.100000E+00
Max. No. of iteration MAXITER, MAXITER1: 200 200

------- Convergence criteria ---------
SMAX = 9.9999999999999995E-07 PEPS = 9.9999999999999995E-07
PEPS1 = 9.9999999999999995E-08
********* End of Input Data Sheet **********

Two-Bladed Damper Seal
3000 rpm, P_{Ratio} = 3.0

********** Input Data Sheet **********

------- Seal Configuration ----------
Number of cavities NC, NW: 4 1
Rotor radius and Seal bottom radius Rr, Rs: 0.635000E-01 0.703580E-01(m)
Seal inside pitch length L: 0.348996E-01(m)
Upstream and Downstream strip height Bs, Bb: 0.673100E-02 0.660400E-02(m)
Upstream and Downstream clearances Hs, Hb: 0.127000E-03 0.254000E-03(m)
Types of Upstream and Downstream clearances: 1 1
Types of seal cavity: 0
Rotor and stator surface roughness : 0.000000E+00 0.000000E+00(m)

---------- Operating Conditions ----------
Supply pressure and Back pressure Ps, Pb: 0.303900E+01 0.101300E+01(Bar)
Gas constant Rg and Temperature T (K)): 0.287000E+03 0.295000E+03
Specific heat ratio Gamma and Gas viscosity EMU(N-s/m**2): 0.140000E+01
0.182000E-04
Pre-swirl velocity ratio UIRATIO: 0.000000E+00
Rotor Rotational Frequency (SPEED): 0.300000E+04(RPM)
Rotor Whirling Frequency (OMEGA): 0.370000E+02(Hz)

----- Empirical Parameters for the partition wall ------
Velocity modification factor BETAw: 0.350000E+00

------ Parameters of Moody Shear Stress Model -------
AMOD= 1.3749999999999999E-03 BMOD= 1000000.000000000
EXPO=0.3333300000000000

----- Parameter relative to Numerical Computation -----
No. of grids in one circumferential cavity NCV: 20
Underrelaxation factors ALFU, ALFP: 0.500000E+00 0.500000E+00
Underrelaxation factors ALFU1, ALFP1: 0.700000E+00 0.700000E+00
Underrelax factor at the partitin wall ALFuw: 0.100000E+00
Max. No. of iteration MAXITER, MAXITER1: 200 200

------- Convergence criteria ---------
SMAX = 9.9999999999999995E-07 PEPS = 9.9999999999999995E-07
PEPS1 = 9.9999999999999995E-08
********* End of Input Data Sheet **********

APPENDIX B

INSTRUMENTAL VARIABLE METHOD AS PERFORMED IN MATHCAD

This page computes the parameters of a system (m,c, and k matrices) given the *FFT* of the response and excitation for two different cases. This page is created for Mathcad Plus 6.0

Read frequency domain data from files

$j := 0,1..250$

$dxx_j := READ(b0c6b1)$ $dyx_j := READ(b0c6b3)$ $fx_j := READ(b0c6b9)$

$dxy_j := READ(b0c6b2)$ $dyy_j := READ(b0c6b4)$ $fy_j := READ(b0c6b10)$

Extract conversion coefficients from data files

$c1 := dxx_{11}$ $\Delta f := dxx_{14}$

$c1 = 4.6$ $\Delta f = 0.8$

Set the lowest analysis frequency (Hz):

$f1 := 1$

$low_f := f1 \cdot \Delta f$

$low_f = 0.8$ Hz

Set the highest analysis frequency (Hz):

$f2 := 110$

$high_f := (f1 + f2) \cdot \Delta f$

$high_f = 90.2$ Hz

Build complex variables from the data files

$i := 0..f2$

$f_i := (i + f1) \cdot \Delta f$ Hz

$\omega_i := f_i \cdot 2 \cdot \pi$ rad/sec

$\omega 2_i := (\omega_i)^2$ (rad/sec)^2

Real counter

$R_i := 2 \cdot i + (21 + 2 \cdot f1)$

Imaginary counter

$I_i := 2 \cdot i + (22 + 2 \cdot f1)$

Displacement variables

$D_{xx_i} := \left[dxx_{(R_i)} \cdot c1 + dxx_{(I_i)} \cdot c1 \cdot i \right]$ $D_{yx_i} := \left[dyx_{(R_i)} \cdot c1 + dyx_{(I_i)} \cdot c1 \cdot i \right]$

$D_{xy_i} := \left[dxy_{(R_i)} \cdot c1 + dxy_{(I_i)} \cdot c1 \cdot i \right]$ $D_{yy_i} := \left[dyy_{(R_i)} \cdot c1 + dyy_{(I_i)} \cdot c1 \cdot i \right]$

Force variables

$$F_{x_i} := \left[fx_{(R_i)} \cdot c1 + fx_{(I_i)} \cdot c1 \cdot i \right] \qquad F_{y_i} := \left[fy_{(R_i)} \cdot c1 + fy_{(I_i)} \cdot c1 \cdot i \right]$$

The following is a filter to remove the synchronous response for rotating tests

Low Pass Value:

$BP1 := 28 \qquad f_{BP1} = 23.6 \quad Hz$

High Pass Value:

$BP2 := 34 \qquad f_{BP2} = 28.4 \quad Hz$

$p := BP1, (BP1 + 1) .. BP2$

$$\Delta Dxx := \frac{D_{xx_{BP2}} - D_{xx_{BP1}}}{(BP2 - BP1) + 1} \qquad \Delta Dyx := \frac{D_{yx_{BP2}} - D_{yx_{BP1}}}{(BP2 - BP1) + 1}$$

$$\Delta Dxy := \frac{D_{xy_{BP2}} - D_{xy_{BP1}}}{(BP2 - BP1) + 1} \qquad \Delta Dyy := \frac{D_{yy_{BP2}} - D_{yy_{BP1}}}{(BP2 - BP1) + 1}$$

*** If the filtering is not desired, just toggle the following equaitons off.

$$\begin{bmatrix} D_{xx_p} \\ D_{xy_p} \\ D_{yx_p} \\ D_{yy_p} \end{bmatrix} := \begin{bmatrix} D_{xx_{p-1}} + \Delta Dxx \\ D_{xy_{p-1}} + \Delta Dxy \\ D_{yx_{p-1}} + \Delta Dyx \\ D_{yy_{p-1}} + \Delta Dyy \end{bmatrix}$$

Computation of the Impedances for each frequency:

$$\begin{pmatrix} H_{xx_i} & H_{xy_i} \\ H_{yx_i} & H_{yy_i} \end{pmatrix} := \begin{pmatrix} F_{x_i} & 0 \\ 0 & F_{y_i} \end{pmatrix} \cdot \begin{pmatrix} D_{xx_i} & D_{xy_i} \\ D_{yx_i} & D_{yy_i} \end{pmatrix}^{-1}$$

Copmputation of the flexibilities for each frequency:

$$\begin{pmatrix} F_{xx_i} & F_{xy_i} \\ F_{yx_i} & F_{yy_i} \end{pmatrix} := \begin{pmatrix} H_{xx_i} & H_{xy_i} \\ H_{yx_i} & H_{yy_i} \end{pmatrix}^{-1}$$

initial point: $i_o = f1$ Correponding to: $\omega_{i_o} = 10.2$ rad/sec

final point: $i_f = f2$ $\omega_{i_f} = 566.7$ rad/sec

Construct a vector whose elements are the flexibility matrices at each frequency (each element of the vertor is a matrix):

$$F_i = \begin{pmatrix} H_{xx_i} & H_{xy_i} \\ H_{yx_i} & H_{yy_i} \end{pmatrix}^{-1}$$

Now, the problem to solve is $F \cdot H = I + E$

where F is the measured flexibilities, H the approximated impedances, I the identity matrix and E the error to be minimized.

The left hand side can be rearranged as to have:

$$A \cdot \begin{pmatrix} k \\ m \\ c \end{pmatrix} = I + E'$$

Now, the equations of each frequency are to be decomposed into real and imaginary part. And stacking all the equations gives an undetermined system of equations (more equations than unknowns) of the same form, where:

A (as a function of the flexibilities) is given by:

$$a(F) = \left| \begin{array}{l} A \leftarrow \mathrm{Re}\left[F_{i_o} \cdot \begin{bmatrix} 1 & 0 & -(\omega_{i_o})^2 & 0 & i \cdot \omega_{i_o} & 0 \\ 0 & 1 & 0 & -(\omega_{i_o})^2 & 0 & i \cdot \omega_{i_o} \end{bmatrix} \right] \\ A \leftarrow \mathrm{stack}\left[A, \mathrm{Im}\left[F_{i_o} \cdot \begin{bmatrix} 1 & 0 & -(\omega_{i_o})^2 & 0 & i \cdot \omega_{i_o} & 0 \\ 0 & 1 & 0 & -(\omega_{i_o})^2 & 0 & i \cdot \omega_{i_o} \end{bmatrix} \right] \right] \\ \text{for } i \in i_o + 1 .. i_f \\ \quad \left| \begin{array}{l} A \leftarrow \mathrm{stack}\left[A, \mathrm{Re}\left[F_i \cdot \begin{bmatrix} 1 & 0 & -(\omega_i)^2 & 0 & i \cdot \omega_i & 0 \\ 0 & 1 & 0 & -(\omega_i)^2 & 0 & i \cdot \omega_i \end{bmatrix} \right] \right] \\ A \leftarrow \mathrm{stack}\left[A, \mathrm{Im}\left[F_i \cdot \begin{bmatrix} 1 & 0 & -(\omega_i)^2 & 0 & i \cdot \omega_i & 0 \\ 0 & 1 & 0 & -(\omega_i)^2 & 0 & i \cdot \omega_i \end{bmatrix} \right] \right] \end{array} \right. \\ A \end{array} \right.$$

<= A = real part of the first frequency

<= stacks what was on A with the imaginary part of the first frequency

<= for loop from the second the the last frequencies.

<= stacks to A the real part of the i^{th} frequency

<= stacks to A the imaginary part of the i^{th} frequency

<= returns the matrix A

Auxiliary matrix of zeros [2x2]:

$zero_{I,1} := 0$

The right hand side of the equation is given by:

$$I := \left| \begin{array}{l} I \leftarrow identity(2) \\ I \leftarrow stack(I, zero) \\ \text{for } i \in i_o + 1 .. i_f \\ \quad \left| \begin{array}{l} I \leftarrow stack(I, identity(2)) \\ I \leftarrow stack(I, zero) \end{array} \right. \\ I \end{array} \right.$$

The least squares solution of the problem (minimum E) is:

$$\begin{bmatrix} k_{xx} & k_{xy} \\ k_{yx} & k_{yy} \\ m_{xx} & m_{xy} \\ m_{yx} & m_{yy} \\ c_{xx} & c_{xy} \\ c_{yx} & c_{yy} \end{bmatrix} = \left| \begin{array}{l} A \leftarrow a(F) \quad \text{<= Matrix A for the measured flexibilities} \\ X_o \leftarrow \left(A^T \cdot A\right)^{-1} \cdot A^T \cdot I \quad \text{<= first approximation of the coefficients} \\ X_1 \leftarrow X_o \cdot 0 \quad \text{<= initialization of the auxiliar variable} \\ \text{while } \max\left(\overrightarrow{|X_o - X_1|}\right) > 10^{-6} \quad \text{<= maximum admissible error} \\ \quad \left| \begin{array}{l} \text{for } i \in i_o .. i_f \quad \text{<= this for loop builds the new vector of flexibilities based on the identified parameters} \\ \quad F_i \leftarrow \begin{bmatrix} X_{o_{0,0}} - (\omega_i)^2 \cdot X_{o_{2,0}} + i \cdot \omega_i \cdot X_{o_{4,0}} & X_{o_{0,1}} - (\omega_i)^2 \cdot X_{o_{2,1}} + i \cdot \omega_i \cdot X_{o_{4,1}} \\ X_{o_{1,0}} - (\omega_i)^2 \cdot X_{o_{3,0}} + i \cdot \omega_i \cdot X_{o_{5,0}} & X_{o_{1,1}} - (\omega_i)^2 \cdot X_{o_{3,1}} + i \cdot \omega_i \cdot X_{o_{5,1}} \end{bmatrix} \\ W \leftarrow a(F) \\ X_1 \leftarrow X_o \quad \text{<= finds the A matrix for the approximated flexibilities} \\ X_o \leftarrow \left(W^T \cdot A\right)^{-1} \cdot W^T \cdot I \quad \text{<= saves the old paramters} \end{array} \right. \\ X_o \quad \text{<= finds the new set of coefficients} \\ \quad \text{<= returns the set of coefficients that fulfills the error criterion} \end{array} \right.$$

The numerical values of the parameters are:

$$\begin{bmatrix} k_{xx} & k_{xy} \\ k_{yx} & k_{yy} \\ m_{xx} & m_{xy} \\ m_{yx} & m_{yy} \\ c_{xx} & c_{xy} \\ c_{yx} & c_{yy} \end{bmatrix} = \begin{bmatrix} 3.511 \cdot 10^5 & 1.088 \cdot 10^4 \\ -403.41 & 3.186 \cdot 10^5 \\ 7.021 & 6.931 \cdot 10^{-3} \\ -0.236 & 6.375 \\ 74.382 & 3.528 \\ -0.403 & 59.553 \end{bmatrix}$$

The approximated impedances are:

$i := i_0 .. i_f$

$$H'_{xx_i} := k_{xx} - (\omega_i)^2 \cdot m_{xx} + i \cdot \omega_i \cdot c_{xx}$$

$$H'_{xy_i} := k_{xy} - (\omega_i)^2 \cdot m_{xy} + i \cdot \omega_i \cdot c_{xy}$$

$$H'_{yx_i} := k_{yx} - (\omega_i)^2 \cdot m_{yx} + i \cdot \omega_i \cdot c_{yx}$$

$$H'_{yy_i} := k_{yy} - (\omega_i)^2 \cdot m_{yy} + i \cdot \omega_i \cdot c_{yy}$$

And the approximated flexibilities:

$$\begin{pmatrix} F'_{xx_i} & F'_{xy_i} \\ F'_{yx_i} & F'_{yy_i} \end{pmatrix} := \begin{pmatrix} H'_{xx_i} & H'_{xy_i} \\ H'_{yx_i} & H'_{yy_i} \end{pmatrix}^{-1}$$

Correlation between test data and curve fit are calculated

$$Corrxx := |corr(F_{xx}, F'_{xx})| \qquad Corryx := |corr(F_{yx}, F'_{yx})|$$

$$Corrxy := |corr(F_{xy}, F'_{xy})| \qquad Corryy := |corr(F_{yy}, F'_{yy})|$$

The final coefficients and associated correlations

$k_{xx} = 3.511 \cdot 10^5$	$k_{xy} = 1.088 \cdot 10^4$	$k_{yx} = -403.41$	$k_{yy} = 3.186 \cdot 10^5$	(N/m)
$c_{xx} = 74$	$c_{xy} = 4$	$c_{yx} = 0$	$c_{yy} = 60$	(N sec/m)
$m_{xx} = 7$	$m_{xy} = 6.9 \cdot 10^{-3}$	$m_{yx} = -0.2$	$m_{yy} = 6.4$	(kg)
$Corrxx = 0.99$	$Corrxy = 0.98$	$Corryx = 0.97$	$Corryy = 0.99$	

APPENDIX C

SENSITIVITY ANALYSIS AS PERFORMED IN MATHCAD

The following analysis transforms the measurement uncertainties from the time domain to the frequency domain. First, the time domain increment and the number of data points is defined. This sheet is created for Mathcad Plus 6.0

Time step

$dt := 0.00015$ sec

Number of samples

$tmax := 8192$

Counter for time step

$t := 0, 1 .. tmax - 1$

Frequency domain increment (inverse of the total sampling time) (Hz)

$$\Delta f := \frac{1}{dt \cdot tmax}$$

$\Delta f = 0.814$ Hz

Define the measurement uncertainties in the time domain

Force

$delf := 0.8$ N

Displacement

$delx := 0.000002$ m

Frequency

$delw := \Delta f \cdot 2 \cdot \pi$ rad/sec

To generate the time domain impulse, the impact must be defined as a magnitude and duration. In this case, the impact will last one time step, dt.

Impact magnitude

$af1 := 4000$ N

Impact duration

$\Delta t1 := dt$ sec

To generate the time domain displacement response, the seal stiffness, damping and mass must be defined

Stiffness

$K1 := 608000$ N/m

Damping

$C1 := 463$ N sec/m

Mass

$M1 := 6.4$ Kg

The following calculations are necessary for the calculation of the free response to the impulse load

Natural frequency

$$\omega 1 := \sqrt{\frac{K1}{M1}}$$

$\omega 1 = 308.221$ rad/sec

Initial velocity

$$v_{01} := \frac{af1 \cdot \Delta t1}{M1}$$

$v_{01} = 0.094$ m/sec

Damping ratio

$$\xi 1 := \frac{C1}{2 \cdot \omega 1 \cdot M1}$$

$\xi 1 = 0.117$

Damped natural frequency

$$\omega_{d1} := \omega 1 \cdot \sqrt{1 - \xi 1^2}$$

$\omega_{d1} = 306.091$ rad/sec

The time domain impulse is generated using the Dirac delta function so that the force is maximum when t=0, and zero for the remaining time. Two forcing functions are created, one which is one magnitude of uncertainty less than the original force, and one that is one magnitude greater than the original force.

$f1_t := \delta(0,t) \cdot (af1 - delf)$

$f2_t := \delta(0,t) \cdot (af1 + delf)$

The displacement response is the exact solution for the free response of a single-degree-of-freedom system to an initial velocity. The initial velocity is a function of the impulse. Two displacement functions are created. One which which responds with one order of magnitude larger displacement than original and responds at a frequency one order of magnitude larger than the original response frequency. The second response is just the opposite.

$$x1_t := e^{-\xi 1 \cdot (\omega 1 + delw) \cdot t \cdot dt} \cdot \left[\left(\frac{v_{01}}{\omega_{d1}} + delx \right) \cdot \sin\left[\left(\omega_{d1} + delw \right) \cdot t \cdot dt \right] \right]$$

$$x2_t := e^{-\xi 1 \cdot (\omega 1 - delw) \cdot t \cdot dt} \cdot \left[\left(\frac{v_{01}}{\omega_{d1}} - delx \right) \cdot \sin\left[\left(\omega_{d1} - delw \right) \cdot t \cdot dt \right] \right]$$

The force and displacement time responses are displayed below.

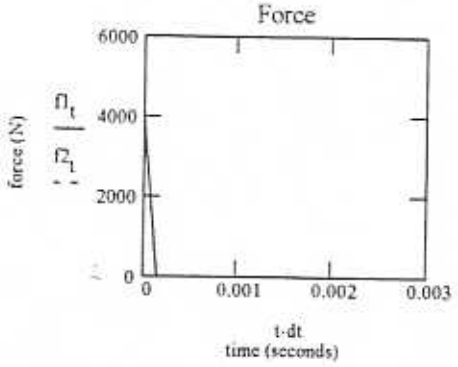

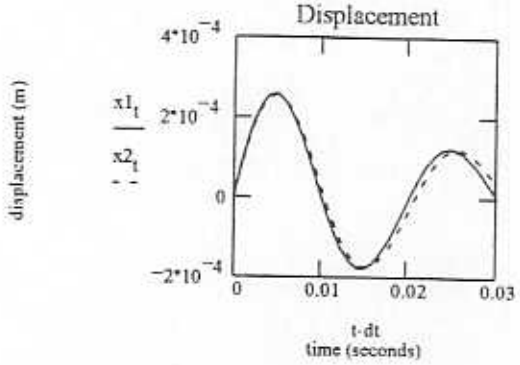

The time domain data is transformed to the frequency domain so that the stiffness and damping coefficients can be identified.

Frequency domain counter

$j := 0, 1 .. 300$

$F1 := \mathrm{fft}(f1)$ $\quad F2 := \mathrm{fft}(f2)$

$X1 := \mathrm{fft}(x1)$ $\quad X2 := \mathrm{fft}(x2)$

Define frequency domain parameters

$f_j := j \cdot \Delta f$ Hz

$w_j := f_j \cdot 2 \cdot \pi$ rad/sec

$w2_j := (w_j)^2$ (rad/sec)^2

The impedances are calculated as follows (seal inertia is not subtracted)

$H1_j := \frac{F1_j}{X1_j}$ N/m $\quad H2_j := \frac{F2_j}{X2_j}$ N/m

The real and imaginary portions of the impedance are displayed separately below

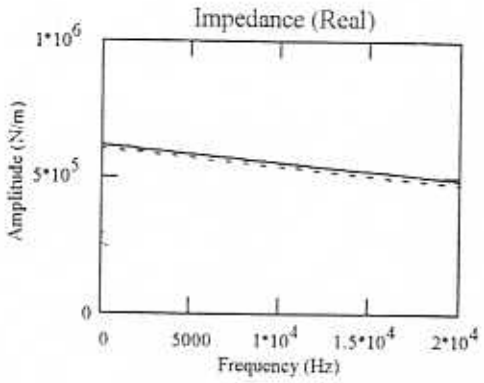

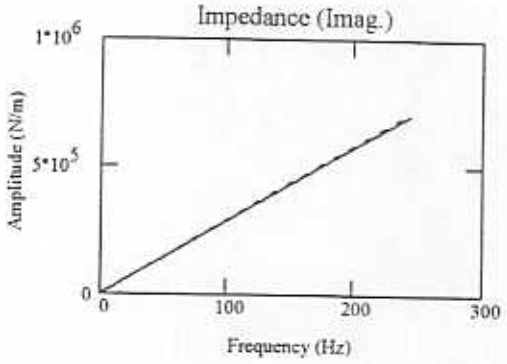

Finally, the stiffness and damping values are identified below, and the uncertainty for each coefficient is the difference between the two identified values

$k1 := \text{intercept}(w2, \text{Re}(H1))$ $\quad k1 = 6.086 \cdot 10^5$ N/m

$c1 := -\text{slope}(w, \text{Im}(H1))$ $\quad c1 = 456.372$ N sec/m

$k2 := \text{intercept}(w2, \text{Re}(H2))$ $\quad k2 = 5.962 \cdot 10^5$ N/m

$c2 := -\text{slope}(w, \text{Im}(H2))$ $\quad c2 = 462.652$ N sec/m

$$\Delta k := \frac{|k1 - k2|}{2} \qquad \Delta k = 6.202 \cdot 10^3 \text{ N/m}$$

$$\Delta c := \frac{|c1 - c2|}{2} \qquad \Delta c = 3.14 \text{ N sec/m}$$

Table C1 - Labyrinth seal force coefficient uncertainties

Speed (RPM)	Pressure Ratio	$U(K_{XX})$ (kN/m)	$U(K_{XY})$ (kN/m)	$U(K_{YX})$ (kN/m)	$U(K_{YY})$ (kN/m)	$U(C_{XX})$ (N sec/m)	$U(C_{XY})$ (N sec/m)	$U(C_{YX})$ (N sec/m)	$U(C_{YY})$ (N sec/m)
0	1.50	5.8	1.0	1.0	5.8	1.0	0.1	0.1	0.1
	1.50	5.8	1.0	1.0	5.7	1.5	0.1	0.1	1.0
	2.00	5.7	1.0	1.0	5.8	0.3	0.1	0.1	0.8
	2.00	5.9	1.0	1.0	5.8	1.2	0.1	0.1	1.0
	2.50	5.8	1.0	1.0	5.9	5.6	0.1	0.1	0.5
	2.50	5.7	1.0	1.0	5.8	1.7	0.1	0.1	0.7
	3.00	6.1	1.0	1.0	5.9	1.4	0.1	0.1	0.5
	3.00	5.6	1.0	1.0	5.8	6.9	0.1	0.1	0.7
1,500	1.50	5.8	1.0	1.0	5.8	0.3	0.1	0.1	0.7
	1.50	5.6	1.0	1.0	5.7	0.3	0.1	0.1	1.3
	1.75	5.8	1.0	1.0	5.7	0.0	0.1	0.1	0.2
	2.00	5.7	1.0	1.0	5.8	3.2	0.1	0.1	1.1
	2.00	5.9	1.0	1.0	5.8	3.8	0.1	0.1	0.5
	2.50	6.0	1.0	1.0	5.8	7.5	0.1	0.1	0.4
	2.50	5.6	1.0	1.0	5.8	3.6	0.1	0.1	1.0
	3.00	6.1	1.0	1.0	5.9	4.3	0.1	0.1	0.2
	3.00	5.7	1.0	1.0	5.8	4.5	0.1	0.1	1.0
3,000	1.50	5.8	1.0	1.0	5.7	2.6	0.1	0.1	0.2
	1.50	5.5	1.0	1.0	5.7	3.2	0.1	0.1	0.5
	1.75	5.8	1.0	1.0	5.8	2.0	0.1	0.1	0.1
	2.00	5.8	1.0	1.0	5.6	1.0	0.1	0.1	0.6
	2.00	5.7	1.0	1.0	5.9	0.4	0.1	0.1	0.4
	2.50	5.6	1.0	1.0	5.8	14.0	0.1	0.1	1.0
	2.50	6.0	1.0	1.0	5.7	9.1	0.1	0.1	0.8
	3.00	6.0	1.0	1.0	5.9	7.2	0.1	0.1	0.3
	3.00	5.8	1.0	1.0	5.9	14.2	0.1	0.1	0.1

Table C2 - Damper seal force coefficient uncertainties

Speed (RPM)	Pressure Ratio	$U(K_{XX})$ (kN/m)	$U(K_{XY})$ (kN/m)	$U(K_{YX})$ (kN/m)	$U(K_{YY})$ (kN/m)	$U(C_{XX})$ (N sec/m)	$U(C_{XY})$ (N sec/m)	$U(C_{YX})$ (N sec/m)	$U(C_{YY})$ (N sec/m)
0	1.50	6.1	1.0	1.0	6.1	2.8	0.1	0.1	3.1
	1.50	6.1	1.0	1.0	6.1	3.0	0.1	0.1	3.1
	2.00	6.1	1.0	1.0	6.1	3.3	0.1	0.1	3.6
	2.00	6.1	1.0	1.0	6.1	3.5	0.1	0.1	3.6
1,500	1.50	6.1	1.0	1.0	6.1	2.9	0.1	0.1	3.1
	1.50	6.1	1.0	1.0	6.1	2.8	0.1	0.1	3.2
	2.00	6.1	1.0	1.0	6.1	3.6	0.1	0.1	3.8
	2.00	6.1	1.0	1.0	6.1	3.6	0.1	0.1	3.8
3,000	1.50	6.1	1.0	1.0	6.1	2.5	0.1	0.1	3.2
	1.50	6.1	1.0	1.0	6.1	3.0	0.1	0.1	3.2
	2.00	6.1	1.0	1.0	6.1	3.6	0.1	0.1	3.6
	2.00	6.1	1.0	1.0	6.1	3.6	0.1	0.1	3.6

APPENDIX D

SAMPLE OF TIME DOMAIN LABYRINTH SEAL RESPONSE AND TRANSFER FUNCTION CURVE FIT FOR NO JOURNAL ROTATION AND PRESSURE RATIO OF 1.5

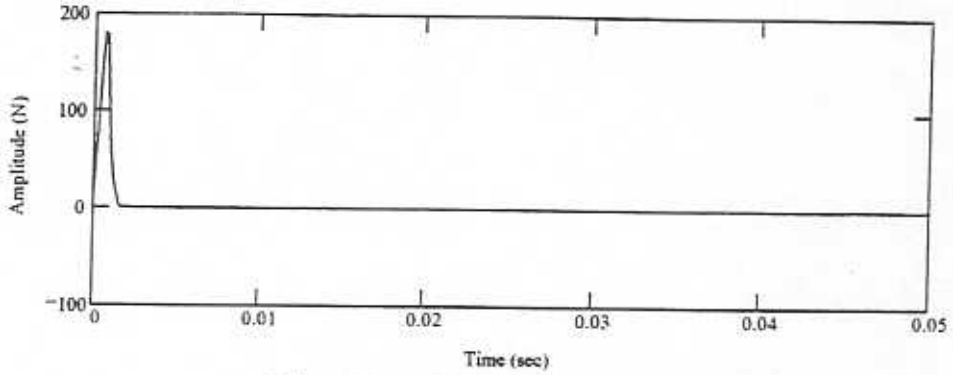

Figure D1 - Time Domain *X* Impact Load

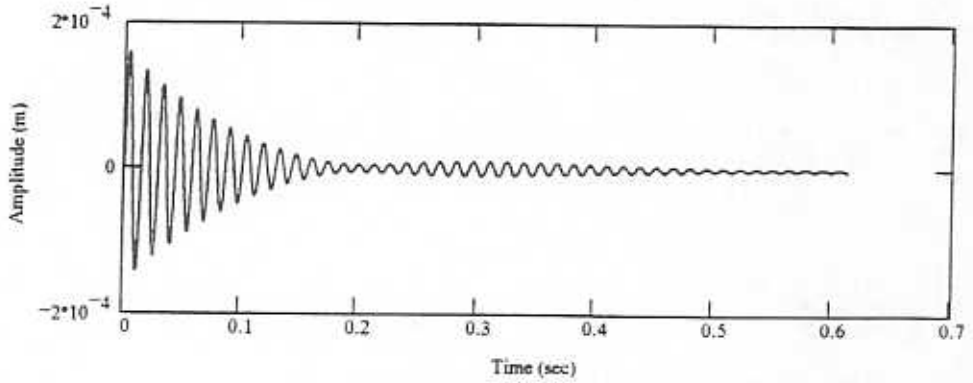

Figure D2 - Time Domain *X* Displacement Response

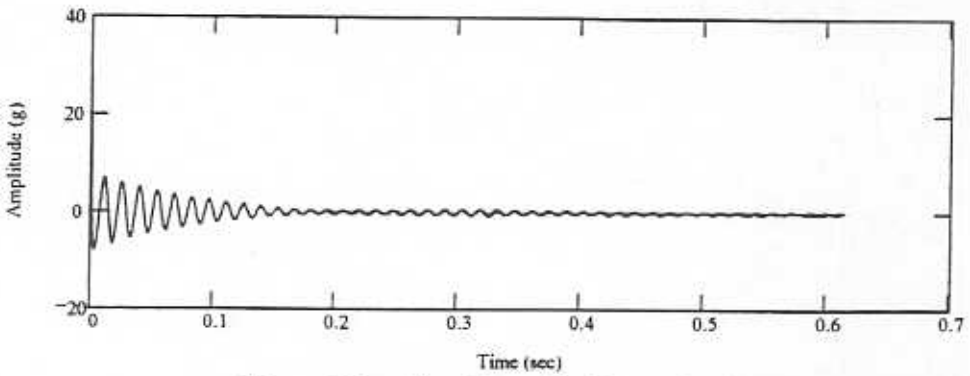

Figure D3 - Time Domain *X* Acceleration Response

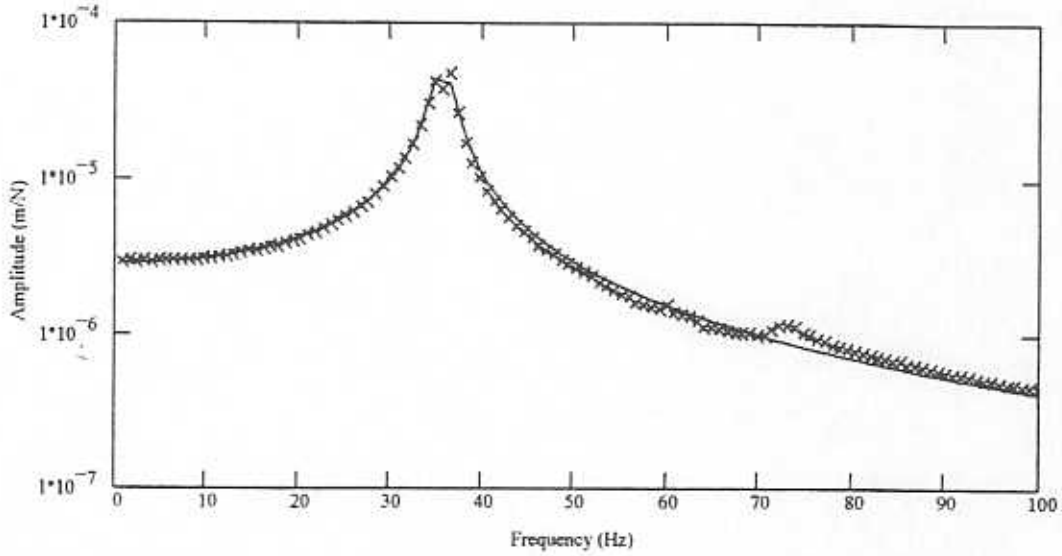

Figure D4 - Test Data and Curve Fit Transfer Functions (Gxx)

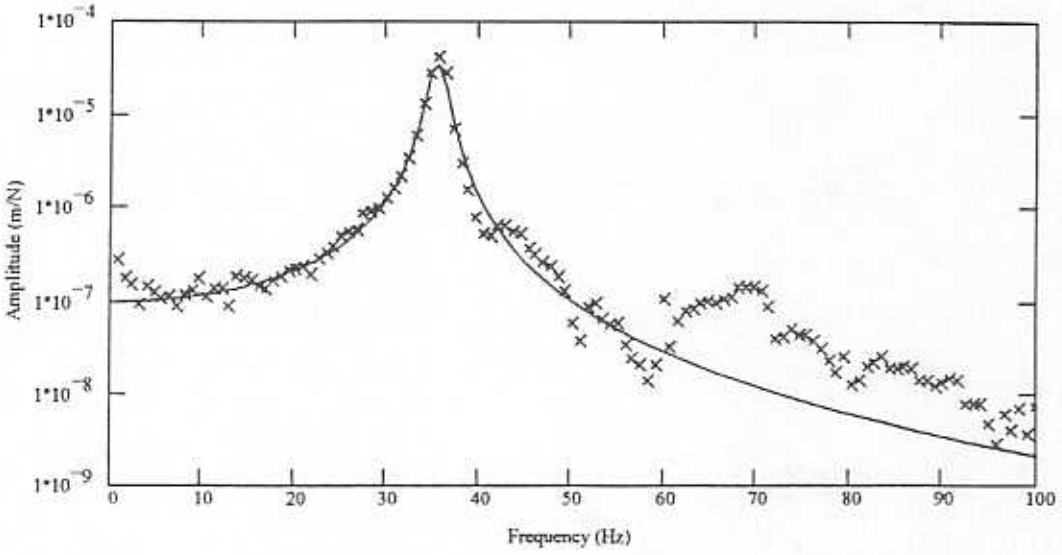

Figure D5 - Test Data and Curve Fit Transfer Functions (Gxy)

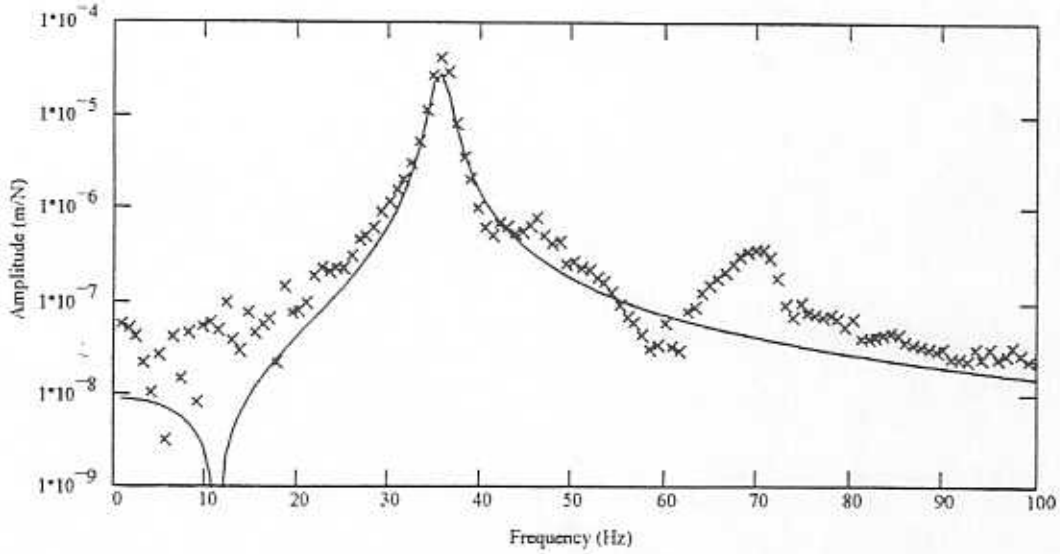

Figure D6 - Test Data and Curve Fit Transfer Functions (Gyx)

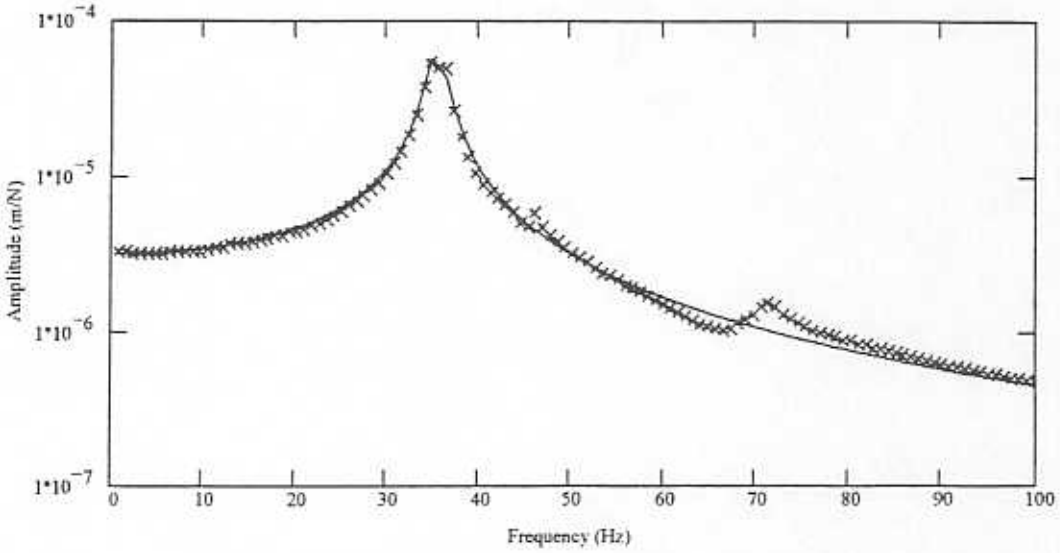

Figure D7 - Test Data and Curve Fit Transfer Functions (Gyy)

APPENDIX E

SAMPLE OF TIME DOMAIN DAMPER SEAL RESPONSE AND TRANSFER FUNCTION CURVE FIT FOR NO JOURNAL ROTATION AND PRESSURE RATIO OF 1.5

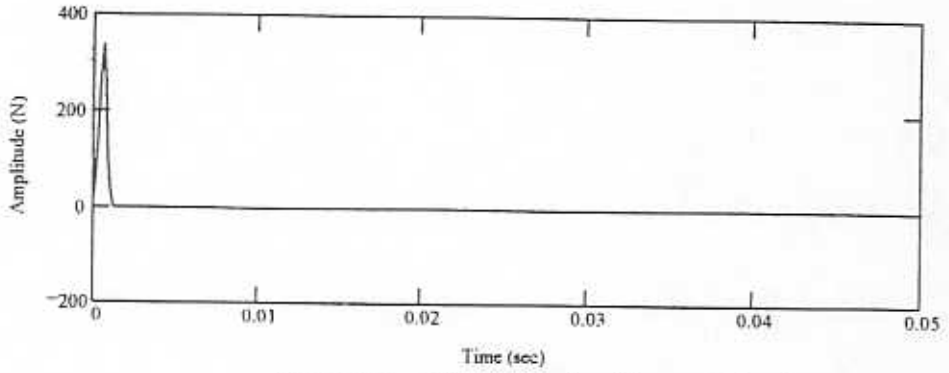

Figure E1 - Time Domain X Impact Load

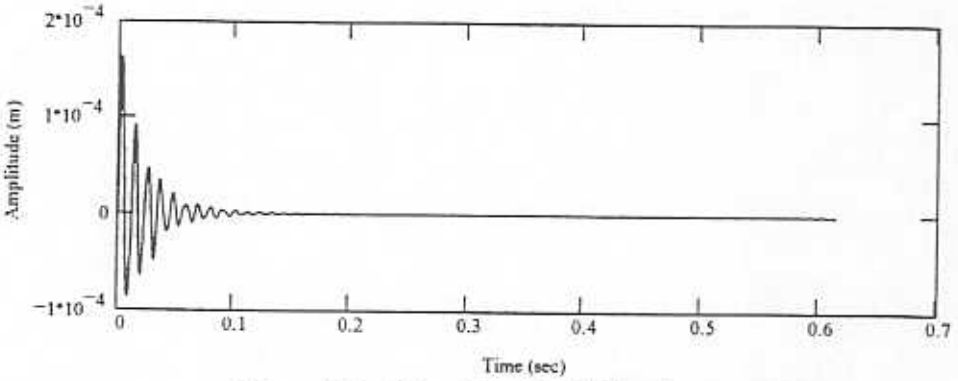

Figure E2 - Time Domain X Displacement Response

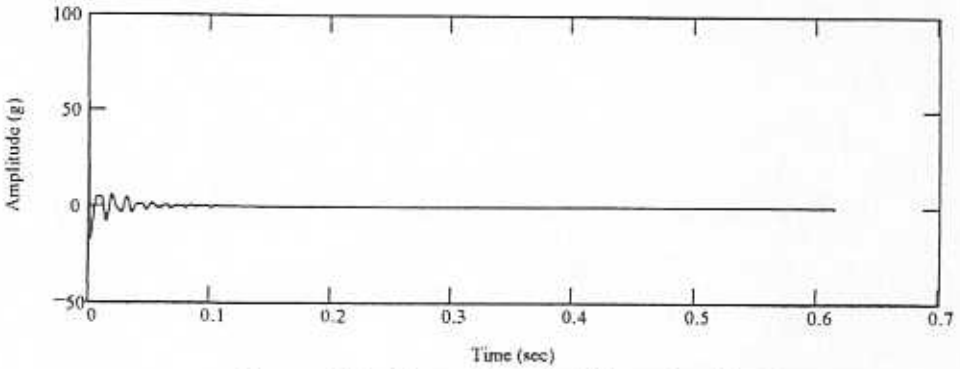

Figure E3 - Time Domain X Acceleration Response

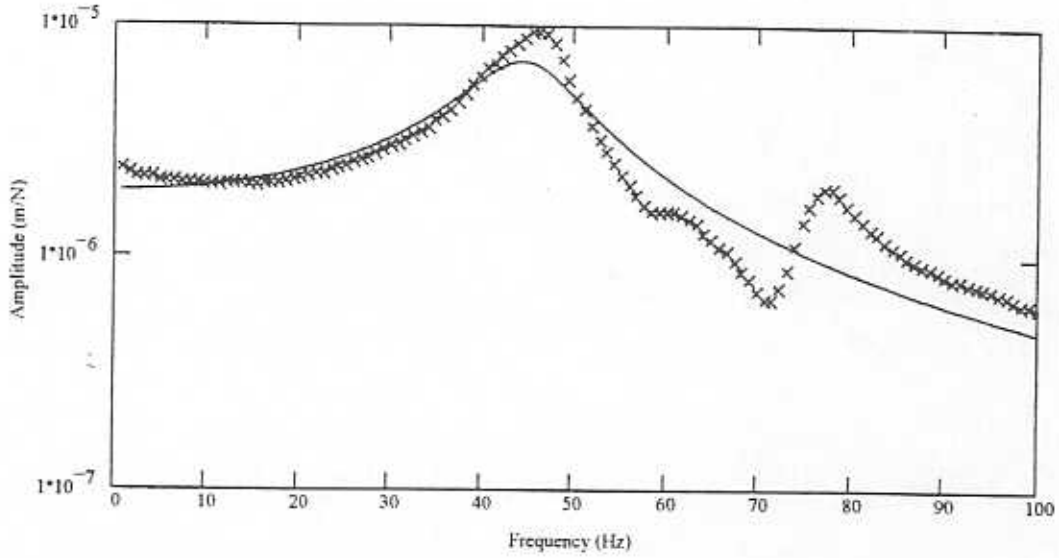

Figure E4 - Test Data and Curve Fit Transfer Functions (Gxx)

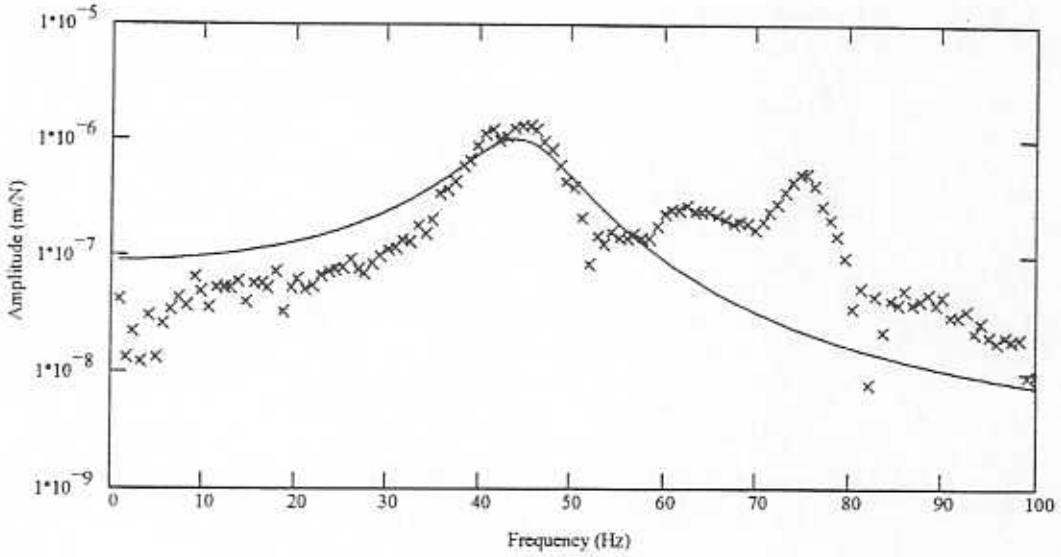

Figure E5 - Test Data and Curve Fit Transfer Functions (Gxy)

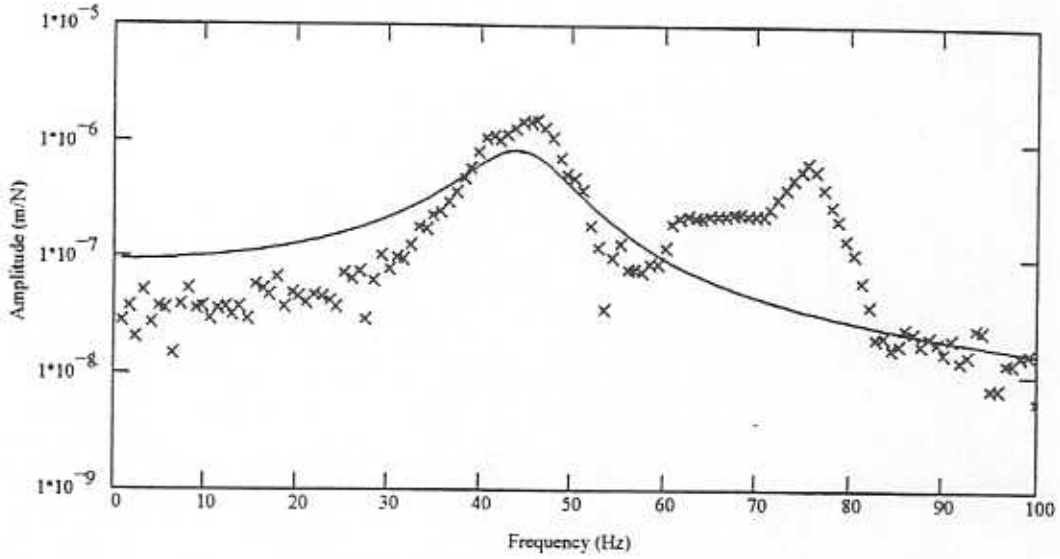

Figure E6 - Test Data and Curve Fit Transfer Functions (Gyx)

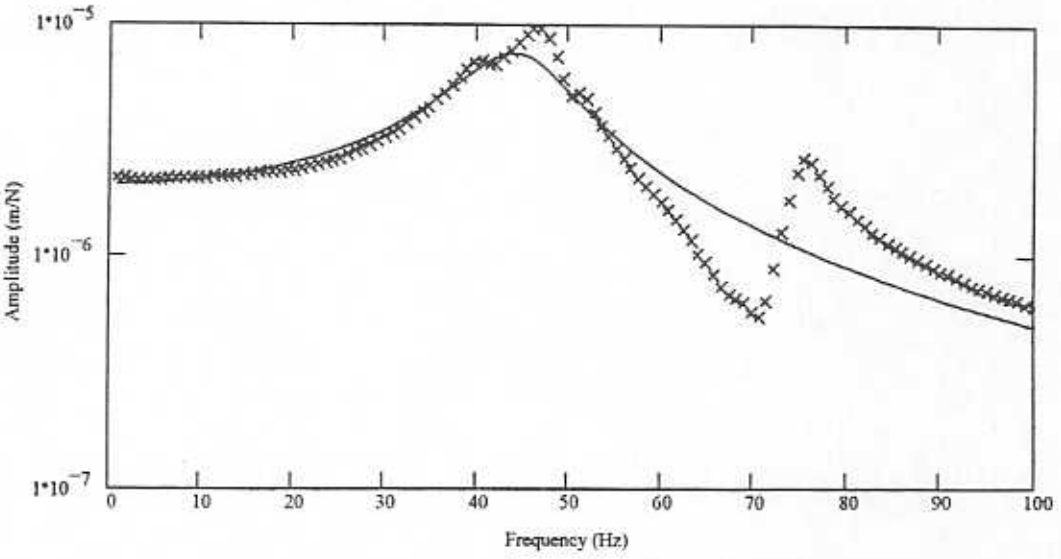

Figure E7 - Test Data and Curve Fit Transfer Functions (Gyy)